Characterisation of Organic Materials for Photovoltaic Devices

Andrew J. Lewis

September 20, 2006

A thesis submitted to the School of Physics and Astronomy, at the University of St Andrews, for the degree of Doctor of Philosophy.

Abstract

This thesis presents an investigation into a wide range of potential materials for organic photovoltaic (PV) devices. A variety of optical techniques are used to define physical parameters for each material such as the photoluminescence quantum yield (PLQY), absorption coefficient and exciton diffusion length. Electrical characterisation is used to determine the optimal structure for devices fabricated with these materials. A number of novel materials are presented in this thesis. These include new polymers, both soluble and precursor, and a relatively new class of material, the conjugated dendrimer. These are highly configurable branching molecular structures that enable fine tuning of material properties.

Work on polymers presented in this thesis investigates how such materials can be improved by testing the effect of small changes to their molecular structure. One of these changes had significant effects upon the overall material characteristics. The introduction of a dipole across a polymer successfully created a charge separating material without the need for an extra species such as C_{60} to be present.

The introduction of the conjugated dendrimer to PV applications allows significant scope for molecular engineering. Dendrimers enable tight control over certain aspects of the molecular properties. Small changes can be made such as colour tuning or solubility that enable optimisation to be performed on the molecular level, rather than on device structure. Such changes produced significantly higher internal quantum efficiencies ($> 90\%$) than typical polymer devices and offer the prospect of power conversion efficiencies in excess of 10%.

Time-resolved luminescence (TRL) spectroscopy was used to characterise the behaviour of photogenerated excitons within organic films. The investigation of exciton diffusion length was performed upon two polymers, each utilising two different time-resolved methods; diffusion to a quencher and exciton-exciton annihilation. It was found that diffusion in polythiophene films is anisotropic and the photoluminescence lifetime is dependent upon film thickness. This is explained by the formation of self-ordered microstructures during the spin coating process. Data modelling was performed which took into account both the thickness variation and the interaction of excitons with a quenching interface producing a much more realistic approach than previously published work.

Contents

Abstract **i**

Contents **iii**

Declarations **vii**

Copyright Declaration **ix**

Acknowledgements **x**

Dedication **xiv**

List of Figures **xv**

1 Introduction **1**

1.1 Background and Motivation 1

1.2 Thesis Structure 5

References **7**

2 Background Theory **10**

2.1 Introduction 10
2.2 Photovoltaic Device Operation 12
2.2.1 Device Efficiency 13
2.2.2 Material Requirements 16
2.3 Semiconductivity in organic materials 18
2.3.1 Conjugation and electron coupling 18
2.3.2 Excitons and Polarons 23
2.4 Absorption and Emission 25
2.5 Photoluminescence Decay 26
2.6 Intermolecular interactions 29
2.6.1 Aggregates (Physical Dimers) 29
2.6.2 Excimers 31
2.7 Molecular Manipulation 33
2.7.1 Conjugated Polymers 34
2.7.2 Conjugated Dendrimers 36
2.8 Photovoltaic Devices 38
2.8.1 Charge Generation, Separation and Transport . . . 38
2.8.2 Heterojunctions 40
2.8.3 Bulk Heterojunctions 41
2.8.4 Grätzel Cells 44
2.9 Summary 46

References **48**

3 Experimental Methods **60**
3.1 Introduction 60
3.2 Material Preparation 61
3.2.1 Soluble Polymers and Dendrimers 61

3.2.2 Precursors 63
3.3 Absorption and Fluorescence Measurements 65
3.4 PLQY 67
3.5 Time-Resolved Luminescence 68
3.5.1 Streak Camera 69
3.5.2 Lifetime measurement 70
3.6 Device Fabrication 71
3.6.1 Substrate Preparation 71
3.6.2 Active Layer Preparation 72
3.6.3 Contact Evaporation 73
3.7 Electrical Characterisation 74
3.7.1 Solar Simulator Characterisation 74
3.7.2 IPCE and APCE Measurements 76
3.8 Summary 77

References **78**

4 Photophysical and Electrical Studies of Polymers **83**
4.1 Introduction 83
4.2 Polymer Materials 86
4.2.1 Dimethoxy-PPV 90
4.2.2 DPFEH-PPV and NDPFEH-PPV 95
4.3 Summary 101

References **103**

5 Photophysical and Electrical Studies of Dendrimers **108**
5.1 Introduction 108
5.2 Dendrimer Materials 111

5.2.1 Porphyrins 111
5.2.2 Ir(ppy)$_3$ 118
5.2.3 Ir(ppy)$_3$ Carbazole 125
5.2.4 Bisfluorene 129
5.2.5 Cyanine Dyes 131
5.3 Discussion 143
5.4 Summary 145

References **146**

6 Exciton Transport in Organic Films **149**
6.1 Introduction 149
6.2 Exciton-Exciton Annihilation 152
6.2.1 Annihilation Constant of MEH-PPV 155
6.2.2 Annihilation Constant of P3HT 161
6.3 Time-Resolved Determination of Exciton Diffusion Length 166
6.3.1 Interface Quenching using MEH-PPV 171
6.3.2 Interface Quenching using P3HT 174
6.4 Comparison and Discussion 177
6.4.1 MEH-PPV 178
6.4.2 P3HT 180
6.5 Summary 185

References **187**

7 General Conclusions **195**

References **199**

A Publications Arising from this Thesis **201**

Declarations

I, Andrew J. Lewis, hereby certify that this thesis, which is approximately 30,000 words in length, has been written by me and it is the record of work carried out by me and has not been submitted in any previous application for a higher degree.

Andrew J. Lewis September 20, 2006

I was admitted as a research student in September 2002 and as a candidate for the degree of Doctor of Philosophy in September 2002; the higher study for which this is a record was carried out in the University of St Andrews between 2002 and 2005.

Andrew J. Lewis September 20, 2006

DECLARATIONS

I hereby certify that the candidate has fulfilled the conditions for the Resolution and Regulations appropriate for the degree of Doctor of Philosophy in the University of St. Andrews and that the candidate is qualified to submit this thesis in application for that degree.

Ifor D.W. Samuel September 20, 2006

Copyright Declaration

Acknowledgements

This is the bit where I thank people for their help and for allowing me to spend lots of money and play with expensive toys. Not to mention deny all knowledge if I happened to break it. Not that I did you understand. Some of us are careful with our equipment.

Right. First out of the hat is Prof. Ifor Samuel. He's the man responsible for allowing me to spend taxpayers money and providing me with guidance, help and direction throughout the whole of my work. Ifor was very generous in providing me with a maintenance grant from his own grant money for which I am especially grateful. Without this opportunity I wouldn't have been able to change the world as we know it.

Next up are the über chemists at the University of Oxford Department of Chemistry. They provided me with all of the funky materials I played with... er..*investigated* for my work. Heading up the Chemistry Crew is their big cheese from Down Under; Dr. Paul Burn. Some say he can wrestle crocs better than that Steve Irwin bloke off the telly and that his hat has more corks than a Bordeaux wine cellar. I'd like to thank

his minions Dr. Graham Webster and Dr. Bimlesh Lochab for polymer synthesis, Peter Deakin for supplying the porphyrins and the cyanine dyes, Sarah Staton for the iridium dendrimer, Dr. Homar Barcena for the bisfluorene dendrimer and Kevin Knights for the carbazole dendrimer. Without their hard work, none of my amazing devices would have been possible. Finally I'd like to thank Aaron Barkhouse, my partner in crime from Nova Scotia. Our work on new and groovy polymers will surely stand the test of time. For the few games of basketball we enjoyed on his vists he claimed he'd only played 'once or twice'. Yeah, and Tiger Woods only plays golf 'now and again'.

Closer to home I must thank Dr. Arvydas Ruseckas for his invaluable assistance with the ultrafast laser systems. I'm in no doubt that I would have lost at least one eye without his help. I am especially grateful to him for explaining the finer points of exciton theory to me. And for tolerating my terrible diagrams on his whiteboard. Guess who didn't do very well in Art at school...

I'd also like to thank the motley (but highly professional) crew that I worked with for the last three years. I'd like to thank Dr. Olivier Gaudin and Dr. Chris Yates for working wonders with our ellipsometer and for providing me with reliable absorption coefficients and refractive indices. I'd also like to thank Dr. Graham Turnbull and Dr. Andrew McNeill for their input and discussions. Although McNeill's 'input' usually consisted of some comments about my Merseyside origins. Not that he can talk, being a Janner from Plymouth.

I would also like to thank Prof. Steve Lee for being my mentor. And for providing the best ever speech at a Christmas Dinner Dance. Really brings a new meaning to the phrase *Head* of School.

Somewhere deep in the bowels of the Physics building, beyond the Chasm of Hopelessness and just left of the Swamp of Despair are a delightful bunch of chaps who do wonderful things with metal and wood. I'd like to thank George Radley and the rest of his workshop posse for making my haphazard designs a reality. Can't forget Jim and the guys in the electronics workshop for building the circuits I required. If I'd have done it myself I'd probably have got lead poisoning from the solder and burnt several fingers. Thanks also to Les Kirk, Paul Robertson and Scott Johnston for being cracking technicians and all round top blokes.

I would also like to convey my eternal gratitude to Mr. George Robb for maintaining the cleanroom and all the equipment in it. Without his talents, I'd have spent more time 'researching' on the internet and 'collaborating' on MSN Messenger. He also plays a mean electric guitar in a cracking Ceilidh band. Buy that man a pint. Hero.

They say in Holland, 'de Boner in de morning is boing boing groovy nice'. There is one man who I'm sure would know. He has the dirtiest windows in Europe, and if your fridge ever breaks, he's the one man who can fix it. Some agree with the Wonder Stuff and say he is the Size of a Cow. They're probably right. He is known to me (and everyone else) as Mark Goossens. I'd like to thank him for being a great friend and colleague throughout the whole of my time at St. Andrews.

My personal thanks also go to Dr. Phillip Wood for his help and support during my three years. If you find any mistakes in this thesis, blame him. He proof read most of it. And no bad thing. When I first wrote this, it looked more like 'Harry Potter and the Renewable Energy Source'.

They do say that behind every great man is a great woman, and my case is no exception. I'd like to thank my wonderful girlfriend Bex for believing in me (millions wouldn't) and her 'motivational tactics' of kicking me out of bed in the morning. Thanks also to all of my family and friends for their help, encouragement and support throughout my time at St. Andrews.

Dedication

I would like to dedicate this thesis to my parents, Jan and Dave, who have continually supported and encouraged me throughout my life. Without their sacrifice and support I wouldn't be where I am today.

List of Figures

2.1 Schematic of the operation of a solar cell device. 12
2.2 Explanation of the Fill Factor. 15
2.3 The A.M. 1.5 solar spectrum. 17
2.4 The structure of polyacetylene. 19
2.5 Structure of Methane and Diamond. 20
2.6 The delocalised cloud of electrons around anthracene and ethene. 21
2.7 Molecular structure of 1,3-butadiene and ethene and the molecular orbitals within a conjugated organic molecule. . 22
2.8 Schematic of a polaron on a polyacetylene chain. 24
2.9 Examples of Frank-Condon transitions. 26
2.10 Jablonski diagram showing an example absorption and emission spectra. 27
2.11 Decay mechanisms from an excited state to the ground state. 28
2.12 Molecular structures of dimers of anthracene. 30
2.13 Exction splitting in dimers of differing geometries. 31
2.14 Aggregate peak in the absorption of PTCDA. 32

2.15 The molecular structure of PPV. 34
2.16 Molecular structures of MEH-PPV and OC_1C_{10}-PPV (MDMO-PPV). 35
2.17 Schematic of a dendrimer molecule. 36
2.18 Schematic showing the operation and charge transport of a single layer polymer device. 39
2.19 Schematic diagram of a bilayer device showing photoinduced charge transfer. 42
2.20 Schematic diagram of a bulk heterojunction device showing photoinduced charge transfer. 43
2.21 Schematic diagram of the structure and operation of a nanoporous Grätzel cell. 44
2.22 Molecular structure of the ruthenium dye, N3. 45

3.1 Molecular structure of [6,6]PCBM. 63
3.2 Structures of two precursor polymers used in this thesis. . 64
3.3 The thermal conversion of a precursor polymer. 64
3.4 Experimental setup for TRL experiments. 69
3.5 Schematic of the operation of a streak camera. 69
3.6 Typical lifetime curve for MEH-PPV. 70
3.7 Schematics showing device structures. 73
3.8 Spectrum of the Solar Simulator output. 75
3.9 Sample chamber illuminated under the solar simulator. . . 76
3.10 Schematic of the IPCE setup. 77

4.1 Absorbance, Absorption and PL of MEH-PPV. 87
4.2 Molecular structures of DM-PPV. 90
4.3 Absorbance, Absorption and PL of DM-PPV. 91

4.4 Molecular structures of DPFEH-PPV and NDPFEH-PPV. . 96
4.5 Absorbance, absorption and PL spectra of DPFEH-PPV and NDPFEH-PPV. 97
4.6 TRL decays for novel polymers. 98
4.7 IV curves for devices fabricated from novel polymers. . . . 100

5.1 Molecular structure of chlorophyll. 112
5.2 Molecular structures of porphyrin dendrimers. 113
5.3 Absorption and absorbance of the free base porphyrin dendrimer in neat film and blend. 114
5.4 IV curve for free base porphyrin devices. 115
5.5 HOMO-LUMO schematic for free base porphyrin device. . 115
5.6 Absorption spectra of the both porphyrin dendrimers in neat film and blend. 116
5.7 IV curve for zinc porphyrin devices. 117
5.8 Molecular structure of IrG1. 118
5.9 Absorption and absorbance of the IrG1 dendrimer in neat film and blend. 119
5.10 IV curves for neat film and blend devices from IrG1. 120
5.11 Contour plot for IrG1 blend device. 122
5.12 Absorption profiles for IrG1 blend device layers. 123
5.13 IPCE and APCE curves for IrG1 blend device. 124
5.14 Molecular structure Iridium Carbazole dendrimer. 125
5.15 Absorption and absorbance of the IrCz dendrimer in neat film and blend. 126
5.16 IV curves for neat film and blend devices from IrCz. 127
5.17 IPCE of IrCz. 128
5.18 Molecular structure Bisfluorene dendrimer. 129

5.19 Absorption and absorbance of the Bisfluorene dendrimer in neat film and blend. 130
5.20 IV curves for neat film and blend devices from IrCz. 131
5.21 Molecular structures of Cyanine dyes 132
5.22 Cyanine dye neat film absorbance spectra. 133
5.23 Cyanine dye-PCBM blend absorbance spectra. 134
5.24 PL of PCD03-10. 135
5.25 PL of PCD03-10. 136
5.26 PL of PCD03-10. 137
5.27 IV curves for PCD03-10 neat film devices. 138
5.28 IV curves for PCD03-10 neat film devices (PEDOT). 138
5.29 IV curves for PCD03-10 blend devices. 139
5.30 IV curves for PCD03-18 neat film devices. 139
5.31 IV curves for PCD03-18 neat film devices (PEDOT). 140
5.32 IV curves for PCD03-18 blend devices. 140
5.33 IV curves for PCD03-19 neat film devices. 141
5.34 IV curves for PCD03-19 neat film devices (PEDOT). 141
5.35 IV curves for PCD03-19 blend devices. 142

6.1 Schematic showing the process involved in exciton-exciton annihilation. 152
6.2 Absorbance spectrum of MEH-PPV. 156
6.3 Time-resolved decay of MEH-PPV at various excitation densities. 157
6.4 Resulting curves from MEH-PPV annihilation analysis. . . 158
6.5 Low power decay curves for MEH-PPV. 159
6.6 Results for the annihilation constant in MEH-PPV. 160
6.7 Molecular structure of P3HT. 161

6.8 Time-resolved decay of P3HT at various excitation densities. 162
6.9 Resulting curves from P3HT annihilation analysis. 163
6.10 Low power decay curves for P3HT. 164
6.11 Results for the annihilation constant in P3HT. 165
6.12 Decay curves for P3HT test sample. 167
6.13 Absorbance spectra for MEH-PPV films. 172
6.14 TRL decays for films of MEH-PPV. 173
6.15 Absorbance spectra for P3HT films. 175
6.16 TRL decays for films of P3HT. 176
6.17 Lamellae ordering in P3HT. 183

Chapter 1

Introduction

1.1 Background and Motivation

For centuries man has strived to find efficient, clean and reliable energy sources. In the modern world there are many sources of energy; these include coal, oil, natural gas and nuclear power. Each of these has its disadvantages, for example, nuclear power produces highly dangerous and long lasting radioactive waste that requires expensive containment. Fossil fuels not only produce high levels of pollution, but will not last forever - it is thought that they themselves will expire in roughly 50 years [1]. Furthermore, the carbon dioxide generated when they are burnt leads to global warming. Because of these drawbacks to more established energy sources, we look to renewable energy sources which are much preferred as they don't produce waste and are readily available. Renew-

able energy sources include such things as fusion (should it ever reach fruition), wind power, hydroelectric generation, geothermal sources and, of course, solar power. Despite each of these being far cleaner than their classic counterparts, many of these sources still have their drawbacks. For example, wind turbines are sometimes disliked by communities as large wind farms can ruin the views of acres of countryside. Solar power, however, is one of the brightest prospects for future energy generation as it is silent and panels can be placed upon walls or rooftops so they don't interfere with views or surroundings. Additionally, the sun itself is the primary source of energy for the whole planet. Solar cells provide us with a great opportunity to harness this energy source for everyday use. Solar cells can be placed almost anywhere, not just on the roof of a building, allowing a much greater flexibility over wind or water power. This could reduce large areas of space being taken up by wind turbines. For example, placing solar cells over Arizona would power the whole of the USA, whereas placing wind turbines over the whole country would not only be unattractive, but also provide insufficient energy [2]. This means that ways must be created to capture this light and convert it to useful electricity in the most efficient, and to some extent, aesthetically pleasing ways possible.

In order to accomplish this there are several things needed. Primarily, materials need to be fabricated for such purposes. Silicon is a prime candidate for solar cells as it is plentiful and has a very broad absorption spectrum. Silicon photocells are well established in energy generation, it is not uncommon for monocrystalline silicon or gallium-arsenide devices to obtain conversion efficiencies (see section 2.2.1) of 24% [3–5]. This

certainly is impressive but the underlying problem with such devices is the cost of production. Production of high quality monocrystalline silicon uses extremely high temperatures making it very costly [5]. It is certainly far too expensive for mass marketing and widespread use. A further disadvantage of silicon and other such crystalline devices is that they are inflexible and generally very brittle, so they have to be kept flat or well supported otherwise they will break and be rendered useless. The most significant disadvantage to silicon is the cost of energy production, both in terms of financial and also environmental cost. Silicon photovoltaics (PVs) need to stay in use for several years to recoup the energy spent on making them [6]. In addition, there are a large number of hazardous chemicals needed to fabricate monocrystalline silicon, and a significant amount of water. Treatment of water both prior to and after fabrication is very expensive and adds significant cost to the production [7]. For these reasons, it is clear that a cheap, clean and easily processable alternative is found. Organic materials are superior to silicon as they fulfill all of the above requirements and are flexible [8] so they can be fashioned into practically any shape desired. They are generally soluble and can be made simply into thin films by various coating methods. Using such methods, material consumption will be dramatically reduced, keeping production costs down.

There are several ways of making films of organic materials. Spin coating is a popular way of performing this because it is quick and provides a film that is of good quality and of known thickness for given conditions. Additionally, there is also doctor blading [9], where an even film is made by dragging a blade across a layer of solution. Drop casting [10] can also

be used to provide thicker films should they be appropriate. Finally, inkjet printing can be used for large scale manufacturing purposes. All of these could be successfully applied to fabricating efficient solar cells for mass production.

There are further advantages to organic materials in devices. They are lightweight, cheap to produce and purify, they can be made for specific needs and most importantly, organic materials can be solution processable. Synthetic chemistry is able to produce changes in molecules at the atomic level [11, 12]. This gives a significant scope for design of materials. For the case of organic LEDs it can mean that a simple change of structure or inclusion of a specific atom can change the emission of the device from red to green. The same is true for solar cells. Where a material can absorb blue light, it is possible to change the molecules to absorb redder light, which is much more suited to the solar spectrum [13].

The operation of an organic solar cell involves several key processes. These are light absorption, charge separation, charge transport and charge extraction. Consequently, in order to better understand organic materials for photovoltaic (PV) use, there are many measurements and experiments that need to be performed. Absorption spectra are essential to investigate a material's suitability for light absorption, as this information is key to the operation of a solar cell device. Time resolved luminescence (TRL) studies are used to determine the fluorescence lifetime of a material. This information can then be used to calculate exciton diffusion lengths, another key property of PV operation. A longer diffusion length is desired to enhance the probability of charge separation. Elec-

trical measurements are performed to understand the conduction and transport properties of a material. The consolidation of this information is required for devices so attributes such as film thickness, contact metal and materials are all optimised.

1.2 Thesis Structure

This thesis will begin in chapter 2 by detailing the background of and physical theory involved in organic materials intended for use in photovoltaic devices. This will include light absorption processes, charge generation and transport, molecular interactions and material manipulation. It will also detail the theory of device operation and then go on to describe different device configurations. Molecular photophysics will be described such as excimer interactions, polaron distortions and aggregates.

Chapter 3 will describe the experimental procedures used in this work including time resolved luminescence measurements and electrical characterisation techniques. Photophysical procedures will be described here as well as material preparation. Device fabrication will be detailed and also the conditions under which these devices were tested.

Chapter 4 will go on to present results of polymer materials characterised with the methods detailed in chapter 3. It will describe the needs and design requirements behind each of the materials used, explaining

(where appropriate) why such materials have been synthesised. Materials are required to separate charge within devices, this chapter will show that organic materials can easily be designed or modified to achieve this goal.

Chapter 5 will continue this trend and present data of a new class of organic materials, conjugated dendrimers. These materials are novel and of particular interest as they are highly efficient, they can be solution processed and also designed to absorb or emit specific wavelengths of light. They can also be blended together without phase separation resulting in broadband light absorption and emission.

In chapter 6 time resolved luminescence techniques have been used in order to obtain information about how charge is transported within an organic film. Results are presented concerning two important properties; the exciton diffusion length and the 3-D annihilation constant. Both of these properties are extremely important in understanding the processes that occur within these materials and also give us insight into how we might better design devices in the future. A mathematical model will also be detailed here in order to describe the decay processes that occur within these films. Surface interactions, film thicknesses and quenching distances are all found to be factors in these decay processes, with the decay time being dependent upon film thickness.

References

[1] Commission of the European Communities, *Green Paper* **769** (2000).

[2] I.D.W. Samuel, Private Communication.

[3] M. Green, K. Emery, K. Buecher, D.L. King, and S. Igari, *Progress in Photovoltaics* **5**, 51 (1997).

[4] J.H. Zhao, A.H. Wang, M.A. Green, and F. Ferrazza, *Applied Physics Letters* **73**, 1991 (1998).

[5] J.J. Dittmer, R. Lazzaroni, Ph. Leclere, P. Moretti, M. Granstrom, K. Petritsch, E.A. Marseglia, R.H. Friend, J.L Bredas, H. Rost, and A.B. Holmes, *Solar Energy Materials and Solar Cells* **61**, 53 (2000).

[6] K. West, in *Risø International Energy Conference - Energy Technologies for post Kyoto targets in the medium term*, 2003.

[7] Y.S. Tsuo, J.M. Gee, P. Menna, D.S. Strebkov, A. Pinov, and V. Zadde, in *2nd World Conference and Exhibition on Photovoltaic Solar Energy Conversion*, 1998.

[8] I.D.W. Samuel, *Philosophical Transactions of the Royal Society of London* **358**, 193 (2000).

[9] M.K. Nazeeruddin, A. Kay, I. Rodicio, R. Humphry-Baker, E. Muller, P. Liska, N. Vlachopolous, and M. Grätzel, *Journal of the American Chemical Society* **115**, 6382 (1993).

[10] S.A. Amautov, E.M. Nechvolodova, A.A. Bakulin, S.G. Elizarov, A. Khodarev, D.S. Martyanov, and D.Y. Paraschuck, *Synthetic Metals* **147**, 287 (2004).

[11] C. Winder, *Sensitization of Low Bandgap Polymer Bulk Heterojunction Solar Cells*, PhD thesis, Universitat Linz, 2001.

[12] S.H. Chanteau and J.M. Tour, *Journal of Organic Chemistry* **68**, 8750 (2003).

[13] D. Muhlbacher, H. Neugebauer, A. Cravino, N.S. Sariciftci, J.K.J. van Duren, A. Dhanabalan, P.A. van Hal, R.A.J. Janssen, and

J.C. Hummelen, *Molecular Crystals and Liquid Crystals* **385**, 205 (2002).

Chapter 2

Background Theory

2.1 Introduction

Plastic materials have existed for decades and are very common in our everyday lives. Computer housings, bags, car dashboards, packaging and countless other examples are all made from plastic. It is cheap to make and easy to mould. However, everyday plastics are all insulators and therefore are unsuitable for electronic devices. Electronics and the devices associated with it require conducting or semiconducting materials. Traditionally, integrated circuits and devices such as diodes and photodiodes are made from silicon. The disadvantages of using silicon have been described in chapter 1. For these reasons we look to the relatively new class of semiconductors, the *conjugated* plastic. Conjugation itself is not a new phenomenon; it has existed in nature for millions of

years forming the basis of processes such as photosynthesis. Chlorophyll, found in plants, is a conjugated molecule and it is this molecule that allows solar light to be converted into energy. The synthesis of conjugated materials has enabled man to fabricate semiconducting plastics for specific needs, including photovoltaic and display devices.

This chapter will describe the operation of a solar cell device from light absorption to charge transport. The requirements of materials will be discussed, together with charge generation, separation and transport. The origin of conjugation and semiconductivity in organic materials will be described. The chemical and physical theory behind atomic and molecular phenomena such as excimers, dimers and polarons within organic materials will also be discussed. The effect of introducing defects into structures will be described and how this affects charge transport. The origins and processes involved in absorption and emission will be described as well as quenching and other non-radiative processes. Molecular design will be introduced and its use to determine material properties and this idea will be then taken further into the design of polymers for specific needs. The dendrimer concept will be introduced as novel molecular design resulting in efficient and easily processable materials. Photovoltaic structure and design will be discussed including monolayer, heterojunction and Grätzel cells.

2.2 Photovoltaic Device Operation

Solar cells require several key processes to occur for operation. These are: light absorption, excition formation (see section 2.3.2), exciton transport leading to charge separation and finally charge transport to the electrodes. The operation of a solar cell is summarised in figure 2.1. Light is absorbed through a transparent electrode (in the majority of cases this is the anode, made of ITO). On absorbing a photon, an electron is then photoexcited into a bound state consisting of the electron and the 'hole' it left behind. It is a bound state due to Coulombic attraction between the two particles. This bound state is called an *exciton*. The exciton then diffuses through the active layer until the charges separate (or recombine). The separated charges then drift to the relevant electrodes, creating a flow of charge.

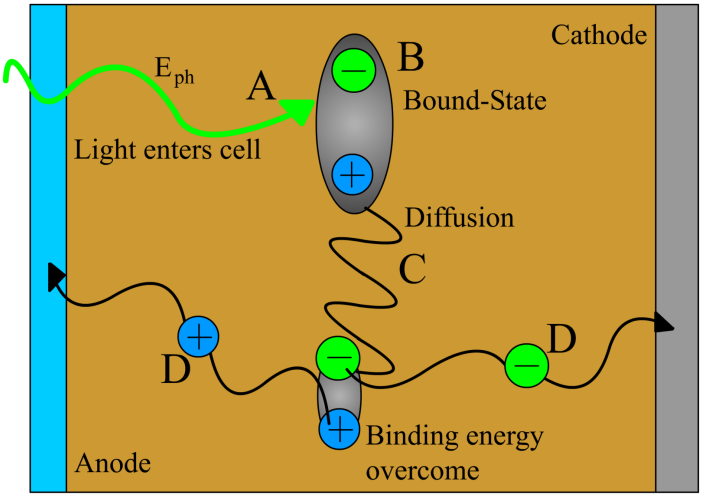

Figure 2.1: Schematic showing the stepwise operation of a solar cell. (A) Light is absorbed. (B) The photon excites an electron and an exciton is formed. (C) The exciton drifts through the material until the charges separate. (D) Charges are transported to the relevant electrodes.

The ultimate goal of a solar cell is to convert solar light energy into electrical energy as efficiently as possible. This is done in several ways. The most obvious, and easiest, to achieve is by making cells large to capture and convert a large amount of light. Whilst not improving the overall efficiency per unit area, it does enable a large mount of power to be generated quickly and simply. An improvement upon this is the introduction of the micro cavity (by using thin films) to prevent (or significantly reduce) the amount of light that escapes. One drawback currently is the fact that there is a large difference in refractive indices between layers of an organic device. This produces large reflection losses. To prevent this, it is possible to add anti-reflection coatings to the devices, but this in turn would add cost to the device production.

2.2.1 Device Efficiency

There are three measurements important to learning how well a device performs under illumination. These are the power conversion efficiency, the Incident Photon to Conducted Electron (IPCE) efficiency and the Absorbed Photon to Conducted Electron (APCE) efficiency. Each of these provides different information about the performance of a device. For example, the conversion efficiency provides overall light power to electrical power performance, whereas the APCE provides the internal quantum efficiency of a device.

Two quantities that are important in measuring the efficiency of a device

are the short circuit current density, J_{SC}, and the open circuit voltage, V_{OC}. J_{SC} is the photocurrent produced at 0 V under illumination and is dependent upon many factors including light intensity, wavelength and material absorption. V_{OC} is the voltage across the device when no current flows. It is highly dependent upon contact materials with their respective work functions and also the material(s) used for the active layer(s) within the cell [1–4].

The device power conversion efficiency, η, is defined as

$$\eta = F.F.\frac{V_{OC}J_{SC}}{P_{in}} \tag{2.1}$$

where $F.F.$ is the fill factor and P_{in} is the incident light power. The fill factor is defined as

$$F.F. = \frac{V_{MX}J_{MX}}{V_{OC}J_{SC}} \tag{2.2}$$

where V_{MX} is the voltage at maximum power, and J_{MX} is the current density at maximum power. The fill factor gives a good indication of the performance of the device. Good rectification will provide a high fill factor. Ideally it should be close to unity. J_{MX} and V_{MX} are shown in figure 2.2. η gives us how well a cell performs overall but it is also desirable to know how efficient cells are at individual wavelengths so that materials can be optimised for light absorption. This is achieved by measuring the Incident Photon to Conducted Electron (IPCE). The IPCE is defined as

$$IPCE = \eta_c = \frac{E_{ph}i_{sc}}{P_{in}e} \tag{2.3}$$

where E_{ph} is the photon energy, i_{sc} is the short circuit current (photocurrent), P_{in} is the input light power and e is the unit electronic charge. This

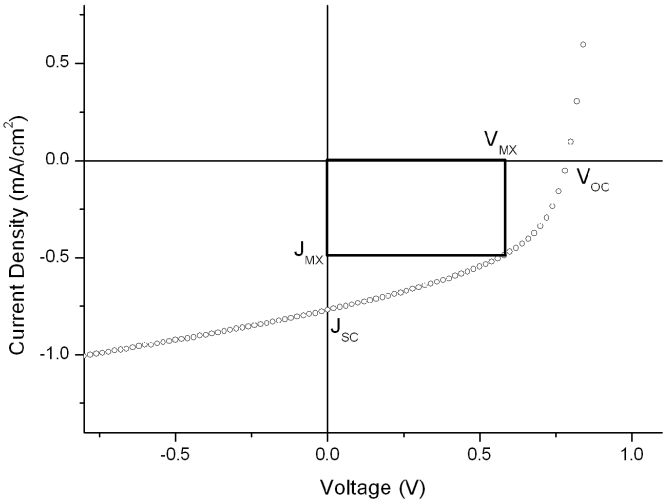

Figure 2.2: The fill factor of a device is found by finding the largest area between the I-V curve and the axes and dividing it by the maximum area possible (J_{SC} and V_{OC}).

produces a monochromatic efficiency for the device. This information can then be used in conjunction with other measurements such as absorption spectra to optimise device and/or material performance. IPCE can be seen as analogous to the monochromatic external quantum efficiency of the device.

The Absorbed Photon to Conducted Electron (APCE) efficiency is gained from knowing the absorption spectrum of the device and the IPCE. This is then defined as

$$APCE = \frac{\eta_c}{1 - T - R} \tag{2.4}$$

where T and R are the transmission and reflectance respectively. This gives the effective internal quantum efficiency for the device. Results are shown and discussed in chapters 4 and 5.

2.2.2 Material Requirements

There are several key requirements for a material to be useful for organic photovoltaic application. These include high, broadband light absorbtion, efficient charge transport, solubility (although this is not essential, see section 3.2.2) and low fluorescence.

Primarily, high, broadband light absorption is desired to be able to make the most of the solar light. Although, the solar spectrum extends well into the infra red, see figure 2.3, most (70%) of the light from the sun is in the optical and near infra-red (300-950 nm) range. This means that we ideally require absorption peaks centred around 690 nm (1.8 eV) [5,6] which will provide an optimal bandgap for materials to absorb light.

The absorption of light is only the first step in the process of extracting useful energy from a solar cell. Once light is absorbed, it needs to be put to good use. Ideally, this is the formation of an exciton. This is essential for the subsequent separation of charge. Once an exciton has been formed there are several processes that can occur, the most undesirable of which is the recombination of the exciton leading to the re-emission of a photon, or non-radiative decay processes such as exciton-exciton annihilation (see chapter 6). Ideally the exciton should diffuse through the film and dissociate into seperate charges, electon and hole. These charges can then be transported to the relevant electrodes. We require the exciton to exist for a substantial time ($>$1 ps, see chapter 6) in order for diffusion and/or hopping to occur.

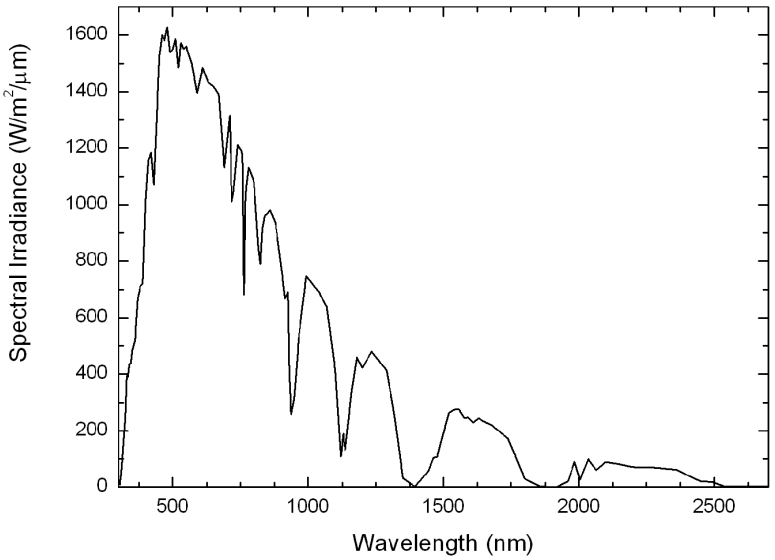

Figure 2.3: The majority of the solar spectrum (A.M. 1.5). There is a small ($<< 1\%$) contribution beyond 3 μm but this is negligible.

In addition, materials need to be able to absorb significant amounts of light in a short distance (nm scale). This is characterised as the absorption coefficient and ideally this should be as high as possible ($>10^5$ cm^{-1}). This means that device film thickness is not as critical an issue for exction diffusion because large amounts of light will still be absorbed whilst allowing excitons to diffuse to interfaces without being quenched within the bulk of the film. If a material does not absorb light strongly, then the film thickness needs to be increased to compensate. This then presents the problem of large diffusion length requirements. A thicker film will reduce the number of excitons reaching an interface to dissociate and hence device efficiency will be reduced.

2.3 Semiconductivity in organic materials

The modern field of organic chemistry has been steadily growing and improving ever since man discovered crude oil and began distilling it for its useful fractions such as kerosene, petrol and bitumen. These materials have been known about and experimented upon for many decades. They all have one thing in common with each other, no matter how dense or volatile the fraction is: they are all based upon carbon atoms. The carbon atom is the essential building block for all organic molecules. Carbon in its pure form exists as three natural allotropes; graphite, fullerenes, for example C_{60} [7] and as one of the most precious and hardest substances on earth; diamond. Each of these are simply made up of a different arrangement of the carbon atoms and it is these differences that determine their material properties. Carbon (and silicon) atoms can join together to form very long chains joined together in different arrangements of bonds to form large molecules. These arrangements determine not only the molecular structure, but also the chemical and physical properties of the molecule. The bond arrangement that we are most interested in for organic semiconductors is that of *conjugation*.

2.3.1 Conjugation and electron coupling

Conjugation arises from a specific arrangement of carbon atoms. This arrangement is a series of alternating single and double bonds within the molecule. In the case of a polymer, the conjugation is manifested

along the backbone of the structure, forming the basis of the molecule and providing the mechanism for a delocalised cloud of electrons. The simplest example of this is polyacetylene, see figure 2.4. Additionally, benzene is also conjugated as it has a delocalised electron cloud above and below the plane of the ring. The process by which conjugation occurs will be described below.

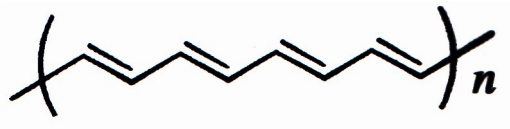

Figure 2.4: The structure of polyacetylene. Taken from [8].

The electronic configuration of carbon is $1s^2 2s^2 2p^2$. This means that there are four electrons in the outer shell of the atom, leaving two s electrons in the inner shell. Of the four outer electrons, the two s electrons are paired while the two p electrons are unpaired. This allows a number of possible combinations of bonding orbitals to be formed. The most basic is that of the case just described where the two p electrons are unpaired. This is the case for single atoms. However, in order to form bonds with other atoms and form molecules, the atoms need to form bonding orbitals. This is achieved my mixing the 2s and 2p orbitals and is known as hybridisation. When the 2s orbitals are allowed to mix with the three 2p orbitals, four equivalent orbitals, all energy degenerate, are created. These are named sp^3 orbitals and form molecules such as diamond, methane and all other saturated hydrocarbons. The structure of these molecules are shown in figure 2.5. In this case the sp^3 orbitals combine in such materials to form σ bonds and are more commonly known as *single bonds*. Further to this, if two of the three p orbitals are al-

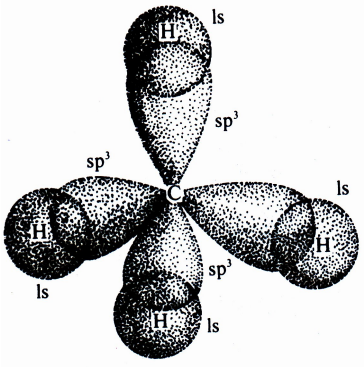

(a) Methane, CH_4, shows a clear sp^3 configuration. Taken from [9].

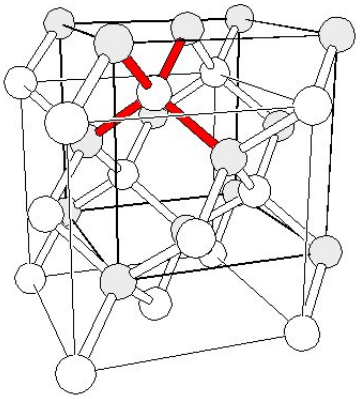

(b) Diamond, a macromolecular structure made up entirely of carbon atoms all joined by sp^3 bonds. Taken from [10].

Figure 2.5: The structures of methane and diamond, methane shows carbon covalently bonded to hydrogen with sp^3 bonding. Diamond bonds carbon to carbon in the same way.

lowed to combine with the s orbital, again four orbitals result, but with differences to the four sp^3 situation. Combining only two of the three p orbitals with the s orbital forms three sp^2 orbitals. These form three coplanar orbitals around the nucleus, each 120° apart. These also form σ bonds with other atoms as with sp^3 orbitals, but the remaining orbital lies perpendicular to this plane, known as a p_z orbital. This orbital can then combine with other p_z orbitals to form a delocalised cloud above and below the plane of the σ bonds. This delocalised cloud is known as the π bond. The combination of a σ bond and a π bond forms another commonly known bond, the *double bond*. It is this combination of alternating single and double bonds that leads to electron delocalisation along the molecule. This alternating combination is known as *conjugation*. The σ bonds hold the molecules together, while the p_z orbitals combine to form the delocalised π orbitals. This hybridisation of orbitals can

be shown clearly using the example of aromatics, made up from benzene rings. Benzene is a conjugated ring of six carbon atoms, with π orbitals above and below the plane of the molecule. Figure 2.6(a) shows the delocalised cloud above and below the plane of a molecule of anthracene. A simliar example is the case of ethene, shown in figure 2.6(b).

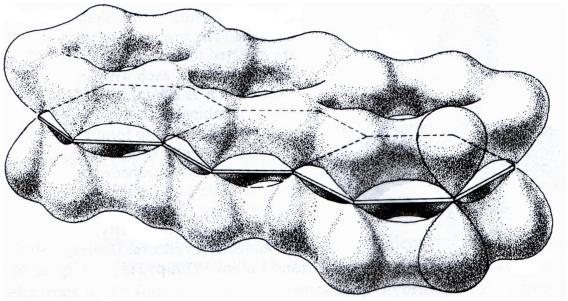

(a) Schematic of the π delocalised cloud above and below the anthracene molecule. Taken from [9].

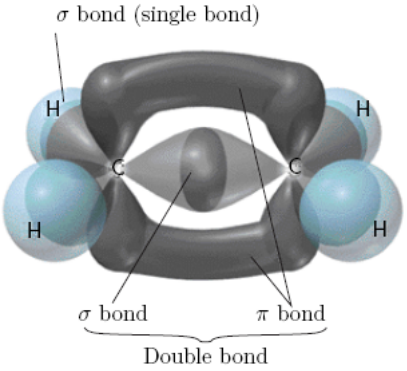

(b) Bonding orbitals between two carbon atoms. This is the arrangement for an ethene molecule. Taken from [11].

Figure 2.6: The delocalised π electron cloud over anthracene and ethene.

By combining many atomic orbitals in a single molecule, there are many degenerate levels formed due to a large number of π bonds formed. Instead of describing each individual atomic orbital, it is more applicable (due to the degeneracy of so many levels) to discuss the *molecular orbital*. This phenomenon arises from the combination of all of the atomic orbitals within the conjugated structure of the organic molecule. This combination of atomic orbitals is described as the Linear Combination of Atomic Orbitals (LCAO). Within a π bond, the electrons are weakly bound and extend across the entire molecule. Figure 2.7 shows the molecular structure of ethene and 1,3-butadiene and also the π molecular or-

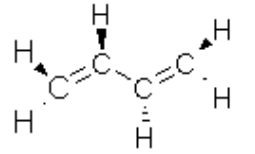

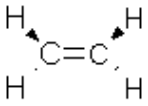

(a) Molecular structure of 1,3-butadiene and ethene.

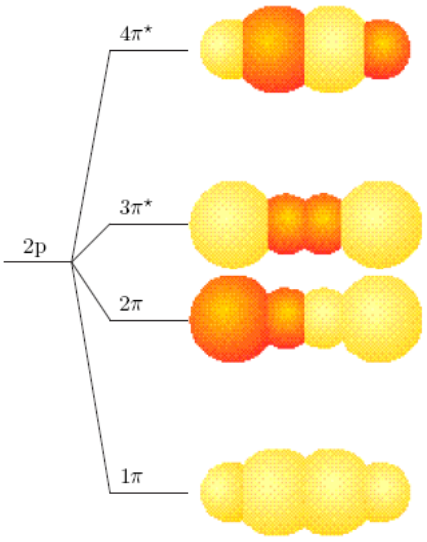

(b) The π orbitals in 1,3-butadiene. Taken from [12]

Figure 2.7: Molecular structure of 1,3-butadiene and ethene and the molecular orbitals within a conjugated organic molecule. The combination of many π bonds forms molecular orbitals which are analogous to valence and conduction bands in inorganic semiconductors.

bitals for 1,3-butadiene. Since there are two electrons within each π bond and two π bonds, there are four electrons in the π orbital. In the ground state the 1π and 2π orbitals are fully occupied. These two orbitals are bonding orbitals. The highest orbital in the ground state, the 2π orbital, is known as the Highest Occupied Molecular Orbital (HOMO). The $3\pi^*$ orbital is known as the Lowest Unoccupied Molecular Orbital (LUMO). Transitions between these levels are known as $\pi \rightarrow \pi^*$ transitions as both are within the π orbitals. Since the π electrons are in the highest occupied orbitals, they are most easily excited into the π^* state.

$N\pi$ orbitals are bonding orbitals and $N\pi^*$ orbitals are anti-bonding or-

bitals. This can be seen to be analogous to the valence and conduction bands in inorganic semiconductors, where the HOMO is the valence band and the LUMO is the conduction band. Band models have only provided limited descriptions of optical and electronic properties [13]. The parity of the orbitals is also an important factor as it affects the absorption and emission of light. In figure 2.7(b) it is clear to see the even parity of the 1π and $3\pi^*$ orbitals (the sign of the wavefunctions remain unchanged under inversion) and the odd parity of the 2π and $4\pi^*$ orbitals (wavefunction sign changes when inverted). This affects the absorption and emission properties of the molecule. The absorption and emission will be discussed in section 2.4.

2.3.2 Excitons and Polarons

Excitation within semiconductors promotes an electron from its ground state, the valence band in inorganic materials, to the conduction band. The organic equivalent to this is the excitation of an electron from the HOMO to the LUMO, $\pi \rightarrow \pi^*$, leaving a hole in the lower level. Since there is a Coulombic attraction between these two particles, they form bound states. These bound states known as *excitons*. Excitons are electron-hole pairs and are treated as quasi-particles. Excitons were first described by Frenkel [14]. This was then expanded upon by Peierls [15] and later by Wannier [16]. There are two distinct types of excitons within organic materials. The first case occurs when an exciton is formed across a small number of conjugated units, approximate radius $<$5 Å, known as a Frenkel exciton. The second case is for much larger excitons where the

electron can be delocalised more than an order of maginitude above the intermolecular separation, usually resulting in a radius of between 40 and 100 Å. This case is referred to as a Wannier-Mott exciton.

Conjugated materials, specifically conjugated polymers in this discussion, are assumed to have conjugation along their entire length during theoretical treatment. Upon excitation, the molecule will suffer a local distortion to its structure. This distortion usually extends several bond lengths. In some cases this distortion is sufficient in reversing the bond conjugation order. This will raise the energy of the molecule and make it slightly more unstable. This combination of an excitation and a distortion is known as a *polaron*. Figure 2.8 shows a schematic of a polaron. The existence of polarons in a chain produce stress on the structure, distorting it. This distortion is known as the Peierls distortion. Polarons can move along a conjugated chain and are able to 'jump' from chain to chain due to their charged properties. It is also possible to simulate

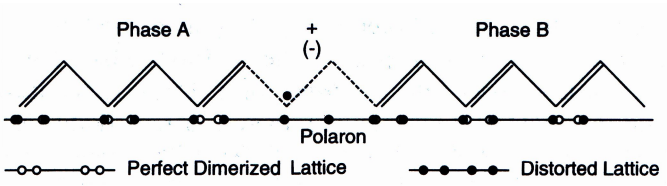

Figure 2.8: Schematic of a polaron on a polyacetylene chain. The defect distorts the chain and destroys the conjugation, but the extra charge present restores it. The polaron is free to move along the chain. Taken from [9].

this effect through doping of a molecule. This adds a charge to the molecule, for example, a hole. This breaks conjugation where the charge is present. The addition of a further charge, either hole or electron, will reform the original conjugation configuration forming either a positive

bi-polaron or a negative bi-polaron respectively [9, 17]. The addition of a hole to such an arrangement could arise from oxidation for example, where the material could have come into contact with air for a period of time. In addition to this, neutral bi-polarons (electron and hole distortions) can be formed, although these are thought to be quickly reduced into excitons due to Coulombic attraction [17, 18].

2.4 Absorption and Emission

The absorption and emission of light within organic materials is similar to inorganic counterparts. When a photon is absorbed, an electron is excited to a higher state and some time later it will relax back to its initial state, emitting a photon as it does so. Figure 2.9 shows the potential surfaces for a typical organic molecule. As electron transitions take place on a timescale of $\sim 10^{-15}$ s (compared with those of nuclear interactions $\sim 10^{-13}$ s) when the electron is excited, there is no time for nuclei to alter their spacial relationships. Therefore transitions are drawn vertically rather than at some angle to the vertical. This is known as a Franck-Condon transition [9]. After excitation, for example from the HOMO to the LUMO, the nuclear coordinates are not in equilibrium and this enables radiationless decay to the lowest vibrational state to occur [9]. After this decay, the electron can then return to the ground state, usually emitting a photon. This is known as relaxation. Since energy has been lost as 'heat' the emitted photon will be of longer wavelength than that of the excitation photon. This difference in the peak of the fundamental

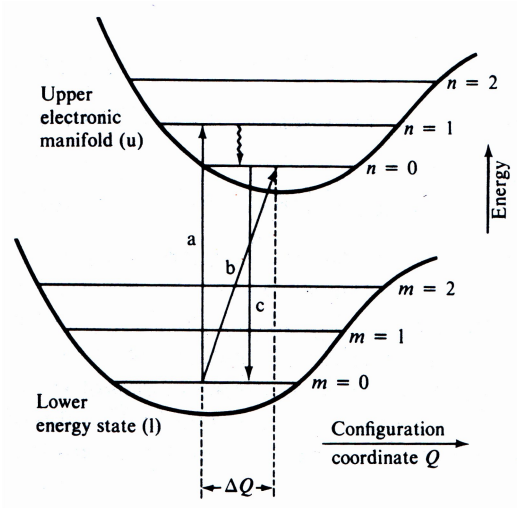

Figure 2.9: Two electronic states, u = upper and l = lower. Several vibronic states have been included. Vertical lines denote Franck-Condon transitions (a), b represents a phonon-less transition and c represents a fluorescence decay. The wavy line denotes a non-radiative transition from a higher vibronic state to the lowest LUMO level. Taken from [9].

absorption band and the fluorescence band is known as the Stokes' shift. This shift can be seen in figure 2.10.

2.5 Photoluminescence Decay

After excitation, there are two ways that the excited species can decay; radiatively and non-radiatively (see figure 2.11). These decays will have a characteristic lifetime varying between materials. From the Einstein relations we know that the rate of decay of excited states is proportional to the number of excited states present. Ignoring intersystem decays and using rate contants for the radiative and non-radiative decays κ_r and κ_{nr}

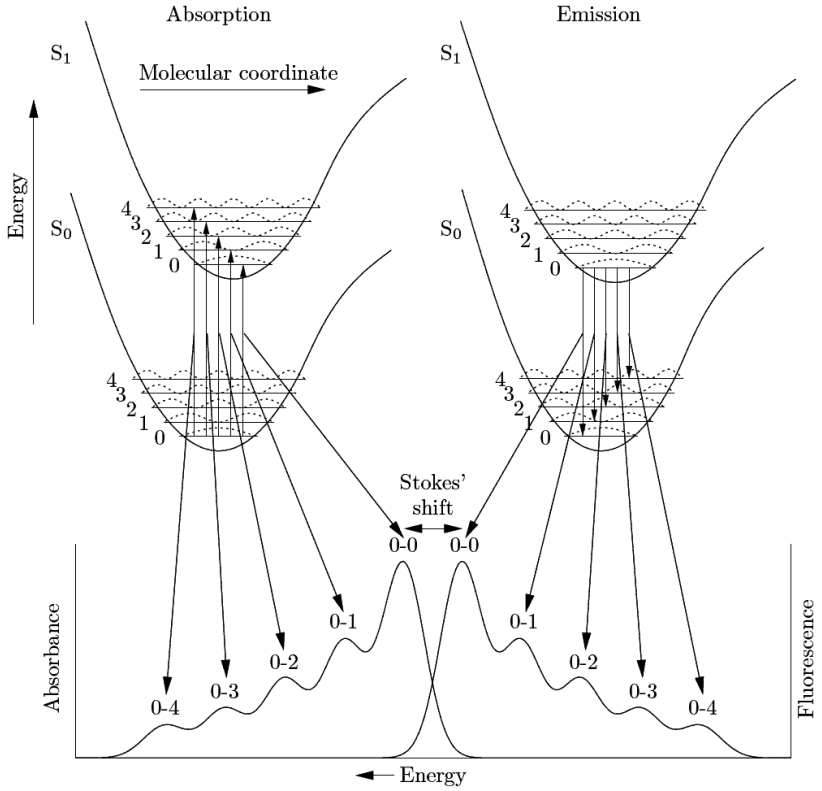

Figure 2.10: Jablonski diagram showing an example absorption and emission spectra. Notice that each vibronic state corresponds to a feature in either spectrum. The Stokes shift is clearly seen here. Taken from [11].

respectively we have equation 2.5.

$$\frac{dN}{dt} = -(\kappa_r + \kappa_{nr})N \tag{2.5}$$

The decay lifetime is then the inverse of these two decay contants

$$\tau = \frac{1}{\kappa_r + \kappa_{nr}} \tag{2.6}$$

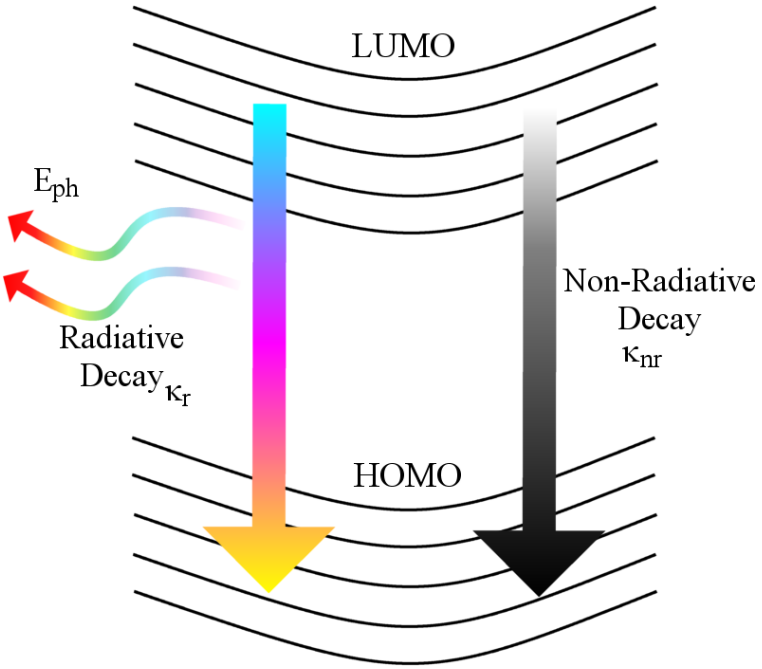

Figure 2.11: Decay mechanisms from an excited state to the ground state. Adapted from [19].

From this the quantum yield (see section 3.4) is then

$$\Phi = \frac{\kappa_r}{\kappa_r + \kappa_{nr}} = \frac{\tau}{\tau_r} \tag{2.7}$$

where $\tau_r = 1/\kappa_r$ is the lifetime the luminescence would have in the absence of non-radiative processes [9, 19, 20]. This is known as the natural lifetime [19]. The only measurable values in equations 2.1 to 2.3 are the lifetime, τ, and the quantum yield, Φ. Thus we need both to determine κ_r and κ_{nr}. The knowledge of κ_r and κ_{nr} is useful in determining exciton diffusion lengths, see chaper 6.

2.6 Intermolecular interactions

In a conjugated film such as those formed when an organic solution is spin-coated onto a substrate, there are many interactions between neighbouring molecules. These interactions modify the properties of the compound (or single element) in a significant way. The result is quantum mechanical splitting of levels due to exchange interactions, for example, electrons can interact between neighbouring molecules. There are two main types of intermolecular interactions, dimers and excimers. Each of these will be discussed in turn.

2.6.1 Aggregates (Physical Dimers)

A dimer is used in chemistry to describe a union between two identical molecules. In organic films this does not happen but a similar process does. In a polymer film, for example, molecules are closely packed and have the opportunity to interact. As all of the molecules are the same (or very similar) these interactions are also known as *dimers*. To avoid confusion, the former will be known as a chemical dimer (chemical union) and the latter as a physical dimer (molecular interaction). The physical dimer is also known as an *aggregate*. The physical dimer will be discussed here. Figure 2.12 shows the difference between the two types of dimer.

Dimers affect both the absorption and the emission of a material. In

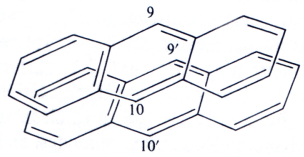

(a) Anthracene physical dimer. Taken from [9].

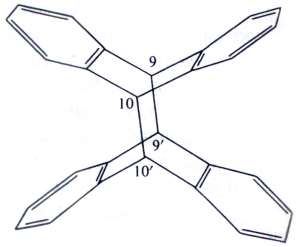

(b) Anthracene chemical dimer, dianthracene. Taken from [9].

Figure 2.12: Molecular structures of physical (a) and chemical (b) dimers of anthracene.

general, aggregate spectra are much broader and possess less strong features than those of monomer spectra [9]. The interactions between molecules causes a shift in their energy levels. This shift can either be blue (positive) or red (negative) mainly depending upon the orientation of the interacting molecules [9]. Figure 2.13 shows the different shifts in emission due to these interactions. Organic molecules generally possess dipoles and it is these dipoles that affect the interactions not only with light, but also between individual molecules. In figure 2.13 one can see the two simple possibilities of dipoles upon dimer interactions where dipoles are either arranged parallel to each other, or head to tail. This results in an energy increase (blue shift) or a decrease (red shift) respectively. The final possibility exists when the two interacting molecules are at some given angle with respect to each other. This results from both parallel and head to tail arrangements being possible. The resultant dipoles add vectorially to produce valid orthogonal solutions to the overlapping wavefunctions to yield both possible energy states. This is known as *band splitting*. Excitations can be transferred back and forth between the two interacting molecules. It can be seen as an wavelike

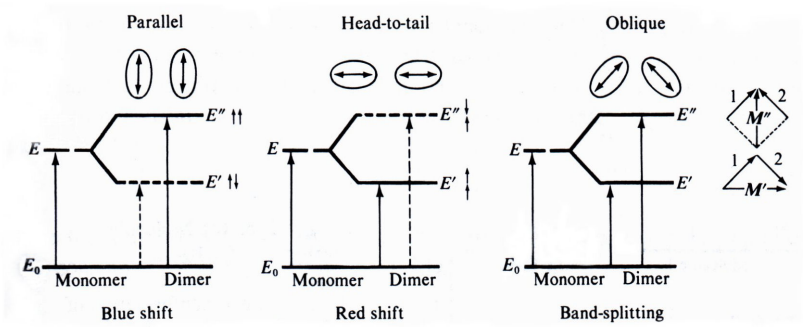

Figure 2.13: Exction splitting in dimers of differing geometries. The orientation of dipoles is shown by short arrows. Dipole-forbidden transitions are shown by dotted arrows. Taken from [9].

oscillation [9]. Provided there are no other loss mechanisms, the energy exchange can proceed indefinitely. Aggregates can be seen when increasing the concentration of molecules in a given environment, for example, moving from dilute solution to a thin film. Using a dilute solution where the molecules are relatively far apart there will be few aggregate contributions to a given spectrum. By contrast, there will be a significant contribution from dimers in a film where the molecules are much closer packed. An example is shown in figure 2.14 where increasing the concentration of 3,4,9,10-perylene tetracarboxylic dianhydride (PTCDA) gives rise to an absorption peak due to aggregates.

2.6.2 Excimers

In the previous section aggregates (physical dimers) were described. For aggregates the molecules are fixed relative to each other and definite absorption and emission bands can be attributed to them (see figure 2.14).

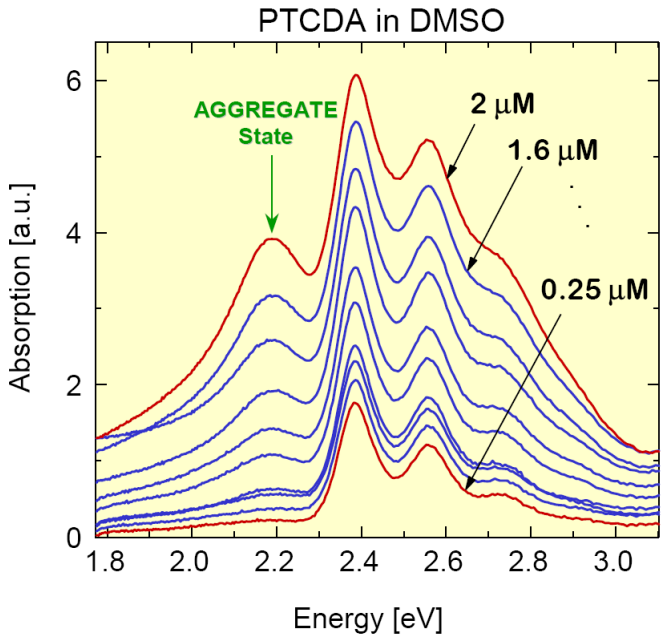

Figure 2.14: Increasing the concentration of a PTCDA solution in DMSO results in the development of an aggregate peak at ~ 2.2 eV. Taken from [21].

There is a class of organic compounds that displays a combination of monomer absorption characteristics and also the broad featureless emission spectrum shown by physical dimers. This class of compounds display what are known as *excimers*. The term excimer is a contraction of 'excited state dimer' and was first used by Stevens and Hutton in 1960 [22]. Excimers are purely excited state as they require an excited molecule to exist. They do not exist in the ground state as they are dissociative [9]. This means that even if the interacting molecules are free to move, they do not form physical dimers because the force between the molecules at dimer separation is repulsive [9]. There are three reactions in such a system:

$$S_1^* \rightarrow S_0 + h\nu_N \tag{2.8}$$

$$S_1^* + S_0 \rightarrow E_1^* \tag{2.9}$$

$$E_1^* \rightarrow S_0 + S_0 + h\nu_E \tag{2.10}$$

Where equation 2.8 shows normal decay from the lowest level of the LUMO (singlet transition) on a single molecule; equation 2.9 shows quenching of an excited state, S_1^*, one one molecule by a ground state, S_0, on a second molecule. This produces excimer E_1^*. Equation 2.10 shows excimer emission to the ground state, giving two ground state molecules and the emitted photon. The starred species denote an excited state.

2.7 Molecular Manipulation

In this section, emphasis will be placed on the importance of material design for their role in photovoltaics. The choice of material for PV applications is critical as a simple change to the molecular structure can drastically alter device performance. Chemistry plays an important role here by synthesising the desired structures suitable for light absorption and charge transport. Polymer design will be discussed first (section 2.7.1) starting from the simplest structures and building upon them. The dendrimer concept will then be discussed in section 2.7.2 describing this novel approach to molecular design providing highly efficient materials with a wide range of emission and absorption properties.

2.7.1 Conjugated Polymers

Conjugated polymers have been investigated for almost 30 years since Shirakawa synthesised the very first example of semiconducting polyacetylene [23]. Since then there have been significant advances in the synthesis of such materials in order to increase their conductivity, make them soluble and alter their optical and electrical properties. A good example of this is poly(*p*-phenylene-vinylene) (PPV), shown in figure 2.15. The addition of the phenyl ring into the polyacetylene backbone increases the conductivity and changes the absorption and emission spectra [24, 25].

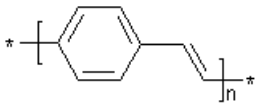

Figure 2.15: The molecular structure of PPV.

As discussed in chapter 1, one of the greatest advantages of organic semiconductors over inorganic is the ability to be solution processed. This enables fast production and low cost fabrication. However, polyacetylene and PPV are both insoluble. In order to facilitate such processes as spin coating and ink-jet printing, the materials need to be modified to enable dissolution into solvents. More recent polymers such as poly[2-methoxy-5-(2'-ethyl-hexyloxy)-1,4-phenylene-vinylene] (MEH-PPV) [6, 26–31], poly[2-methoxy-5-(3',7'-dimethyl-octyloxy)-1,4-phenylene-vinylene] (MDMO-PPV) [3–6, 26, 32–52] (MDMO-PPV is also known as OC_1C_{10}-PPV) and poly[9,9'-dioctyl-fluorene-*co*-benzo-thiadiazole] (F8BT) [1, 2, 53, 54] are soluble in a wide variety of organic solvents due to the addition of side

groups to the polymer backbone (see figure 2.16). Because of such side groups the molecules dissolve relatively quickly in common solvents such as chlorobenzene, chloroform, tetrahydrofuran (THF) and toluene.

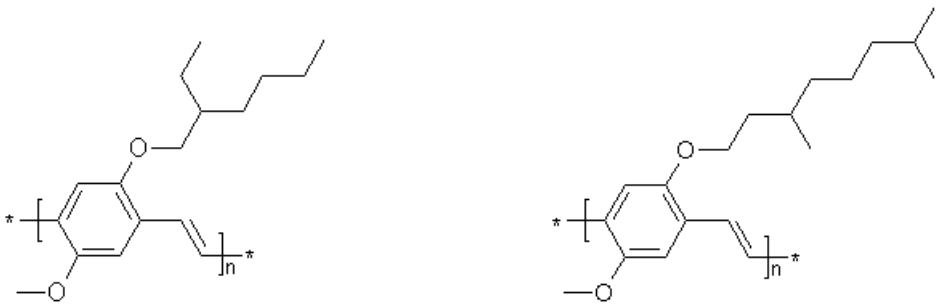

(a) MEH-PPV. (b) OC_1C_{10}-PPV.

Figure 2.16: Molecular structures of MEH-PPV and OC_1C_{10}-PPV (MDMO-PPV).

Further to the solublising additions, there are many other polymers that can be used for PV devices such as poly[3-hexyl-thiophene-2,5-diyl] (P3HT) [55–57] and several specially designed polymers that are investigated as part of this thesis. These specially designed polymers have been synthesised for the specific application of PV devices. The polymers have been designed for high light absorption, charge separation and transport properties and solubility in common solvents. Their characterisation is detailed in chapter 4.

2.7.2 Conjugated Dendrimers

Designing molecules for a specific purpose is one of the core ideas for organic devices. For the case of LEDs we require efficient charge transport, specific spectral luminescence and solution processing. These properties were successfully manifested in the form of the *conjugated dendrimer* by Halim, Samuel and Burn [58]. The conjugated dendrimer is built up of three main parts; the core, the dendrons and the surface groups, see figure 2.17. The core controls the emission (or absorption) of light, the dendrons are responsible for charge transport and molecular separation and the surface groups control the solubility of the molecules. This means that, in the case of LEDs, molecules can be synthesised to

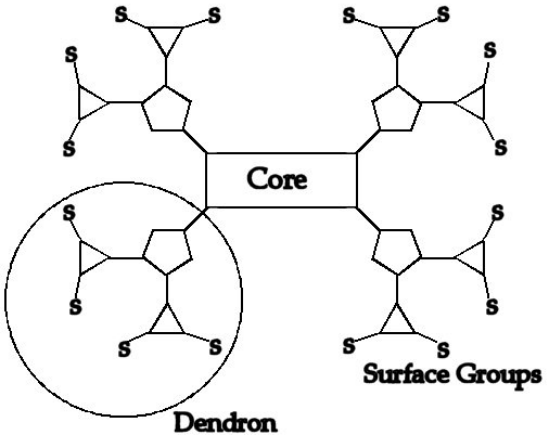

Figure 2.17: Schematic of a dendrimer molecule. The core, dendrons and surface groups are shown. Adapted from [20].

emit red, green or blue light to suit a display device simply by changing the core of the dendrimer [59, 60] whilst keeping the surface groups the same. This means that the processing properties remain identical whatever the colour of emission. The dendrons are positioned around the core to 'shield' it from its neighbouring molecules preventing core-

core interactions and to space the molecules within the film [58, 61–63]. The size of a dendrimer can be increased by adding to the existing dendrons, in a fractal fashion. The number of dendron 'layers' is known as the generation number of the dendrimer [61]. Increasing the generation of the dendrons around the core will increase the separation of the cores [58, 61]. For the case of LEDs, it is important to reduce core-core interactions as this produces luminescence quenching [61]. Luminescence quenching is desireable for solar cells to reduce loss mechanisms by re-emission of light. However, since thin film solar cells are excitonic devices [64–66] requiring charge separation, core-core interactions can also be detrimental as excitons could be quenched by these interactions before charges are separated (see section 2.8.1 for a fuller description). Chapter 5 details the characterisation of several types of dendrimer and their usefulness as photovoltaic materials.

Since the physical size of the dendrimer can be finely tuned by altering the generation number, the mobility and charge carrying properties of the materials can be adjusted to suit the required purpose. In the case of solar cells, it is desirable to have materials with high mobilities for both electrons and holes to maximise charge transport efficiencies. It has been shown that changing the dendrimer generation has a significant effect upon the mobility of the material [61].

One of the greatest advantages of conjugated dendrimers is their processability. This enables many different cores to be mixed together without phase separation [20], providing the ability to absorb a wide range of wavelengths of light. By blending (mixing) several dendrimers with dif-

fering cores, we are able to access much more of the solar spectrum for light absorption. This in turn should yield much more efficient devices. The results for dendrimer device work are shown and discussed in chapter 5.

2.8 Photovoltaic Devices

The fabrication of efficient solar cell devices are a significant part of material characterisation. This section will detail the ideal requirements of a material for use in PV devices and then go on to describe the operational theory of thin film devices. This will include the processes of exciton creation from light absorption, the subsequent diffusion of the excitons through the film, charge separation from exciton dissociation and finally the transport of these charges through the device. The final part of this section, 2.8.4, will describe the operation of another configuration of solar cell; the Grätzel cell [67]. Grätzel cells are a relatively new class of solar cell that have provided high efficiency light conversion ($>$10%) whilst being thin film organic devices.

2.8.1 Charge Generation, Separation and Transport

Initially within a solar cell, photons are absorbed resulting in the creation of an exciton. After exciton formation, we require the separation of

the bound electron-hole pair. This is achieved by fabricating a cell with differing work functions on the electrodes. Figure 2.18 shows a simple monolayer device. Charges are attracted to the electrodes due to the

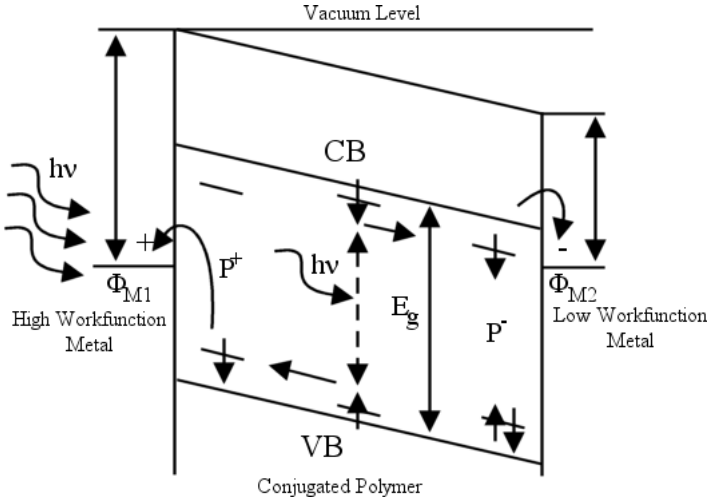

Figure 2.18: Schematic showing the operation and charge transport of a single layer polymer device. E_g is the bandgap, P^+ and P^- are positive and negative polarons respectively. Adapted from [26].

'built in' voltage generated by the different work functions of the anode and cathode. This 'built in' voltage across the cell can provide an electric potential that is sufficient to overcome the exciton binding energy ($<$1 eV) [68–71] and separate the charges. Excitons 'migrate' through the material(s), characterised by the exciton diffusion length, see chapter 6. This process is limited in a single layer (or single material) device as the potential created is not usually sufficient to overcome this binding energy, however, the introduction of *heterojunctions* and *bulk heterojunctions* can provide a solution, see sections 2.8.2 and 2.8.3.

Charge transport can occur in several ways. The most direct is that of a polaron movement along a molecule. The defect formed from the ad-

dition of a charge will force the molecule to reduce its energy. This is done by pushing the defect to the end of the molecule, taking the charge with it. From here the possibility of charge hopping is presented. Since an excited state is essentially a dipole, there can be dipole-dipole interactions. Oscillating dipoles can induce oscillation in neighbouring molecules, transferring energy. This is known as *Förster transfer*. Excitons themselves can also 'hop' from the excited molecule to a neighbour, exciting that instead. Since an excited electron 'jumps' from the excited molecule to the ground state molecule neighbour, a hole must jump the same way as well to balance the charge. This is known as *Dexter transfer*. Energy is lost in every hop or oscillation, so this can only occur as long as it is favourable, giving rise to the characteristic exciton diffusion length, see chapter 6. Consequently, this leads to a problem of maximum useful film thickness. If a film is too thick then an exciton (or separated charge) will most likely not reach a contact before it decays, reducing efficiency. The alternative to this is having a thin film ($\sim$ 20 nm) but then the problem of insufficient light absorption arises. If the active layer in a cell is too thin, there may not be sufficient useful light absorbed. This could be improved using a material with a high absorption coefficient.

2.8.2 Heterojunctions

Heterojunctions are common in inorganic devices providing such structures as p-n diodes. The organic analogue to this is the bilayer device. These have been very successful for LEDs producing high quantum efficiencies [72], so the same theory was applied to solar cells. This con-

figuration is ideal for the formation of excitons, which are essential for cell operation, at the interface between the two organic layers. In the case of LEDs, subsequent exciton decay led to the emission of photons. This is undesirable for solar cells as excitons would still need to diffuse to this interface. This means that light would need to be absorbed within one diffusion length of this interface. An example of this is shown in figure 2.19. In this configuration, charges are still limited to moving to the n-type layer (for electrons) and the p-type (for holes). Charge separation can still only occur at the p-n interface. The solution to this, and another benefit of organic materials, is the *bulk heterojunction*.

2.8.3 Bulk Heterojunctions

Since organic materials are (generally) soluble, they can be blended together. This means that p-type materials (polymers for example) and n-type materials (fullerenes) can be interdissolved in the same solution, see section 3.2.1. When a film is spun from this solution, it forms an interpenetrating network of molecules, both p and n-type. This has a significant advantage over the bilayer configuration as charge separation can now occur over the entire bulk of the film, effectively removing the problem of exciton diffusion through the entire film thickness. Light absorption can occur throughout the entire film and, as such, charge transport is benefitted. Figure 2.20 shows a schematic of such a configuration. It is possible to see that photoinduced charges can hop to their preferred carriers and then be easily transported to respective electrodes. This device configuration is used for majority of the device work in this thesis,

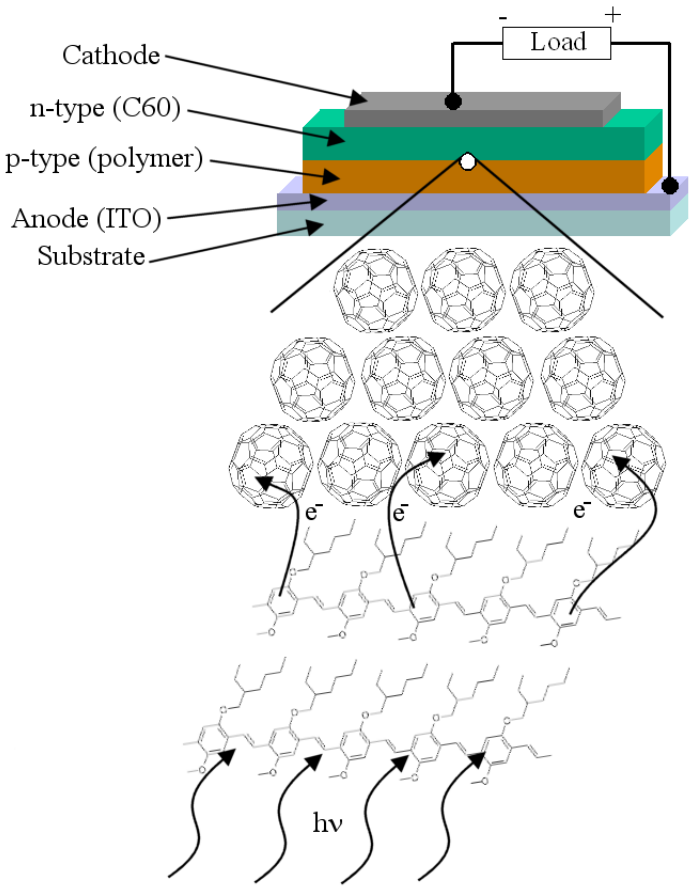

(a) Charge transfer interface in a bilayer device, and typical device structure.

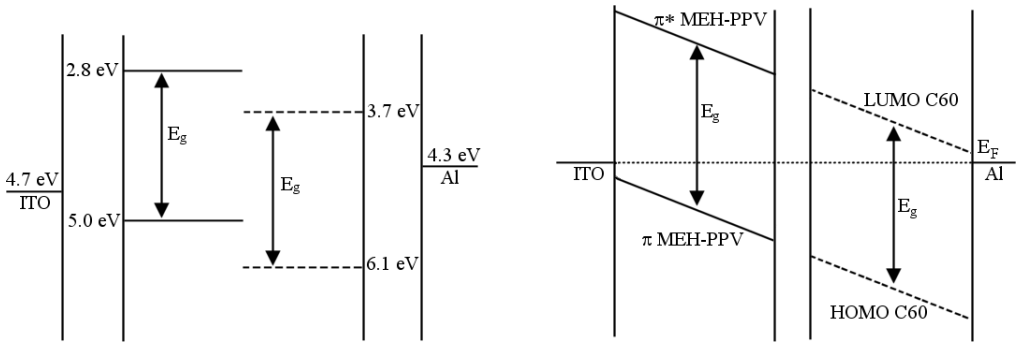

(b) (c)

Figure 2.19: Schematic diagram of a bilayer device showing photoinduced charge transfer, (a). The device is represented under open circuit (b) and under short circuit (c). Adapted from [26].

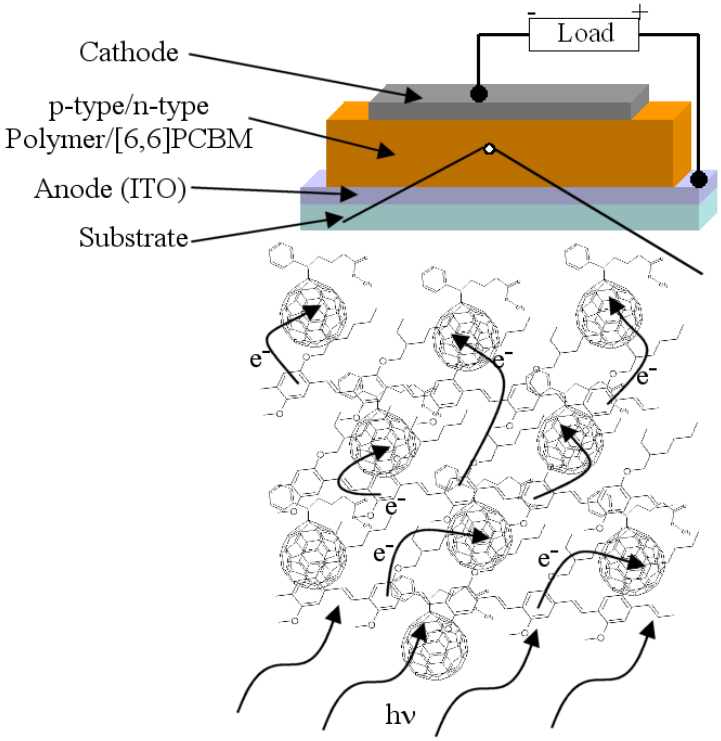

(a) Charge transfer interface in a bulk device, and typical device structure.

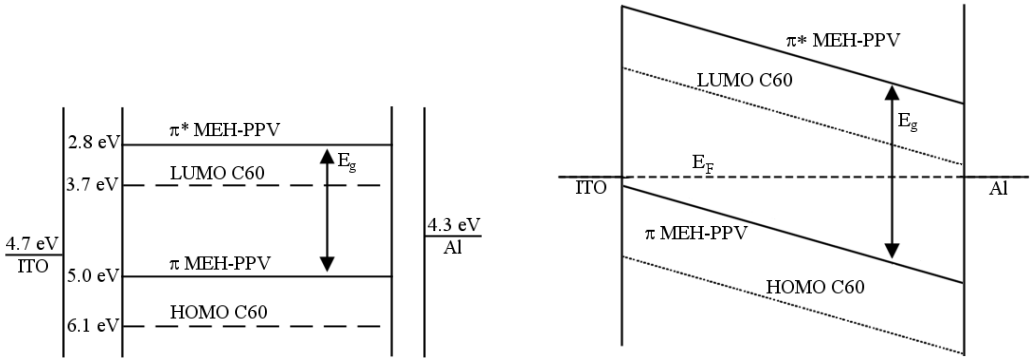

Figure 2.20: Schematic diagram of a bulk heterojunction device showing photoinduced charge transfer within the interpenetrating network formed from the blend (a). The device is represented under open circuit (b) and under short circuit (c). Adapted from [26].

and results are described in chapters 4 and 5.

2.8.4 Grätzel Cells

Further to the thin film bulk heterojunction devices described in section 2.8.3, there is another type of device configuration that can be used, the Grätzel cell. This device was first conceived by Michael Grätzel in 1993 [67] and they were shown to be highly efficient (over 10% power conversion efficiency) [67, 73–75]. Unlike bulk heterojunctions which,

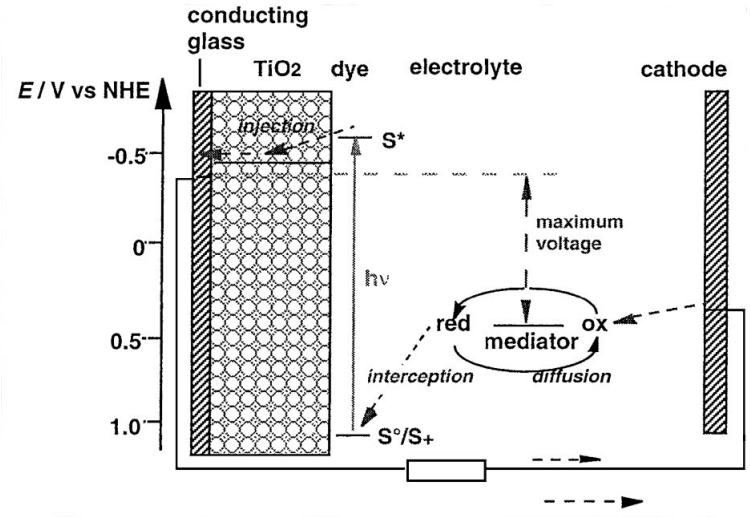

Figure 2.21: Schematic diagram of the structure and operation of a nanoporous Grätzel cell. The TiO_2 layer is fused to the anode and a redox reaction enables the cell to function. Current flow within the device is indicated by the dashed arrow at the bottom of the diagram. Taken from [73].

once spun cast, are dry, the Grätzel cell is wet. The structure of a Grätzel cell is shown in figure 2.21. The construction of such a cell is remarkably different to that of a monolayer device. The majority of the volume of the cell is made from nanocrystalline TiO_2 in anatase (sponge-like)

form. This structure forms a semi-rigid structure with a large surface area to volume ratio, ideal for efficient charge transfer. The TiO_2 film is spread onto the substrate (usually ITO coated glass) by doctor blade to create a layer a few micrometers thick [67]. This is then baked to form the anatase structure which is then soaked in the (usually, though not always) Ruthenium based dye, N3 [67, 74, 76, 77] (see figure 2.22). This process is known as sensitisation. The TiO_2 soaks up the dye which forms the light-absorbing material. The remaining contact can either be a metal (such as aluminium) or another layer of ITO coated glass. The cell will not work like this however as it relies upon a redox reaction to function. Upon light absorption the dye is oxidised, transferring its electrons to the TiO_2 layer. In order for the reaction to complete, the introduction of an electrolyte is necessary, making the cell 'wet'. This electrolyte (usually iodine based [74, 78]) is in turn oxidised by transferring an electron from itself to the dye. The redox reaction is completed by the transfer of an electron from the cathode to the electrolyte.

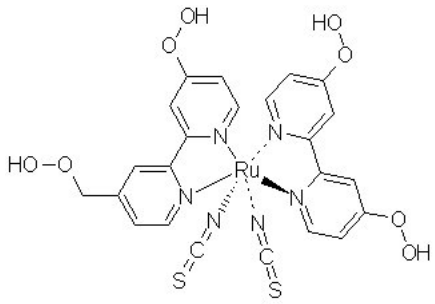

Figure 2.22: Molecular structure of the ruthenium dye, N3, used in the majority of dye-sensitised cells.

Despite the high efficiency of these devices, they are restricted in their use because of the inconvenience of the electrolyte. As it is liquid, the

cells are wet and thus encapsulation (and transport) is problematic. Cells can be regenerated should the electrolyte eventually evaporate, but this does not solve the encapsulation problem. To combat this, there has been considerable effort put into combining polymers with the TiO_2 structure [79–86]. This has not only the advantage of being 'dry', but also attempts to solve the poor charge transport properties of polymers. Since the porous structure has a large surface area there is considerable scope for charge transfer from the polymer to the nanoporous structure [87–89]. Since the transfer is efficient, device conversion efficiencies in excess of 3% have been reported [82, 86].

2.9 Summary

In this chapter the origin of semiconductivity in organic materials has been discussed including orbital interactions, bonding species and the origin of semiconductivity in organic materials. Device operation and material requirements have been described including exciton formation, charge separation and charge transport. The role of absorption and emission in devices has been discussed. Photoabsorption in organic materials has been described, resulting in the formation of excitons. Chemical defects and polarons have been described. Several common device structures have been introduced and their operation has been described. Intermolecular interactions such as dimers have been described. The role of synthetic chemistry in organic device design has been put forward and the subsequent nanoengineering necessary for molecular manipula-

tion has been detailed. The introduction of the dendrimer has been made as novel molecular design to incorporate processability, emission and absorption tuning and mobility control.

References

[1] C.M. Ramsdale, J.A Barker, A.C. Arias, J.D. MacKenzie, R.H. Friend, and N.C. Greenham, *Journal of Applied Physics* **92**, 4266 (2002).

[2] H.J. Snaith, N.C. Greenham, and R.H. Friend, *Advanced Materials* **16**, 1640 (2004).

[3] C.J. Brabec, A. Cravino, D. Meissner, N.S. Sariciftci, T. Fromherz, M.T. Rispens, L. Sanchez, and J.C. Hummelen, *Advanced Functional Materials* **11**, 374 (2001).

[4] C.J. Brabec, A. Cravino, D. Meissner, N.S. Sariciftci, M.T. Rispens, L. Sanchez, J.C. Hummelen, and T. Fromherz, *Thin Solid Films* **403-404**, 368 (2002).

[5] C. Winder, G. Matt, J.C. Hummelen, R.A.J. Janssen, N.S. Sariciftci,

and C.J. Brabec, *Thin Solid Films* **403-404**, 373 (2002).

[6] C.J. Brabec and N.S. Sariciftci, *Monatschefte fur Chemie Chemical Monthly* **132**, 421 (2001).

[7] H.W. Kroto, J.R. Heath, S.C. O'Brien, R.F. Curl, and R.E. Smalley, *Nature* **318**, 162 (1985).

[8] I.D.W. Samuel, *Philosophical Transactions of the Royal Society of London* **358**, 193 (2000).

[9] M. Pope and C.E. Swenberg, *Electronic Processes in Organic Crystals and Polymers*, Oxford Science Publications, UK, 1999.

[10] *http://www.fhi-berlin.mpg.de/th/personal/hermann/diamond-lat.gif*.

[11] P. Wood, *Conformational Disorder and the Degree of Conjugation in Conjugated Polymers*, PhD thesis, University of St. Andrews, 2002.

[12] P.W. Atkins, *Molecular Quantum Mechanics*, chapter 10, p. 275, Oxford University Press, 1983.

[13] A.J. Heeger, S. Kivelson, J.R. Schrieffer, and W.P. Su, *Reviews of Modern Physics* **60**, 781 (1988).

[14] J. Frenkel, *Physical Review* **37**, 1276 (1931).

[15] R. Peierls, *Annals of Physics* **13**, 905 (1932).

[16] G.H. Wannier, *Physical Review* **52**, 191 (1937).

[17] M. Halim, *Light Emission From Conjugated Dendrimers and Polymers*, PhD thesis, University of Durham, 1999.

[18] A. Ruseckas, Private Communication.

[19] I.D.W. Samuel, G. Rumbles, and R.H. Friend, *Primary Photoexcitations in Conjugated Polymers: Molecular Exciton versus Semiconductor Band Model*, chapter 7, pp. 140–173, World Scientific Publishing Company, 1998.

[20] J.P.J. Markham, *Highly Efficient Dendrimers and Polymers for Solution Processed Organic Light Emitting Diodes*, PhD thesis, University of St. Andrews, 2003.

[21] *http://hackman.mit.edu/6977/handouts/6.977.lecture.7.pdf*.

[22] B. Stevens and E. Hutton, *Nature* **186**, 1045 (1960).

[23] H. Shirakawa, E.J. Louis, A.G. MacDiarmid, C.K. Chang, and A.J. Heeger, *Journal of the American Chemical Society: Chemical Com-*

munications **16**, 578 (1977).

[24] K. Seki, S. Asada, T. Mori, H. Inokuchi, I. Murase, T. Ohnishi, and T. Noguchi, *Solid State Communications* **74**, 677 (1990).

[25] N. Sato, M. Logdlund, R. Lazzaroni, W.R. Salaneck, J.L. Bredas, D.C.C. Bradley, R.H. Friend, and K.E. Ziemelis, *Chemical Physics* **160**, 299 (1992).

[26] C.J. Brabec, N.S. Sariciftci, and J.C. Hummelen, *Advanced Functional Materials* **11**, 15 (2001).

[27] S. Alem, R. deBettignies, J.M. Nunzi, and M. Cariou, *Applied Physics Letters* **84**, 2178 (2004).

[28] J.J. Dittmer, K. Petritsch, E.A. Marseglia, R.H. Friend, H. Rost, and A.B. Holmes, *Synthetic Metals* **102**, 879 (1999).

[29] R.H. Friend, R.W. Gymer, A.B. Holmes, J.H. Burroughes, R.N. Marks, C. Taliani, D.D.C. Bradley, D.A. Dos Santos, J.L. Bredas, M. Logdlund, and W.R. Salaneck, *Nature* **397**, 121 (1999).

[30] H. Kim, Y. Kim, S.H. Park, K. Lee, Y. Jin, J. Kim, and H. Suh, *Applied Physics Letters* **86** (2005).

[31] S.H. Kwon, S.Y. Paik, and J.S. Yoo, *Synthetic Metals* **130**, 55 (2002).

[32] T. Martens, J.D'Haen, T. Munters, Z. Beelen, L. Goris, J. Manca, M. D'Olieslaeger, D. Vanderzande, L. DeSchepper, and R. Andriessen, *Synthetic Metals* **138**, 243 (2003).

[33] C. Winder, C. Lungenschmied, G. Matt, N.S. Sariciftci, A.F. Nogueira, I. Montanari, J.R. Durrant, C. Arndt, U. Zhokhavets, and G. Gobsch, *Synthetic Metals* **139**, 577 (2003).

[34] J.K.J. van Duren, V.D. Mihailetchi, P.W.M. Blom, T. van Woudenbergh, J.C. Hummelen, M.T. Rispens, R.A.J. Janssen, and M.M. Wienk, *Journal of Applied Physics* **94**, 4477 (2003).

[35] E.A. Katz, D. Faiman, S.M. Tuladhar, J.M. Kroon, M.M. Wienk, T. Fromherz, F. Padinger, C.J. Brabec, and N.S. Sariciftci, *Journal of Applied Physics* **90**, 5343 (2001).

[36] M. Svensson, F. Zhang, S.C. Veenstra, W.J.H. Verhees, J.C. Hummelen, J.M. Kroon, O. Inganäs, and M.R. Andersson, *Advanced Materials* **15**, 988 (2003).

[37] F. Padinger, T. Fromherz, P. Denk, C.J. Brabec, J. Zettner, T. Hierl, and N.S. Sariciftci, *Synthetic Metals* **121**, 1605 (2001).

[38] H. Neugebauer, C. Brabec, J.C. Hummelen, and N.S. Sariciftci, *Solar Energy Materials and Solar Cells* **61**, 35 (2000).

[39] C.J. Brabec, S.E. Shaheen, C. Winder, N.S. Sariciftci, and P. Denk, *Applied Physics Letters* **80**, 1288 (2002).

[40] C.J. Brabec, S.E. Shaheen, T. Fromherz, F. Padinger, J.C. Hummelen, A. Dhanabalan, R.A.J. Janssen, and N.S. Sariciftci, *Synthetic Metals* **121**, 1517 (2001).

[41] T. Fromherz, F. Padinger, D. Gebeyehu, C. Brabec, J.C. Hummelen, and N.S. Sariciftci, *Solar Energy Materials and Solar Cells* **63**, 61 (2000).

[42] M.T. Rispens, A. Meetsma, R. Rittberger, C.J. Brabec, N.S. Sariciftci, and J.C. Hummelen, *Chemistry Communications* , 2116 (2003).

[43] C.J. Brabec, F. Padinger, J.C. Hummelen, R.A.J. Janssen, and N.S. Sariciftci, *Synthetic Metals* **102**, 861 (1999).

[44] V. Dyakonov, D. Godovsky, J. Meyer, J. Parisi, C.J. Brabec, N.S. Sariciftci, and J.C. Hummelen, *Synthetic Metals* **124**, 103 (2001).

[45] D. Muhlbacher, C.J. Brabec, N.S. Sariciftci, B.V. Kotov, V.I. Berendyaev, B.M. Rumyantsev, and J.C. Hummelen, *Synthetic Metals* **121**, 1609 (2001).

[46] L. Goris, M.A. Loi, A Cravino, H. Neugebauer, N.S. Sariciftci,

I. Polec, L. Lutsen, E. Andries, J. Manca, L. DeSchepper, and D. Vanderzande, *Synthetic Metals* **138**, 249 (2003).

[47] V. Dyakonov, *Applied Physics A* **79**, 21 (2004).

[48] M. Al-Ibrahim, H.Klaus Roth, U. Zhokhavets, G. Gobsch, and S. Sensfuss, *Solar Energy Materials and Solar Cells* **85**, 13 (2005).

[49] D. Chirvase, Z. Chiguvare, M. Knipper, J. Parisi, V. Dyakonov, and J.C. Hummelen, *Journal of Applied Physics* **93**, 3376 (2003).

[50] H. Frohne, S.E. Shaheen, C.J. Brabec, D.C. Mullen, N.S. Sariciftci, and K. Meerholz, *A European Journal of Chemical Physics and Physical Chemistry* **9**, 795 (2002).

[51] R.A.J. Janssen, J.C. Hummelen, and N.S. Sariciftci, *Materials Research Society Bulletin* **30**, 33 (2005).

[52] S.E. Shaheen, C.J. Brabec, N.S. Sariciftci, F. Padinger, T. Fromherz, and J.C. Hummelen, *Applied Physics Letters* **78**, 841 (2001).

[53] M. Stoessel, G. Wittmann, J. Staudigel, J. Blassing, W. Roth, H. Klausmann, W. Rogler, J. Simmerer, A. Winnacker, M. Inbasekaran, and E.P. Woo, *Journal of Applied Physics* **87**, 4467 (2000).

[54] A.C. Arias, J.D. MacKenzie, R. Stevenson, J.J.M. Halls, M. Inbasekaran, E.P. Woo, D. Richards, and R.H. Friend, *Macromolecules* **34**, 6005 (2001).

[55] D. Chirvase, Z. Chiguvare, M. Knipper, J. Parisi, V. Dyakonov, and J.C. Hummelen, *Synthetic Metals* **138**, 299 (2003).

[56] V.R. Nikitenko, H. Heil, and H. von Seggern, *Journal of Applied Physics* **94**, 2480 (2003).

[57] Z. Chiguvare, J. Parisi, and V. Dyakonov, *Journal of Applied Physics* **94**, 2440 (2003).

[58] M. Halim, J.N.G. Pillow, I.D.W. Samuel, and P.L. Burn, *Advanced Materials* **11**, 371 (1999).

[59] S.C. Lo, N.A.H. Male, J.P.J. Markham, S.W. Magennis, P.L. Burn, O.V. Salata, and I.D.W. Samuel, *Advanced Materials* **14**, 975 (2002).

[60] M. Halim, J.N.G. Pillow, I.D.W. Samuel, and P.L. Burn, *Synthetic Metals* **102**, 1113 (1999).

[61] J.M. Lupton, I.D.W. Samuel, R. Beavington, P.L. Burn, and H. Bassler, *Advanced Materials* **13**, 258 (2001).

[62] M.J. Frampton, S.W. Magennis, J.N.G. Pillow, P.L. Burn, and I.D.W.

Samuel, *Journal of Materials Chemistry* **13**, 235 (2003).

[63] J.N.G. Pillow, M. Halim, I.D.W. Samuel, and P.L. Burn, *Macromolecules* **32**, 5985 (1999).

[64] B.A. Gregg, *Journal of Physical Chemistry B* **107**, 4688 (2003).

[65] M.A. Green, *Physica E* **14**, 11 (2002).

[66] B.A. Gregg and M.C. Hanna, *Journal of Applied Physics* **93**, 3605 (2003).

[67] M.K. Nazeeruddin, A. Kay, I. Rodicio, R. Humphry-Baker, E. Muller, P. Liska, N. Vlachopolous, and M. Grätzel, *Journal of the American Chemical Society* **115**, 6382 (1993).

[68] B.A Gregg, J. Sprague, and M.W. Peterson, *Journal of Physical Chemistry B* **101**, 5362 (1997).

[69] J.J.M. Halls, K. Pichler, R.H. Friend, S.C. Moratti, and A.B. Holmes, *Applied Physics Letters* **68**, 3120 (1996).

[70] D. Moses, J. Wang, A.J. Heeger, N. Kirova, and S. Brazovski, *Proceedings of the National Association of Sciences of the USA* **98**, 13496 (2001).

[71] T. Stubinger and W. Brutting, *Journal of Applied Physics* **90**, 3632 (2001).

[72] J.P.J. Markham, S.C. Lo, S.W. Magennis, P.L. Burn, and I.D.W. Samuel, *Applied Physics Letters* **80**, 2645 (2002).

[73] M. Grätzel, *Journal of Sol-Gel Science and Technology* **22**, 7 (2001).

[74] A. Hagfeldt and M. Grätzel, *Accounts of Chemical Research* **33**, 269 (2000).

[75] M. Grätzel, *Pure Applied Chemistry* **73**, 459 (2001).

[76] S.K. Deb, R. Ellingson, S. Ferrere, A.J. Frank, B.A. Gregg, A.J. Nozik, N. Park, and G. Schlichthorl, Photochemical Solar Cells Based on Dye-Sensitization of Nanocrystalline TiO_2, in *2^{nd} World Conference and Exhibition on Photovoltaic Solar Energy Conversion*, 1998.

[77] P. Wang, S.M. Zakeeruddin, J.E. Moser, M.K. Nazeeruddin, T. Sekiguchi, and M. Grätzel, *Nature Materials* **2**, 402 (2003).

[78] Y. Liu, A. Hagfeldt, X.R. Xiao, and S.E. Lindquist, *Solar Energy Materials and Solar Cells* **55**, 267 (1998).

[79] S. Spiekermann, G. Smestad, J. Kowalik, and L.M. Tolbert amd

M. Grätzel, *Synthetic Metals* **121**, 1603 (2001).

[80] C.D. Grant, A.M. Schwartzberg, G.P. Smestad, J. Kowalik, L.M. Tolbert, and J.Z. Zhang, *Journal of Electroanalytical Chemistry* **522**, 40 (2002).

[81] C.D. Grant, A.M. Schwartzberg, G.P. Smestad, J. Kowalik, L.M. Tolbert, and J.Z. Zhang, *Synthetic Metals* **132**, 197 (2003).

[82] A.C. Arango, L.R. Johnson, V.N. Bliznyuk, Z. Schlesinger, S.A. Carter, and H.H. Horhold, *Advanced Materials* **12**, 1689 (2000).

[83] B. van der Zanden, A. Goossens, and J. Schoonman, *Synthetic Metals* **121**, 1601 (2001).

[84] K.M. Coakley, Y. Liu, M.D. McGehee, K.L Frindell, and G.D. Stucky, *Advanced Functional Materials* **13**, 301 (2003).

[85] T.J. Savenije, J.M. Warman, and A. Goossens, *Chemical Physics Letters* **287**, 148 (1998).

[86] K.M. Coakley and M.D. McGehee, *Applied Physics Letters* **83**, 3380 (2003).

[87] A.C. Arango, S.A. Carter, and P.J. Brock, *Applied Physics Letters* **74**, 1698 (1999).

[88] P.A. van Hal, M.P.T. Christiaans, M.M. Wienk, J.M. Kroon, and R.A.J. Janssen, *Journal of Physical Chemistry B* **103**, 4352 (1999).

[89] N.A. Anderson, E. Hao, X. Ai, G. Hastings, and T. Lian, *Chemical Physics Letters* **347**, 304 (2001).

Chapter 3

Experimental Methods

3.1 Introduction

This chapter will detail the experimental techniques and methods employed to characterise the materials used to make solar cells within this thesis. The processing of organic semiconductors is one of the main advantages of these materials as it is quick and relatively simple. Material consumption is low, typically only using milligrams when making a solution. The entire process from spin-coating onto a substrate to metal cathode deposition using thermal evaporation will be described here as will the testing procedures that follow fabrication. Time-resolved luminescence (TRL) methods will be explained and the operation of appropriate equipment, for example the Streak Camera, will be described. Photophysical measurements are discussed here including Photoluminescence

Quantum Yield (PLQY).

3.2 Material Preparation

Materials used in this work can be broken down into three categories. These are soluble polymers, soluble dendrimers and precursor polymers. Preparation of each of these will be discussed in turn.

3.2.1 Soluble Polymers and Dendrimers

One of the first common conjugated polymers was PPV. The biggest inconvenience of this polymer is that, like many of the conjugated polymers, it is rigid and insoluble. This can be overcome by two methods. The first is the addition of solublising side groups to the chain backbone allowed it to be dissolved in common solvents. Two common PPV-derivatives that are soluble are MEH-PPV and OC_1C_{10}-PPV. The second is the use of precursor polymers, which will be discussed in section 3.2.2. In order to make a solution, a small amount of solid polymer (of order mg) was allowed to dissolve in a chosen solvent, usually chlorobenzene. The solutions were sirred in all cases to ensure complete dissolution. Dissolving was performed at room temperature. Dissolution time varies with molecular weight and number of solubilising groups. Once a solution is made it can be simply spin-coated onto a chosen sub-

strate. Polymers generally form more viscous solutions as they have relatively higher molecular weights. Viscosity can be controlled by altering the concentration of the solution. Due to the varying types of polymers characterised, the amount of polymer used varied according to molecular weight. Typically, concentrations of approximately 5 mg/ml were used for device work based on polymers. See chapters 4 and 6 for full details. Concentrations used were chosen to provide the film thickness required. The dissolving procedure was identical in every case for all polymers used. This involved weighing out the desired weight of material, transferring it to a sample bottle, adding the desired volume of chosen solvent via pipette and then adding a magnetic follower. This ensured good, thorough stirring of the solution.

Dendrimer materials are much lower molecular weights and so in order to be able to spin a good quality film with reasonable thickness for a device, typically of order 60 nm or more, then 20 mg/ml of material was used. This is due to lower viscosity of the resulting solution compared to that of polymers. There were several dendrimer materials used in this work but all were of similar molecular weight ($M_w \sim 2000$) so concentrations were kept constant. The dendrimer materials used and results gained from them are described in chapter 5.

Organic PVs based on bulk heterostructures need to be fabricated using blends of two or more materials, which are described in section 2.8.3. A blend is a mixture of two or more materials in the same solution. Typically blends were made up of organic semiconductor (polymer or dendrimer) combined with an electron accepting material. In the majority of

cases the electron accepting material was [6,6]-phenyl-C_{61}-butyric-acid methyl ester, [6,6]PCBM (see figure 3.1). [6,6]PCBM is a derivative of

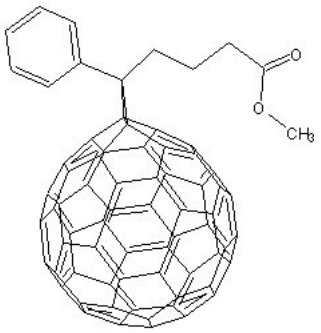

Figure 3.1: Molecular structure of [6,6]PCBM.

C_{60} and has been functionalised in order to increase charge separation properties and also to improve solubility. It is widely used within organic solar cell devices [1–25]. In the case of polymer blends, ratios of polymer:PCBM were typically 1:4 by weight (usually 5:20 mg/ml) and 1:2 for dendrimers.

3.2.2 Precursors

As mentioned in section 3.2.1, there is more than one way to produce a conjugated polymer film. The first has been described, involving soluble conjugated polymer spun from solution. However, not all polymers will dissolve due to a lack of solubilising groups. A solution to this problem is to use a soluble precursor polymer [1, 26, 27]. These materials were first introduced to combat the insolubility problem by Greenham and Friend [28, 29].

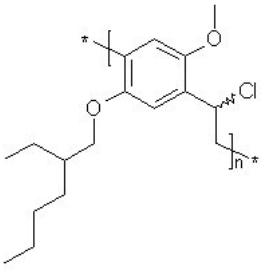

(a) Molecular structure of Chloro precursor of MEH-PPV.

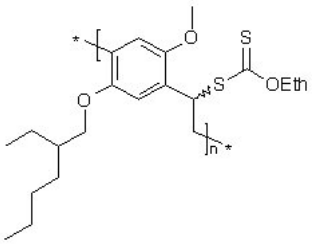

(b) Molecular structure of Xanthate precursor of MEH-PPV.

Figure 3.2: Structures of two precursor polymers used in this thesis. The side groups solublise the polymer and are removed when heated under vacuum.

Precursor polymers are structurally very similar to their soluble counterparts but lacking the solublising side groups. In order for them to be soluble, they are non-conjugated and possess a removable solubilising group. In this work they were either chloro groups (a single chlorine atom) or xanthate groups (a sulphur based group). Both of these variants are shown in figure 3.2. To remove this side group and conjugate the polymer, thermal conversion is needed. During this process the side group leaves the polymer chain as shown in figure 3.3. When this occurs, the leaving group also removes a hydrogen atom from the neighbouring carbon atom to which it was bonded. This leaves behind a vinylene (double bond) linkage on the chain and creates the conjugation required.

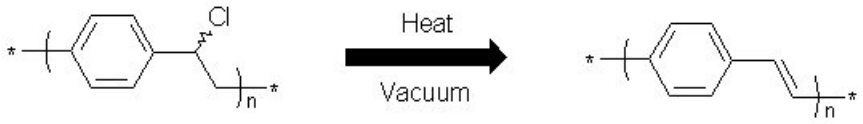

Figure 3.3: The thermal conversion of a precursor polymer. Upon heating, the side group leaves the backbone leaving a vinylene linkage behind.

The solution was spun cast onto substrates and placed in an evacuated (2×10^{-3} mbar) oven and baked for an extended period. The temperature of this bake depended upon the side group. For chloro group removal the conversions were performed at 130°C, the xanthate groups required higher temperatures, performed at 230°C. All conversions were performed over eight hours. An advantage of using a precursor material enables the fabrication of multilayered devices using several polymer materials. A second layer could be spun on top of a converted precursor (which is insoluble) without interdissolving occurring.

3.3 Absorption and Fluorescence Measurements

The absorption of light is one of the key processes within solar cells so it is one of the most useful measurements taken during characterisation. It can tell us a significant amount of information about which parts of a molecule absorb which wavelengths of light and by how much. This is essential information when designing molecules for PV applications. Simply by varying a side group on a polymer, for example, can have dramatic effects upon the absorbing properties of the molecule. Such differences are discussed in chapter 4.

Absorbance was directly measured on organic films using a Varian Cary-300 UV-Vis Spectrophotometer. This was a straightforward measurement using two identical substrates, one with the organic film on, the other kept clean and used as a reference. This way, samples could be

on varying substrates but only the absorbance of the film would be measured. A baseline scan was taken before samples were measured using two blank substrates. Absorbance (optical density) is calculated by comparing the measurement beam to the reference beam. Both samples are illuminated with the same intensity. The sample beam will be dimmer (assuming absorption has occurred) than the reference beam when compared. The spectrometer measures transmission, given as

$$T = \frac{I_{sample}}{I_{ref}} \tag{3.1}$$

where I_{sample} is the light intensity measured through the sample and I_{ref} is the intensity after the reference. Absorption of the sample films is then calculated by using the relation

$$A = -\log(T) \tag{3.2}$$

where A is the absorbance of the film. Reflection is not accounted for in the absorbance measurements. Since the refractive index for a sample is higher than that of air, there will be no accounting for the reflection caused by the interface between organic material and the substrate. The instrument correction only allows for reflection at a clean substrate/air interface.

For a quartz substrate reflection losses are approximately 4% per surface at normal incidence. Reflection losses are dependent heavily upon the materials at the interfaces due to the differing refractive indexes of the organic layers. For most of the organic materials used in this work the refractive index, n, is unknown. For approximations, unless otherwise

stated, n for organic layers will be assumed to be 1.8 for all wavelengths. This is comparable to MEH-PPV [30].

Photoluminescence (PL) measurements were performed using a Jobin-Yvon Fluoromax 2 fluorimeter. Samples were illuminated with a monochromated Xenon source and the emission was recorded through another monochromator by a photomultiplier tube in photon counting mode. Readings were subsequently corrected for the quantum efficiency of the photomultiplier tube within the spectrometer (correction supplied by Jobin-Yvon). It is desired that photovoltaic materials should not fluoresce as this is an energy loss mechanism.

3.4 PLQY

The photoluminescence quantum yield (PLQY) is defined as

$$\Phi = \frac{number\ of\ photons\ emitted}{number\ of\ photons\ absorbed} \tag{3.3}$$

PLQY measurements were performed using an integrating sphere [31, 32]. An integrating sphere is a hollow sphere internally coated in a highly reflective but diffusing material. The light output at one aperture of the sphere is proportional to the total light produced by a sample within the sphere. The PLQY gives an upper limit on the EL efficiency within an organic layer [31]. PLQY measurements are performed primarily for emissive materials but it is also a useful measurement for PV

materials. For emissive purposes, such as LEDs, a high PLQY is desired. The opposite is true for photovoltaics. Light emitted after absorption will provide a loss mechanism for such devices and is therefore undesirable. In this case a low PLQY is desired.

Organic samples were spin coated onto quartz disks of diameter 12 mm. Samples were made with suitable thickness to achieve optical densities of >0.3. This enabled a significant amount of absorption ($>50\%$) to ensure a large fraction of the absorbed photons are measured accurately. Samples were illuminated by approximately 0.05 mW of laser light. Unless otherwise stated, all PLQY measurements used a laser excitation wavelength of 488 nm. Samples placed in the integrating sphere were under a nitrogen flow to prevent oxidation of the films.

3.5 Time-Resolved Luminescence

Time-resolved luminescence (TRL) measurements were carried out in order to investigate exciton dynamics within polymers and the results and discussion are presented in chapter 6. Samples were illuminated (kept under vacuum, $\sim 2\times10^{-5}$ mbar) with a frequency doubled output of a Ti:Sapphire femtosecond laser (800 nm doubled to 400 nm) and the emission was resolved by a Hamamatsu streak camera, see section 3.5.1. Figure 3.4 shows a schematic for the experimental setup. Chapter 6 describes two experimental methods requiring TRL; exciton diffusion to an interface and exciton-exciton annihilation.

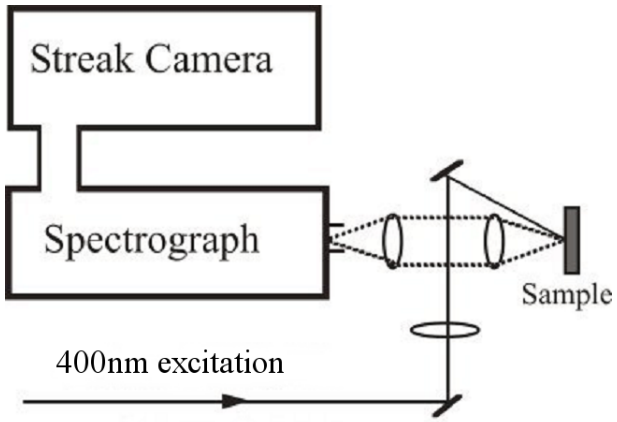

Figure 3.4: Experimental setup for time-resolved luminescence experiments.

3.5.1 Streak Camera

A streak camera enables time-resolved measurements to be taken. The operation of a streak camera is shown in figure 3.5. Light emitted from

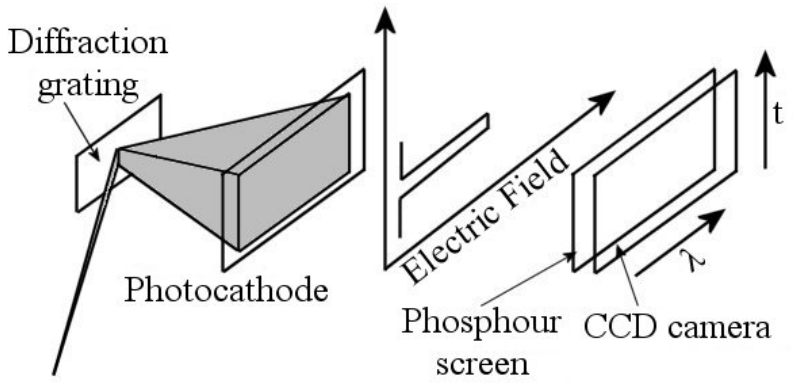

Figure 3.5: Schematic of the operation of a streak camera. Adapted from [33].

a sample is dispersed by a spectrograph and is then incident upon a photocathode where it is converted into electrons. These electrons are then accelerated by a scanning electric field along the streak tube. These

electrons hit a phosphor screen and the photons emitted by this are detected by a CCD camera. The time resolution of the streak camera was $\sim$ 1-2 ps and originates from the electric field scanning up and down the tube. This causes the electrons to be accelerated and strike the anode at different positions. From this we get a 2D image of the intensity containing both temporal and spectral information.

3.5.2 Lifetime measurement

Once a streak camera image was obtained, the fluorescence lifetime was calculated by first integrating across the spectral window. This decay

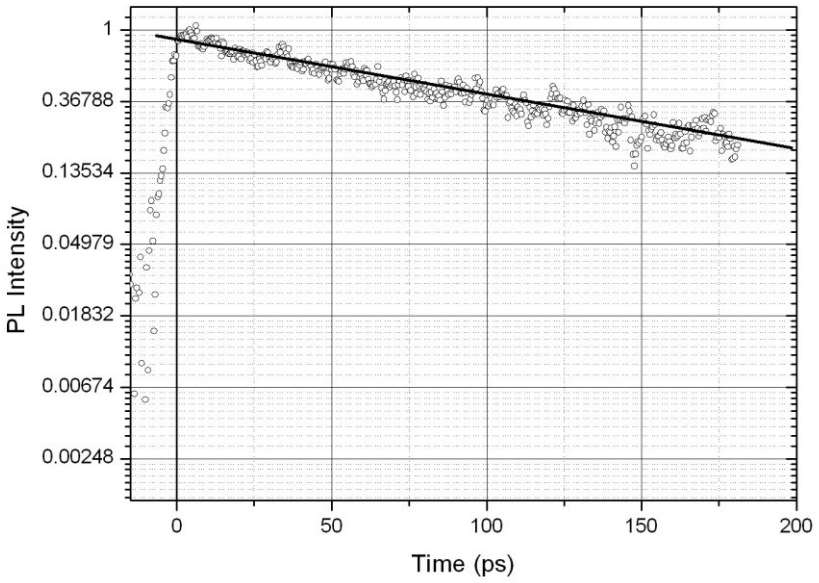

Figure 3.6: Typical lifetime curve for MEH-PPV. Sample was illuminated at 400 nm with 40 μW at 50 kHz.

curve was normalised to the peak of the output. 'Time zero' is placed at the point on the rise of the curve where the (normalised) intensity is equal to 0.5. A typical output is shown in figure 3.6. Once the curve has been aligned properly, the lifetime, τ, is then calculated by fitting an monoexponential or biexponential decay. Using a logarithmic scale (base e) the decay curve, assuming no quenching, should be a straight line. The lifetime is then found at the point where this line falls to $1/e$ of the peak. This is the lifetime discussed in section 2.5.

3.6 Device Fabrication

Device fabrication can be broken down into several parts. These are: substrate preparation, active layer (which includes anode preparation) deposition and finally, contact evaporation. Each of these will be discussed in turn.

3.6.1 Substrate Preparation

Substrates were prepared using Indium Tin Oxide (ITO) coated glass cut into 12 mm squares. These were then etched using concentrated hydrochloric acid (HCl, 37%). The etching was achieved by covering the required area, a central strip 4 mm wide, with tape extending beyond the edges of the substrate. Once prepared, the substrate was placed into

a bath of HCl for approximately 10 minutes to allow the bare ITO to be etched off. After etching had occurred, the substrates were washed briefly in excess cold water to remove the acid. Substrates were then dried in nitrogen. To clean the substrates, they were immersed in Acetone and ultrasonicated for 12 minutes. They were then dried in nitrogen. The process was repeated using Isopropyl Alcohol (IPA) for a further 12 minutes. Substrates were then dried in nitrogen. If needed, substrates were then ashed in oxygen for six minutes at $\sim 10^{-2}$ mbar.

3.6.2 Active Layer Preparation

The active layer(s) of the device are the simplest to prepare. Before this layer was made, the anode was prepared. After substrate preparation, a dual layer of poly[3,4-ethylene-dioxy-thiophene]:poly[4-styrene-sulphonate] (PEDOT:PSS, Baytron-P) was spun at 2000 rpm onto the ITO. This ensured a good covering of the anode and enabled good wetting of the substrate due to PEDOT smoothing the ITO roughness. PEDOT thickness was $\sim$ 60 nm. Once spun, the PEDOT was allowed to dry in air for 15 minutes. The active layer was then spun onto the PEDOT layer, spin speeds varied depending upon desired film thickness but were usually 1600 rpm for devices. This gave an active layer of $\sim$ 80-100 nm for polymers and $\sim$ 60 nm for dendrimer films. Films were then placed into an evaporator immediately after spinning to ensure as little degradation as possible. PEDOT was used in all devices fabricated from a polymer as it smooths the substrate and provides a more stable anode. PEDOT was also used in all dendrimer devices, unless otherwise stated.

3.6.3 Contact Evaporation

Thermal evaporation was performed at 1×10^{-6} mbar. Calcium was evaporated onto the active layer at 0.1 nm/s to give a thickness of 10 nm. Aluminium contacts were then evaporated at 0.3 nm/s to give a thickness of 100 nm. Devices were then left to cool before removal and testing. A schematic of a typical device is shown in figure 3.7. Contacts were 2 mm wide, producing devices 4×2 mm to provide and active area of 8 mm^2. Each substrate had four devices on, as shown in figure 3.7(b).

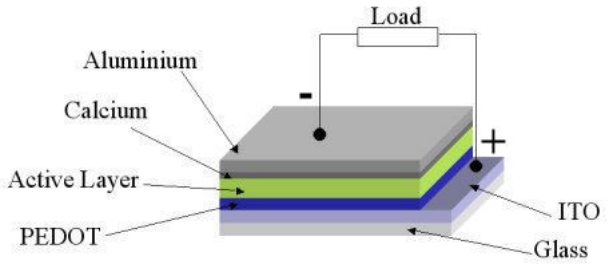

(a) Schematic of a typical organic PV device.

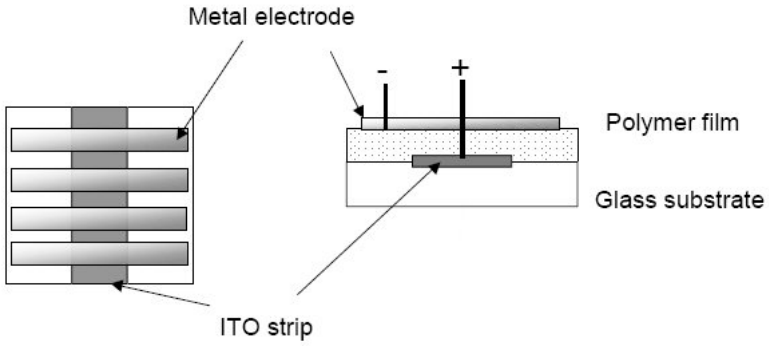

(b) Schematic showing contact arrangement within a typical device. Adapted from [34].

Figure 3.7: Schematics showing device structure and contacts. Not to scale.

3.7 Electrical Characterisation

Characterisation of a device is the final step in assessing the usefulness of a material for PV applications. Testing devices is necessary to see if any of the characterisitics, such as film thickness, material properties or device structure, affect the device significantly. When optimising devices, there are many factors that can be varied. These include film thickness, contact thickness, contact metal(s) and also anode properties. The ashing of the ITO anode, for example, will change the work function of this material, changing the effectiveness of the device.

This section will describe the processes and techniques involved in the final testing procedures. Aside from photophysical measurements, all characterisation performed was electrical. This characterisation falls into two primary types; broadband (solar) testing and monchromatic testing. These will each be described in turn.

3.7.1 Solar Simulator Characterisation

Device testing to calculate the energy conversion efficiency, η, was performed under a solar simulator, purchased from KHS, Germany. Output was A.M. 1.5 (global) at 100 mW/cm^2. The output spectrum of the simulator is shown in figure 3.8. It should be noted that the simulator output extends beyond that shown here, but the useful light is within the region displayed, since this is where the materials tested absorbed light.

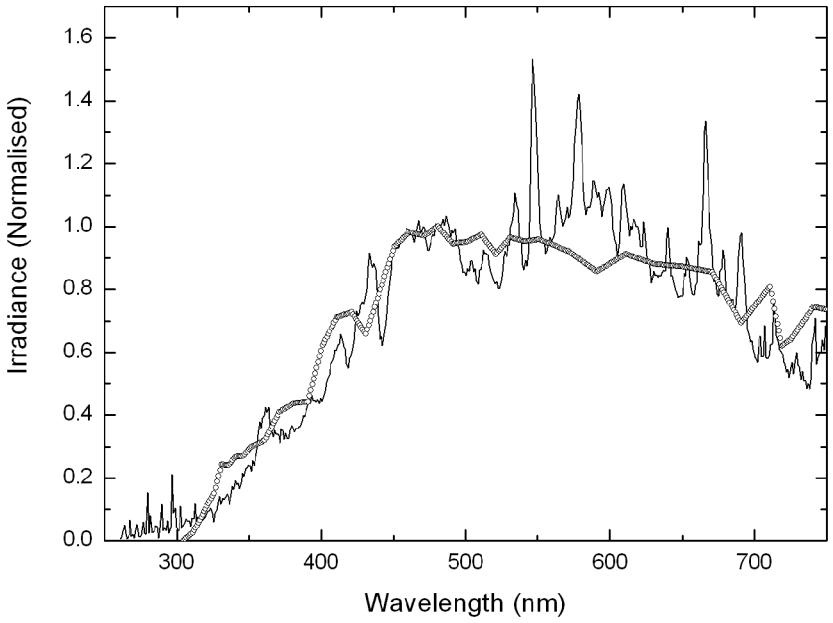

Figure 3.8: Spectrum of the Solar Simulator output (solid line) and the A.M. 1.5 Solar Spectrum (open circles).

Devices were placed in a holder with sprung-loaded contacts to ensure a good contact and also to ensure that the aluminium cathode was not damaged during testing. This holder was then placed in a chamber and evacuated to $\sim 10^{-5}$ mbar. The testing chamber is shown in figure 3.9. Devices were tested individually by placing a voltage across the device and measuring the current generated by the light. Typically the voltage applied ranged from -2 to +2 V. The time between each voltage step was typically 200 ms, with each step being 0.02 V. Results are shown in chapters 4 and 5.

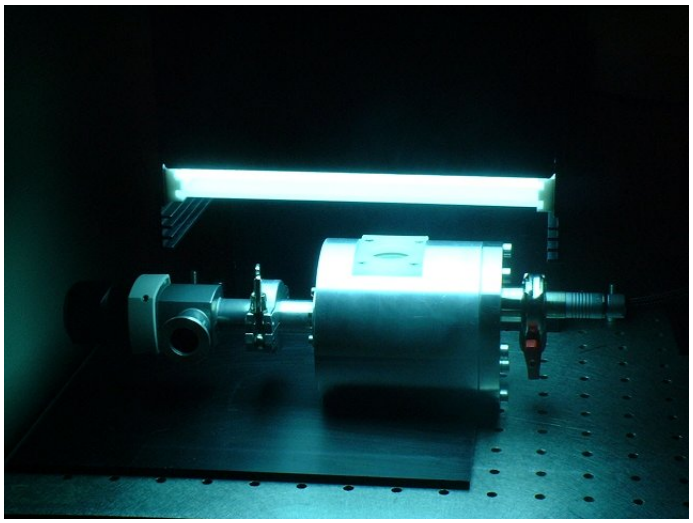

Figure 3.9: Sample chamber illuminated under the solar simulator.

3.7.2 IPCE and APCE Measurements

To test the Incident Photon to Conducted Electron (IPCE) efficiency of the cells, they were each tested under monochromatic light. Using a Xenon lamp source, cells were illuminated with light from 300 to 800 nm in steps of 1 nm. The experimental setup is shown in figure 3.10. The photocurrent generated at 0 V was then recorded. The power at each wavelength was calculated by first illuminating an NPL calibrated photodiode placed where the sample would be. Simultaneously, another photodiode was placed near a quartz window, to capture a small fraction of light reflected from this window. The readings from both photodiodes were recorded. By using the current generated by the NPL photodiode it was possible to calculate the monochromatic power for each wavelength. This way, by using the reference photodiode, the exact power incident on the sample was known for each wavelength.

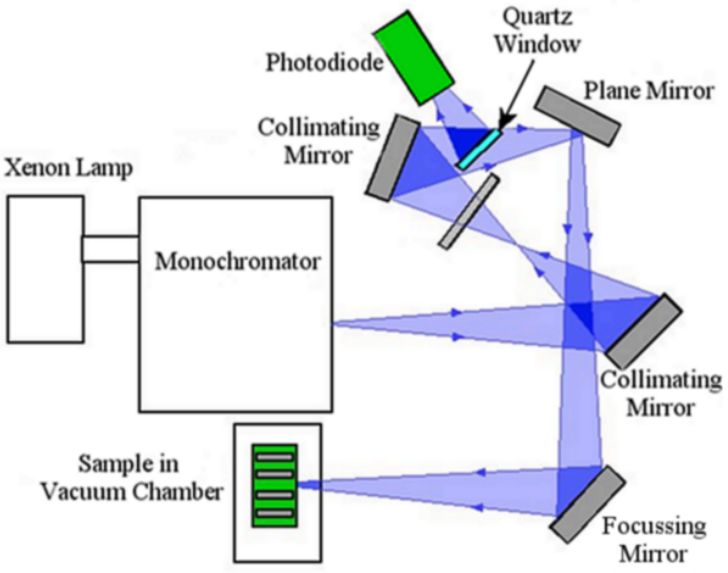

Figure 3.10: Schematic of the IPCE setup. Light was collimated because it was highly divergent emerging from the monochromator.

3.8 Summary

This chapter has detailed the experimental procedures used in this work. The preparation of materials has been described, including the preparation of precursor polymers. For devices, the cleaning and preparation of substrates has been described, going on to device fabrication techniques and finally contact evaporation. Experimental characterisation techniques have also been described, including absorption and fluorescence measurements, TRL experiments and PLQY measurements. The operation and use of experimental equipment such as a Streak Camera has been described. Measurement techniques have been given presenting sample results where appropriate. All of these techniques are used in the work presented in this thesis.

References

[1] T. Munters, T. Martens, L. Goris, V. Vrindts, J. Manca, L. Lutsen, W. DeCeuninck, D. Vanderzande, L. DeSchepper, J. Gelan, N.S. Sariciftci, and C.J. Brabec, *Thin Solid Films* **403-404**, 247 (2002).

[2] E.A. Katz, D. Faiman, S.M. Tuladhar, J.M. Kroon, M.M. Wienk, T. Fromherz, F. Padinger, C.J. Brabec, and N.S. Sariciftci, *Journal of Applied Physics* **90**, 5343 (2001).

[3] M. Svensson, F. Zhang, S.C. Veenstra, W.J.H. Verhees, J.C. Hummelen, J.M. Kroon, O. Inganäs, and M.R. Andersson, *Advanced Materials* **15**, 988 (2003).

[4] C. Winder, G. Matt, J.C. Hummelen, R.A.J. Janssen, N.S. Sariciftci, and C.J. Brabec, *Thin Solid Films* **403-404**, 373 (2002).

[5] F. Padinger, T. Fromherz, P. Denk, C.J. Brabec, J. Zettner, T. Hierl,

and N.S. Sariciftci, *Synthetic Metals* **121**, 1605 (2001).

[6] H. Neugebauer, C. Brabec, J.C. Hummelen, and N.S. Sariciftci, *Solar Energy Materials and Solar Cells* **61**, 35 (2000).

[7] C.J. Brabec, S.E. Shaheen, C. Winder, N.S. Sariciftci, and P. Denk, *Applied Physics Letters* **80**, 1288 (2002).

[8] C.J. Brabec, S.E. Shaheen, T. Fromherz, F. Padinger, J.C. Hummelen, A. Dhanabalan, R.A.J. Janssen, and N.S. Sariciftci, *Synthetic Metals* **121**, 1517 (2001).

[9] C.J. Brabec and N.S. Sariciftci, *Monatschefte fur Chemie Chemical Monthly* **132**, 421 (2001).

[10] T. Fromherz, F. Padinger, D. Gebeyehu, C. Brabec, J.C. Hummelen, and N.S. Sariciftci, *Solar Energy Materials and Solar Cells* **63**, 61 (2000).

[11] M.T. Rispens, A. Meetsma, R. Rittberger, C.J. Brabec, N.S. Sariciftci, and J.C. Hummelen, *Chemistry Communications* , 2116 (2003).

[12] C.J. Brabec, F. Padinger, J.C. Hummelen, R.A.J. Janssen, and N.S. Sariciftci, *Synthetic Metals* **102**, 861 (1999).

[13] V. Dyakonov, D. Godovsky, J. Meyer, J. Parisi, C.J. Brabec, N.S. Sariciftci, and J.C. Hummelen, *Synthetic Metals* **124**, 103 (2001).

[14] D. Muhlbacher, C.J. Brabec, N.S. Sariciftci, B.V. Kotov, V.I. Berendyaev, B.M. Rumyantsev, and J.C. Hummelen, *Synthetic Metals* **121**, 1609 (2001).

[15] L. Goris, M.A. Loi, A Cravino, H. Neugebauer, N.S. Sariciftci, I. Polec, L. Lutsen, E. Andries, J. Manca, L. DeSchepper, and D. Vanderzande, *Synthetic Metals* **138**, 249 (2003).

[16] V. Dyakonov, *Applied Physics A* **79**, 21 (2004).

[17] M. Al-Ibrahim, H.Klaus Roth, U. Zhokhavets, G. Gobsch, and S. Sensfuss, *Solar Energy Materials and Solar Cells* **85**, 13 (2005).

[18] C.J. Brabec, N.S. Sariciftci, and J.C. Hummelen, *Advanced Functional Materials* **11**, 15 (2001).

[19] D. Chirvase, Z. Chiguvare, M. Knipper, J. Parisi, V. Dyakonov, and J.C. Hummelen, *Journal of Applied Physics* **93**, 3376 (2003).

[20] S. Alem, R. deBettignies, J.M. Nunzi, and M. Cariou, *Applied Physics Letters* **84**, 2178 (2004).

[21] C.J. Brabec, A. Cravino, D. Meissner, N.S. Sariciftci, T. Fromherz,

M.T. Rispens, L. Sanchez, and J.C. Hummelen, *Advanced Functional Materials* **11**, 374 (2001).

[22] H. Frohne, S.E. Shaheen, C.J. Brabec, D.C. Mullen, N.S. Sariciftci, and K. Meerholz, *A European Journal of Chemical Physics and Physical Chemistry* **9**, 795 (2002).

[23] C.J. Brabec, A. Cravino, D. Meissner, N.S. Sariciftci, M.T. Rispens, L. Sanchez, J.C. Hummelen, and T. Fromherz, *Thin Solid Films* **403-404**, 368 (2002).

[24] R.A.J. Janssen, J.C. Hummelen, and N.S. Sariciftci, *Materials Research Society Bulletin* **30**, 33 (2005).

[25] S.E. Shaheen, C.J. Brabec, N.S. Sariciftci, F. Padinger, T. Fromherz, and J.C. Hummelen, *Applied Physics Letters* **78**, 841 (2001).

[26] D.A. Halliday, D.C.C. Bradley, P.L. Burn, R.H. Friend, and A.B. Holmes, *Synthetic Metals* **41-43**, 931 (1991).

[27] W. Bijnens, M. Van Der Borght, J. Manca, W. De Ceuninck, L. De Schepper, D. Vanderzande, J. Gelan, and L. Stals, *Optical Materials* **9**, 150 (1998).

[28] N.C. Greenham and R.H. Friend, *Solid State Physics* **49**, 1 (1995).

[29] M. Pope and C.E. Swenberg, *Electronic Processes in Organic Crystals and Polymers*, Oxford Science Publications, UK, 1999.

[30] A. Boudrioua, P.A. Hobson, B. Matterson, I.D.W. Samuel, and W.L. Barnes, *Synthetic Metals* **111-112**, 545 (2000).

[31] N.C. Greenham, I.D.W. Samuel, G.R. Hayes, R.T. Phillips, Y.A.R.R. Kessener, S.C. Moratti, A.B. Holmes, and R.H. Friend, *Chemical Physics Letters* **241**, 89 (1995).

[32] J.C. deMello, H.F. Wittmann, and R.H. Friend, *Advanced Materials* **9**, 230 (1997).

[33] P. Wood, *Conformational Disorder and the Degree of Conjugation in Conjugated Polymers*, PhD thesis, University of St. Andrews, 2002.

[34] J.P.J. Markham, *Highly Efficient Dendrimers and Polymers for Solution Processed Organic Light Emitting Diodes*, PhD thesis, University of St. Andrews, 2003.

Chapter 4

Photophysical and Electrical Studies of Polymers

4.1 Introduction

The use of conjugated polymers in PV devices is widespread, not only because of the number of different polymer materials available, but also because they are heavily studied organic semiconductors. They have been in existence since 1977 when Shirakawa *et al.* discovered semiconductivity in polymers [1]. In the following 30 years, conjugated polymers have been successfully used as light emitting materials, ultimately leading to the fabrication of LEDs. Device efficiencies were initially low, but have steadily risen as our understanding of materials, device structures and electrode optimisation has increased [2, 3]. Material understand-

ing is key to producing suitable conjugated polymers for a particular purpose, such as light emission for LEDs or light absorption for PV devices. This includes the understanding of charge transport, exciton formation and interactions with light. In furthering our knowledge of these properties, significantly more efficient materials have been synthesised. This evolution has produced many variants of original polymers (such as MEH-PPV being a variant of PPV) and also a wide range of new polymers (such as polyfluorenes) for a broad number of uses. More recently, they have been applied to light absorbing roles such as solar cells and photodiodes [4–7].

Conjugated polymers are well-suited to solar cell applications as they have strong, broadband light absorption. They have been shown to display high efficiency ($\sim$3%) when blended with electron transporting materials such as PCBM [8–11]. The versatility of polymer materials for PV devices makes them ideal candidates for this purpose. As discussed in chapter 2, they can be modified in order to improve conduction, solubility and absorption (and emission) colour. The additional groups can include methyloxy and hexyloxy for solubility control. Additionally, thiophene and/or fluorene rings can be included for absorption and emission tuning. Should one require tighter molecular packing, it is possible to remove the solublising groups altogether. This will result in an insoluble (or very low solubility) polymer prepared using a precursor film. The preparation of precursors was discussed in chapter 3.

In developing new materials for polymer photovoltaics there are a number of issues that need to be addressed. These include light absorption,

exciton diffusion, charge separation and charge transport properties. Polymers are hole transporters. Unfortunately, as discussed in previous chapters, monolayer devices are not usually suitable for producing efficient light conversion due to their low exciton separation ability and poor charge transport. Monolayer polymer devices produce low efficiencies, typically 0.001%- 0.01%. To improve this situation, the addition of electron acceptors/transporters such as C_{60} (and derivatives thereof) is employed.

In order to improve charge separation, novel polymers have been developed specifically for PV applications. This chapter focusses on one such polymer. The addition of suitable side groups onto the polymer chain creates a dipole across the polymer molecule. This dipole enhances the separation of charges from an exciton. In addition, because of such a dipole, the absorption properties will be affected providing the opportunity for tuning the material to absorb desired wavelengths. This effect can be seen in comparatively lower PLQY and reduced fluorescence from TRL measurements. These results will be discussed in section 4.2.2.

This chapter presents results for electrical and photophysical measurements performed upon a number of novel polymers. The following section begins with the motivation behind these new polymers and will then present results from these materials, discussing them in terms of success in their desired functions.

I would like to acknowledge Olivier Gaudin for the measurement of the absorption coefficient of MEH-PPV by ellipsometry. I would also like to

thank Paul Burn and his group at the University of Oxford for synthesising the polymers used in this work. Specifically, I would like to thank Dr. Bimlesh Lochab for the novel dipole polymers and Dr. Graham Webster for DM-PPV synthesis. Data taken as part of the charge separating work was performed in collaboration with Aaron Barkhouse using the polymers supplied by the Burn group.

4.2 Polymer Materials

Two of the most common materials studied over the last decade or so are MDMO-PPV and MEH-PPV. They have been extensively studied in device applications, including LEDs [12], PVs [8] and lasers [13]. They have been widely studied and characterised, which makes them good choices for device materials. The current literature reports device performance in excess of 2.5% for MEH-PPV and MDMO-PPV blends with PCBM [8, 11, 14, 15]. The absorption, absorbance and PL spectra of MEH-PPV are shown in figure 4.1. In this chapter, there are several conjugated polymer materials that have been investigated. Each of the these polymers is based upon poly[phenylene-vinylene] (PPV). The focus in this work is centred upon material characterisation to determine which molecular attributes affect such properties as luminescence efficiency, absorption coefficients and exciton quenching properties.

One of the more significant problems facing conjugated polymers at present is their charge separating and transporting abilities. Within conju-

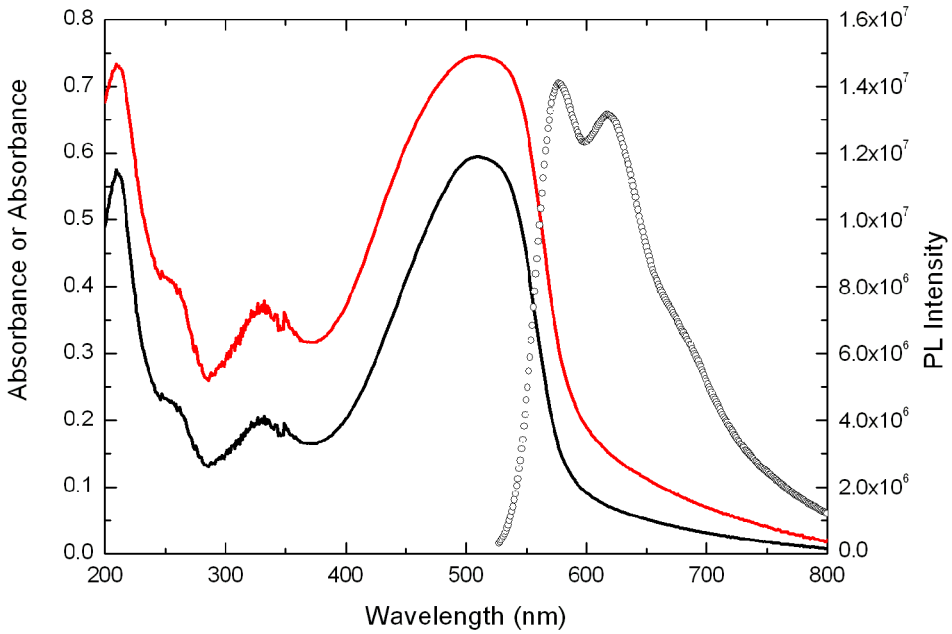

Figure 4.1: Absorbance (A, black line), Absorption ($1-10^{-A}$, red line) and PL spectra (open circles) of MEH-PPV.

gated polymers, excitons are strongly bound (typically the exciton binding energy lies between 0.3 and 1 eV [16–18]) which results in neutral excitations. This means that charge separation from bound states is less effective, which in turn results in lower device efficiency. Currently, one solution to this problem is the use of blends in the active layer of a device. The mixing of a hole transporter (polymer) with an electron transporter (fullerene) increases the probability for excitons to separate and charge to be transported. The difference in HOMO and LUMO of the two materials allows charges to be separated and move relatively freely to the relevant electrodes. This process has been investigated here in terms of charge separation by introducing a dipole across the polymer backbone which is intended to enhance charge separation from the excited state.

The conjugated polymer in a solar cell device is seen as the 'workhorse' as it is the material primarily responsible for light absorption (although within a blend the electron transporter will also absorb light, but the majority of this light is ultraviolet, which is scarce in the solar spectrum). There are, therefore, a number of material requirements. Firstly, light needs to be absorbed. This is obviously fundamental to a solar cell. This means that the absorbance of the (polymer) material in question needs to be high (A $>$0.3) in the green/red (500-800 nm) area of the optical spectrum (and, indeed if possible, far into the infra red) since this is where a significant proportion of the light from the sun is situated.

Currently there are polymers that absorb blue/green or blue-green/green-red light but not both (MEH-PPV and P3HT respectively). However, the bandgap of these materials is still too large ($>$2.2 eV). Ideally, the bandgap of such a material should be $\sim$ 1.8 eV [10, 14, 15, 19] as this is a good compromise between suitable absorption and the minimisation of internal loss through phonons and other non-radiative processes. Several low bandgap materials have been synthesised for this purpose such as the polymers poly[N-dodecyl-2,5-bis(2'-thienyl)pyrrole-(2,1,3-benzothiadiazole)] (PTPTB) [9, 19, 20], poly[5,6-dithiooctylisothianaphtene] (PDOST) [21] and poly[2,7-(9-(2'-ethylhexyl)-9-hexyl-fluorene)-*alt*-5,5-(4',7'-di-2-thienyl-2',1',3'-benzothiadiazole)] (PFDTBT) [7, 14]. However, these materials have not yet produced devices with high ($>$3%) efficiency. A further complication of these low bandgap polymers is their difficulty to synthesise. They are not only time consuming to synthesise, but also the resulting devices require considerable care in order to maintain the V_{OC} and efficiency [14, 20].

Light absorption can also be enhanced by increasing the absorption coefficient of a material. This could be achieved by increasing molecular packing within the film by removing solublising side groups from a molecule. Side groups take up a relatively large amount of space within a film and this space could be put to better use by increasing the density of conjugated material. This idea has been manifested in the synthesis of the polymer poly[2,5-dimethoxy-1,4-phenylene-vinylene] (Dimethoxy-PPV, DM-PPV) [22]. The loss of side groups provides the opportunity for tighter molecular packing, affording the possibility for higher light absorption due to more absorption sites within the film. Section 4.2.1 presents results for this material.

Charge separation (and its subsequent transport) within a conjugated polymer film is essential to the operation of a PV device. This can be performed in two ways. The first is to use an electron accepting/transporting material (such as C_{60}). This approach have been used by Sariciftci *et al.* and Yoshino *et al.* [15,23,24]. The alternate approach to this the method taken in this thesis, is to attempt to increase charge separation on the polymer molecule itself by introducing a strong dipole across the conjugated backbone. Once charge has been separated due to this dipole, the hopping and/or diffusion of charges can then occur. Additionally, as charges are separated on the molecule as opposed to separated by the potential difference between the two transporting species within a blend, the possibility of a single species performing as an active layer presents itself. These possibilities are investigated in section 4.2.2 where two new polymers are introduced specifically designed for these purposes.

4.2.1 Dimethoxy-PPV

In order to increase device efficiency, one of the most obvious improvements that can be made to a material is its ability to absorb more light. This can be done in a number of ways, including changing its light absorbing centres (from, for example, phenyl to thiophene rings) or the doping of the material with elements such as Iodine to change the shape of the absorbtion spectrum. Additionally, one could simply increase the molecular density of the material in an attempt to absorb more light. The latter case has been chosen here because it is straightforward to

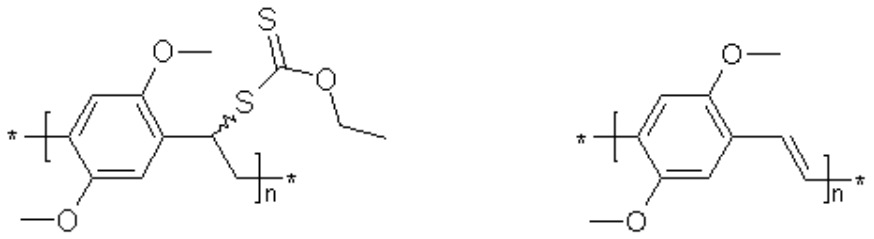

(a) Precursor form of DM-PPV.

(b) Conjugated form of DM-PPV.

Figure 4.2: Molecular structures of DM-PPV. The material is insoluble in conjugated form so it needs to be converted from precursor form.

alter a conjugated polymer by removing its side groups. This is the situation for poly[2,5-dimethoxy-1,4-phenylene-vinylene] (Dimethoxy-PPV, DM-PPV). This is another PPV derivative, very similar to MEH-PPV and MDMO-PPV, but lacking the solublising groups. The molecular structure of DM-PPV is shown in figure 4.2. Since the molecule has no solublising groups, it is synthesised and supplied in precursor form (Xanthate precursor) and is prepared as described in chapter 3. Once prepared, it is similar in appearance in thin film to MEH-PPV and MDMO-PPV.

Films are generally of good quality, with little aggregation visible.

DM-PPV has been briefly studied previously in terms of synthesis and conversion routes [25] and the optical properties of a converted film [26]. The work performed here was to test for tighter molecular packing, increasing the suitability for PV applications. Photophysical characterisation was also performed since films have been prepared differently to those reported previously. The polymer used in this work was prepared using the xanthate precursor route, whereas the material studied by Halliday *et al.* [25] utilised a number of leaving groups, involving different conversion processes (heat or acid + heat). This in turn produced a range of bandgaps. Figure 4.3 shows the absorption and PL spectra

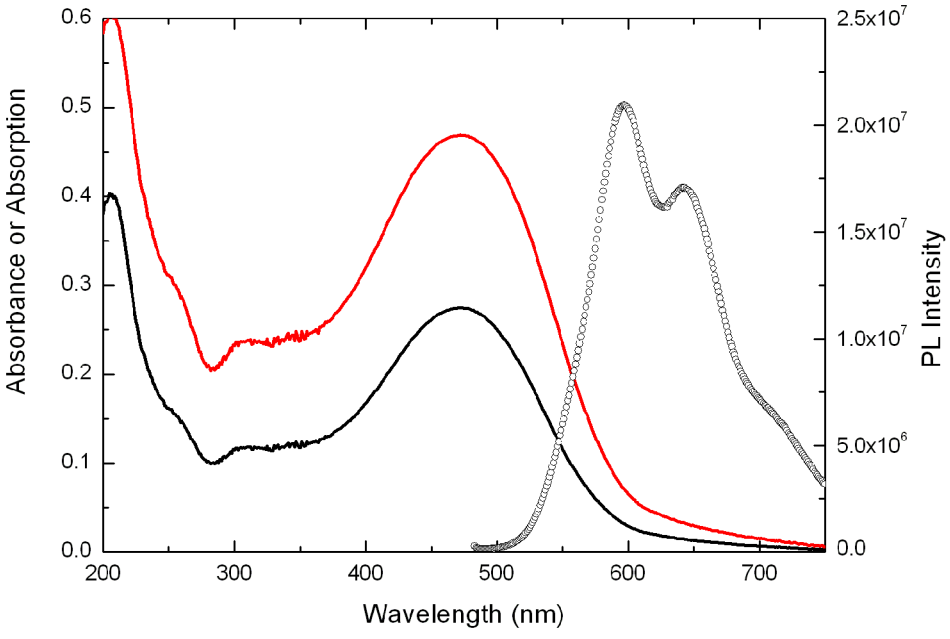

Figure 4.3: Absorbance (A, black line), Absorption ($1-10^{-A}$, red line) and PL spectra (open circles) of DM-PPV.

for DM-PPV. The absorption spectrum is very similar to that of MEH-PPV, as desired. The PL spectra is also very similar to MEH-PPV. This indicates that the solublising side groups are not responsible for light absorption or emission. In order to test whether DM-PPV absorbs more light per unit film thickness than MEH-PPV, the absorption coefficient is needed. This was calculated by measuring the film thickness with a Dektak profilometer and using the absorbance spectrum. Equation 4.1 shows the relationship between light intensity and absorbance.

$$I = I_0 e^{-\alpha d} \tag{4.1}$$

using

$$A = -\log(T) \tag{4.2}$$

gives

$$-\log\left(\frac{I}{I_0}\right) = \frac{\alpha d}{\ln 10} \tag{4.3}$$

so

$$\alpha = \frac{A \ln 10}{d} = \frac{A}{d \log(e)} \tag{4.4}$$

where A is the film absorbance, d is the film thickness, I is the intensity at d, I_0 is the incident light intensity and α is the absorption coefficient. Using 4.4, the calculated absorption coefficient for DM-PPV is $\alpha = 2.14 \times 10^5$ cm^{-1} at absorption maximum (472 nm). For MEH-PPV, the measured absorption coefficient at absorption maximum (497 nm) is $\alpha = 2.04 \times 10^5$ cm^{-1} and $\alpha = 1.83 \times 10^5$ cm^{-1} at 472 nm. There is a clear difference at at 472 nm, in favour of DM-PPV. There is a 17% increase in absorbance purely by removing the side groups from the MEH-PPV molecule. This could translate into a significant device performance increase if DM-PPV

were to be used in a device. However, comparing the peaks, there is a blue-shift of the spectrum. This is undesirable for PV applications since redder absorbing materials are favoured. This could imply that the removal of side groups has in fact blue-shifted the absorption. This is a surprising result since the inclusion of (asymmetric) side chains tends to produce curled or twisted chains, which can blue-shift absorption [27, 28]. Having no or symmetric substitution would lead to much straighter, more conjugated chains which would imply redder absorption.

In addition to this, comparing the entire absorption spectrum of DM-PPV to that of MEH-PPV, there is little difference between the two. Integrating across the spectra of each material and normalising each film to the same thickness (30 nm) reveals that there is an almost identical ($<< 1\%$ difference) match between absorbed light across the spectrum. This implies that there is little or no difference in the absorption of the film as a whole, even if certain parts have been improved. The UV peak will be contributing to this which perhaps skews the result slightly. However, overall there is no improvement. If one ignores the effect of this UV peak then there is an increase in absorption in the visible part of the spectrum, as desired. This accounts for the 17% improvement.

The PLQY of DM-PPV was also measured in order to compare it to MEH-PPV. The PLQY was measured to be $\sim 5\%$. This is considerably lower than MEH-PPV ($\sim 13\%$). A possible reason for this is the tighter molecular packing. This would encourage chromophore-chromophore interactions, providing a quenching route for excitons generated in the film, reducing the PL efficiency.

An estimate for the increased packing can be made quite simply. The physical size of the polymer backbone is approximately 2 Å [28]. The benzene ring can be seen as the widest point on the backbone, making it 2 Å across. The side chain is approximately twice this size, being six carbon atoms in length, rather than the three forming the width of the benzene ring. Therefore the length of the side chain is approximately 5-6 Å. This is most likely a slight overestimate since the atoms will be in close contact with each other in a single bond. However, this removal of the side chain will significantly decrease the physical width of a molecule by up to 0.5 nm, approximately a 66% reduction of the total polymer width. This means that we could expect an increase of up to 66% in the absorption coefficient. Since the result gained is 13%, it is not beyond this (somewhat crude) estimate and therefore not unbelievable.

The presented results can also indicate a poor quality film or one with low conjugation. Upon inspection of the absorption spectrum of DM-PPV, it is noticed that the UV peak (200 nm) is noticeably taller than the 'optical' peak (472 nm). This is a feature of the precursor conversion process. Precursor polymers have no conjugation and are therefore UV (or very blue) absorbing. During conversion the absorption spectrum of precursors becomes much redder (i.e. the 'optical' peak becomes more significant) and simultaneously, the UV peak shrinks as there is more conjugation created [29]. The spectrum of DM-PPV here implies that there has been an incomplete (or poor) conversion process. This conclusion is supported by a blueshift compared to MEH-PPV and the relatively poor PLQY. This could mean that the conversion time was not long enough. Conversion conditions are determined by the material sup-

pliers. Further investigation of this material and conversion conditions may yield better results.

4.2.2 DPFEH-PPV and NDPFEH-PPV

One of the most significant processes in the operation of a PV device is that of charge separation. There are currently two dominant ways of achieving this; either at an interface with a layer of organic or inorganic semiconductor [30] or with dispersed molecules with a different ionisation potential within a blend [31]. The disadvantage of the former approach is that excitons need to diffuse a long way (> 30 nm) through the organic layer to reach the interface. This is unlikely, since most organic semiconductors have diffusion lengths of approximately 10 nm (see chapter 6). The latter approach is more common for PVs, and has produced high efficiencies [4, 11, 15], but includes materials that are expensive to produce (PCBM).

There is an alternative to these methods. Instead of using two materials, it is possible to synthesise polymers to absorb light and separate charge on the same molecule. This is the approach taken here. PPV derivatives have been synthesised to test whether light can be absorbed and charges can be effectively separated on the same molecule, without the need for a dopant. Figure 4.4 shows the molecular structures of these novel materials. By introducing a strong dipole across the molecule, it is possible to induce charge separation. This was achieved by introducing a fluorene

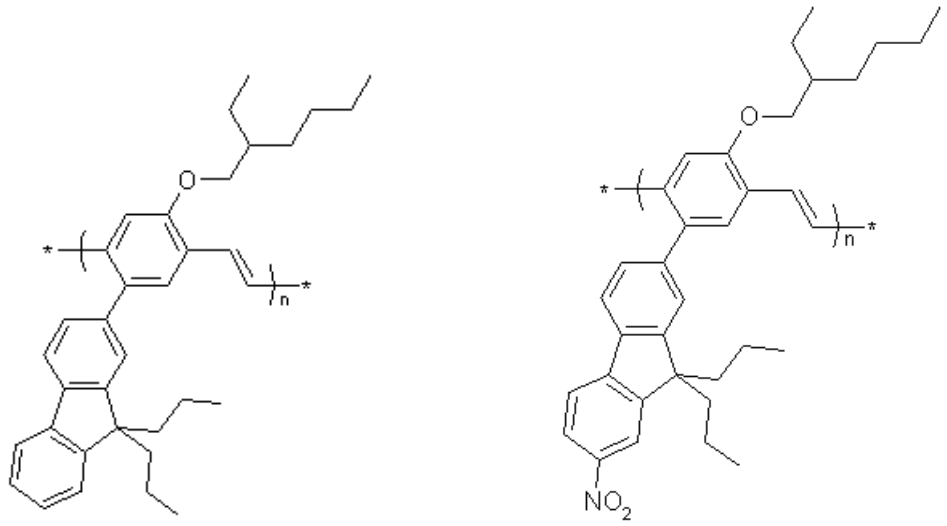

(a) DPFEH-PPV. (b) NDPFEH-PPV.

Figure 4.4: Molecular structures of DPFEH-PPV and NDPFEH-PPV. Materials differ only by the nitro group on the base of the fluorene group.

group with a nitro (NO_2) group at the base. To test whether the presence of this group leads to enhanced charge separation, the same polymer was synthesised without this nitro group. The polymers are both based upon PPV and their IUPAC names are poly[2-(9,9'-dipropyl-fluorene)-5-(2'-ethyl-hexyloxy)-1,4-phenylene-vinylene] (DPFEH-PPV) and poly[2-(3-nitro-9,9'-dipropyl-fluorene)-5-(2'-ethyl-hexyloxy)-1,4-phenylene-vinylene] (NDPFEH-PPV).

In order to test whether charge separation was occurring, several measurements were performed. These include absorption and PL spectra, PLQY, TRL spectroscopy and determination of the absorption coefficient for each material. This gives a complete photophysical view of the materials. Absorbance, absorption and PL spectra for both polymers are shown in figure 4.5 and TRL results are shown in figure 4.6. Photo-

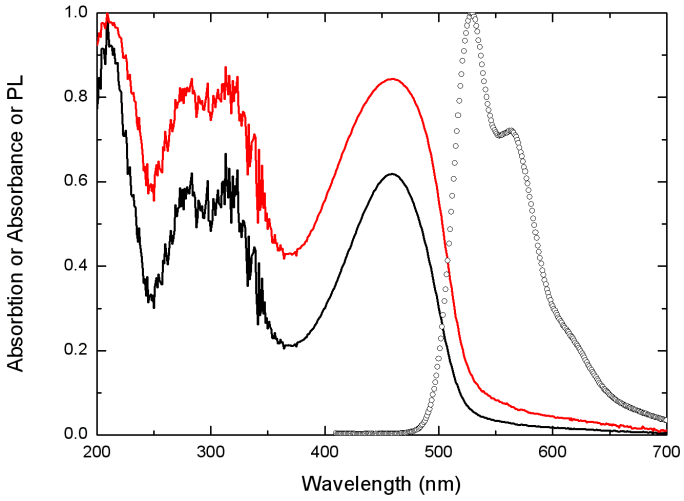

(a) DPFEH-PPV.

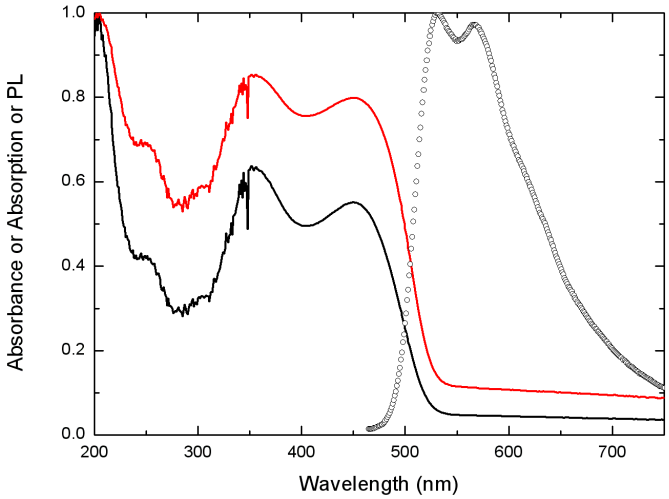

(b) NDPFEH-PPV.

Figure 4.5: Absorbance (A, black line), absorption ($1 - 10^{-A}$, red line) and PL (open circles) of DPFEH-PPV and NDPFEH-PPV.

physical results are summarised in table 4.1. Upon examining these

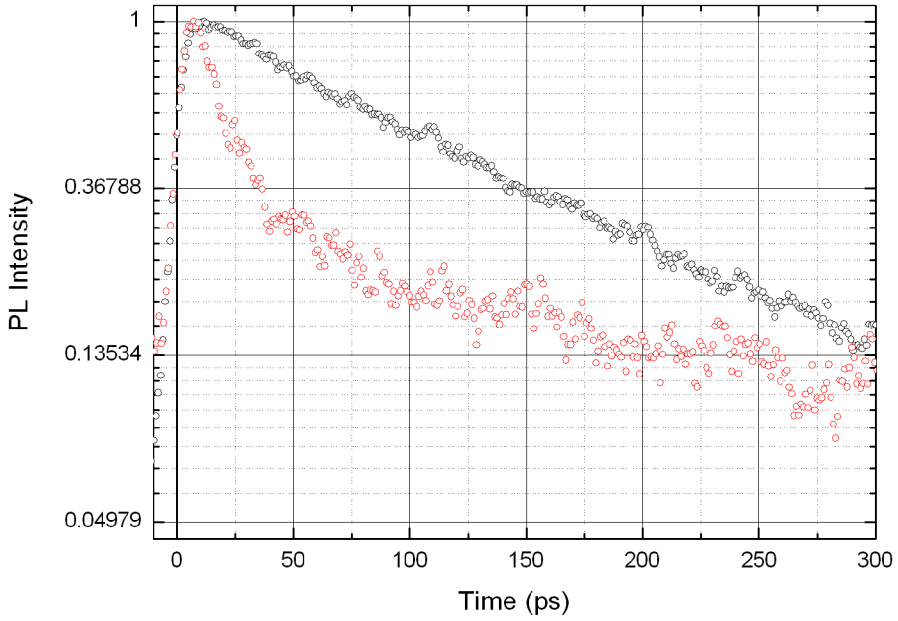

Figure 4.6: TRL decays of DPFEH-PPV (black circles) and NDPFEH-PPV (red circles). There is a clear difference between the two.

Polymer	**PLQY**	**Abs. Peak**	τ (ps)	α ($\times 10^5$ cm^{-1})
DPFEH-PPV	8%	460 nm	140	1.66
NDPFEH-PPV	$\sim$ 1%	449 nm	36	1.56

Table 4.1: A summary of the results for photophysical characterisation of the polymers DPFEH-PPV and NDPFEH-PPV.

results, there are a number of observations. Firstly, the absorption spectra are noticeably different. There is a similar peak around 450 nm in both cases, this is produced by the PPV backbone. There is a significant contribution from the NO_2 group around 350 nm. It is assumed to quench the contribution from the fluorene group as the peak at 300 nm in DPFEH-PPV is no longer present in the polar molecule. The PL spec-

tra are also slightly different. Initial PL measurements of DPFEH-PPV proved to be poor and were later re-performed in (separate) later work by Aaron Barkhouse [32]. The shape of the spectrum has a significant shoulder at around 550 nm. In the case of NDPFEH-PPH, the PL spectrum is similar to MEH-PPV.

The quenching process could be due to an intramolecular charge transfer process, as can be seen from the reduction in PL lifetime and PLQY. This is supported by light-induced electron spin resonance (LESR) work performed by Elizabeth Thomsen [33] which shows charge separation occurring across the NDPFEH-PPV molecule.

Devices from these polymers were also fabricated to test their charge separating ability, and to test their suitability as PV materials. IV curves are shown in figure 4.7. Reasonably high values for V_{OC} were observed for neat polymer films, while this decreased when PCBM was added. Since these were neat films, the expected V_{OC} would be the difference between the work functions of the two metal contacts (approximately 2 V) which is seen. Device characteristics are shown in the graph insets. Devices consisted of a standard configuration (ITO/PEDOT/Active/Ca/Al) (see chapter 3) with an active layer of approximately 100 nm.

From this presented data there are a number of conclusions that can be made. Primarily, the polymer with a nitro group added successfuly separates charge on the molecule as desired. This is supported by the lower PLQY, faster PL decay and improved device performance in neat film. This indicates that the desired effect is occurring. However, when

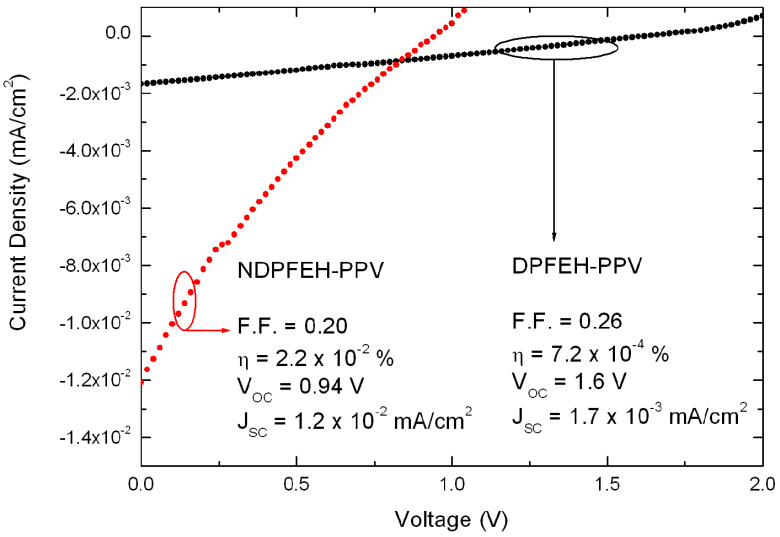

(a) IV curves for neat polymer films.

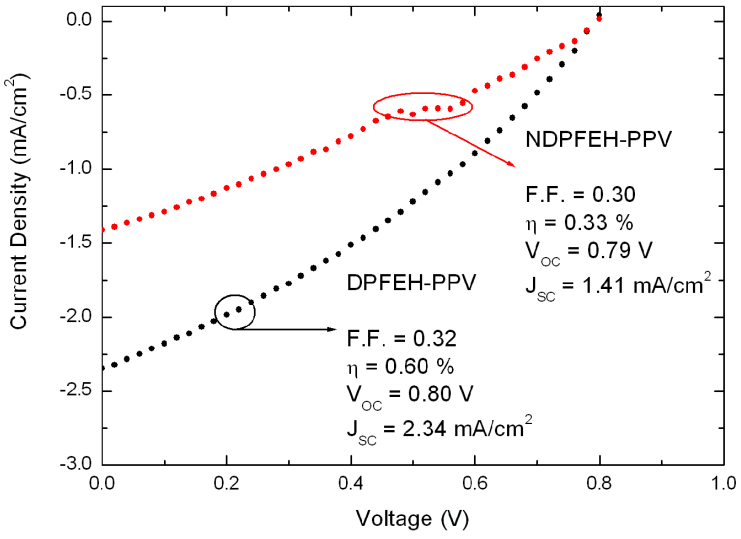

(b) IV curves for polymer-PCBM blends.

Figure 4.7: IV curves for devices fabricated from DPFEH-PPV (black) and NDPFEH-PPV (red).

placed into a blend, the non-polar molecule, DPFEH-PPV, is superior by a factor of two. This could possibly indicate that the nitro group is too strong an electron acceptor as it inhibits the transfer of an electron to the PCBM once the exciton has been separated, effectively acting as an electron trap. Charge transfer can occur directly to PCBM from DPFEH-PPV as there is no (or a very small) dipole across the molecule. This is reflected in a (relatively) high device efficiency. This is not the case for the polar molecule, NDPFEH-PPV. Once charge is separated, it is possibly being hindered by the highly electronegative nitro group so the electron cannot easily hop to the PCBM molecule. Since the nitro group is acting as an electron trap due to its high electron affinity, it will reduce efficiency within the device. Further investigation into this effect will be performed by reducing the electron affinity of the added group, but is beyond the scope of this thesis.

4.3 Summary

This chapter has presented results for preliminary characterisation for a number of novel polymers as potential materials for PV devices. It has introduced possible improvements that can be made to molecules by altering different aspects of their structure and tested these modifications with some success. The removal of solublising side groups from a molecule of MEH-PPV possibly results in tighter molecular packing which in turn leads to a higher absorption coefficient. This is beneficial for PV devices where a significant amount of light needs to be absorbed. The

scope for molecular design to give photoinduced charge separation has also been investigated. This is to enable charge separation on a single molecule without the need for adding an electron acceptor. The modifications in this case were successful, but the possibility of the effect being too strong has been suggested due to the electron trapping nature of the nitro group used. In both cases, the molecular manipulation of PPV derivatives has successfully resulted in improvement of material performance.

References

[1] H. Shirakawa, E.J. Louis, A.G. MacDiarmid, C.K. Chang, and A.J. Heeger, *Journal of the American Chemical Society: Chemical Communications* **16**, 578 (1977).

[2] R.H. Friend, *International Union of Pure and Applied Chemistry* **73**, 425 (2001).

[3] C.W. Tang and S.A. Vanslyke, *Applied Physics Letters* **51**, 913 (1987).

[4] C.J. Brabec, N.S. Sariciftci, and J.C. Hummelen, *Advanced Functional Materials* **11**, 15 (2001).

[5] D. Chirvase, Z. Chiguvare, M. Knipper, J. Parisi, V. Dyakonov, and J.C. Hummelen, *Synthetic Metals* **138**, 299 (2003).

[6] M.M. Wienk, J.M. Kroon, W.J.H. Verhees, J. Knol, J.C. Hummelen, P.A. van Hal, and R.A.J. Janssen, *Angewandte Chemie International Edition* **115**, 3493 (2003).

[7] M. Svensson, F. Zhang, S.C. Veenstra, W.J.H. Verhees, J.C. Hummelen, J.M. Kroon, O. Inganäs, and M.R. Andersson, *Advanced Materials* **15**, 988 (2003).

[8] S.E. Shaheen, C.J. Brabec, N.S. Sariciftci, F. Padinger, T. Fromherz, and J.C. Hummelen, *Applied Physics Letters* **78**, 841 (2001).

[9] C. Winder, G. Matt, J.C. Hummelen, R.A.J. Janssen, N.S. Sariciftci, and C.J. Brabec, *Thin Solid Films* **403-404**, 373 (2002).

[10] C.J. Brabec, S.E. Shaheen, T. Fromherz, F. Padinger, J.C. Hummelen, A. Dhanabalan, R.A.J. Janssen, and N.S. Sariciftci, *Synthetic Metals* **121**, 1517 (2001).

[11] V. Dyakonov, *Applied Physics A* **79**, 21 (2004).

[12] G. Gustafsson, G.M. Treacy, Y. Cao, F. Klavetter, N. Colaneri, and A.J. Heeger, *Synthetic Metals* **57**, 4123 (1993).

[13] I.D.W. Samuel and G.A. Turnbull, *Materials Today* **7**, 28 (2004).

[14] R.A.J. Janssen, J.C. Hummelen, and N.S. Sariciftci, *Materials Re-*

search Society Bulletin **30**, 33 (2005).

[15] C.J. Brabec and N.S. Sariciftci, *Monatschefte fur Chemie Chemical Monthly* **132**, 421 (2001).

[16] M. Scheidler, U. Lemmer, R. Kersting, S. Karg, W. Riess, B. Cleve, R. F. Mahrt, H. Kurz, H. Bassler, E. O. Gobel, and P. Thomas, *Physical Review B* **54**, 5536 (1996).

[17] S. F. Alvarado, P. F. Seidler, D. G. Lidzey, and D. D. C. Bradley, *Physics Review Letters* **81**, 1082 (1998).

[18] V. Gulbinas, Y. Zaushitsyn, V. Sundström, D. Hertel, H. Bassler, and A. Yartsev, *Physical Review Letters* **89**, 107401 (2002).

[19] D. Muhlbacher, H. Neugebauer, A. Cravino, N.S. Sariciftci, J.K.J. van Duren, A. Dhanabalan, P.A. van Hal, R.A.J. Janssen, and J.C. Hummelen, *Molecular Crystals and Liquid Crystals* **385**, 205 (2002).

[20] C.J. Brabec, C. Winder, N.S. Sariciftci, J.C. Hummelen, A. Dhanabalan, P.A. van Hal, and R.A.J. Janssen, *Advanced Functional Materials* **12**, 709 (2002).

[21] L. Goris, M.A. Loi, A Cravino, H. Neugebauer, N.S. Sariciftci, I. Polec, L. Lutsen, E. Andries, J. Manca, L. DeSchepper, and

D. Vanderzande, *Synthetic Metals* **138**, 249 (2003).

[22] P. L. Burn, D. D. C. Bradley, A. R. Brown, R. H. Friend, and A. B. Holmes, *Synthetic Metals* **41**, 261 (1991).

[23] K. Yoshino, X.H. Yin, S. Morita, T. Kawai, and A.A. Zakhidov, *Solid State Communications* **85**, 85 (1993).

[24] K. Yoshino, T. Akashi, K. Yoshimoto, S. Morita, R. Sugimoto, and A.A. Zakhidov, *Solid State Communications* **90**, 41 (1994).

[25] D.A. Halliday, D.C.C. Bradley, P.L. Burn, R.H. Friend, and A.B. Holmes, *Synthetic Metals* **41-43**, 931 (1991).

[26] W. Bijnens, M. Van Der Borght, J. Manca, W. De Ceuninck, L. De Schepper, D. Vanderzande, J. Gelan, and L. Stals, *Optical Materials* **9**, 150 (1998).

[27] M. Kemerink, J.K.J van Duren, A.J.J.M. van Breemen, J. Wildeman, M.M. Wienk, P.W.M. Blom, H.F.M. Schoo, and R.A.J. Janssen, *Macromolecules* **38**, 7784 (2005).

[28] M. Kemerink, J.K.J van Duren, P. Jonkheijm, W.F. Pasveer, P.M. Koenraad, R.A.J. Janssen, H.W.M. Salemink, and J.H. Wolter, *Nanoletters* **3**, 1191 (2003).

[29] P.L. Burn, Private Communication.

[30] K.M. Coakley and M.D. McGehee, *Applied Physics Letters* **83**, 3380 (2003).

[31] D. Chirvase, Z. Chiguvare, M. Knipper, J. Parisi, V. Dyakonov, and J.C. Hummelen, *Journal of Applied Physics* **93**, 3376 (2003).

[32] A. Barkhouse, Private Communication.

[33] E.A. Thomsen, Private Communication.

Chapter 5

Photophysical and Electrical Studies of Dendrimers

5.1 Introduction

Over the last 25 years, the evolution of organic materials as semiconductors has produced a wide range of molecular structures. These range from high molecular weight ($M_w > 10^5$) polymers such as OC_1C_{10}-PPV [1] down to small molecules such as $Ir(ppy)_3$ [2, 3]. Each of these materials has unique properties which can be applied to specific requirements. For example, polymers are solution processable which makes fabrication much easier. Since this high degree of flexibility exists due to molecular manipulation, (see section 2.7) it is possible to create a molecule to perform a certain task. By progressively changing aspects of a material

and characterising these changes, it is possible to create a material that is highly efficient and very well suited to its purpose. These incremental changes not only allow further understanding of organic semiconductor behaviour, but using this knowledge can allow us to improve upon existing materials, or even create completely new classes. This methodical approach to material synthesis has been successfully performed recently by Halim, Samuel and Burn and resulted in the creation of the *conjugated dendrimer* [4]. The structure and design of conjugated dendrimers is described in section 2.7.2. The dendrimer molecule consists of three main parts: the core, dendrons and surface groups, to control light emission or absorption, spacing and processability respectively.

The synthesis of conjugated dendrimers has presented the possibility of colour tunability for both absorption and emission whilst still retaining simple processability. This extremely useful attribute has enabled simple fabrication of high efficiency LEDs [5] producing blue, green and red emission simply by changing the core (chromophore) of the material. Further tuning can be achieved by using conjugated dendrons. The conjugation can either be kept between the dendrons and the core (redshifting the emission and absorption) or broken, which will raise the energy of the molecule, blueshifting the absorption and emission (electron delocalisation occurs in the case of IrG1 whilst keeping conjugation. This has a similar effect to breaking conjugation, see section 5.2.2). Ideally in the case of solar cells, it is desirable to have a red absorbing material due to the abundance of red photons in the solar spectrum. Until now, however, the majority of conjugated dendrimer materials have been green or red emitting in order to work towards RGB emission for LEDs. This lim-

its the absorption to shorter wavelengths such as green, blue or, in the case of blue emitters, UV. Certainly absorbing blue and UV light is not useful for PV devices as there are very few photons of this energy in the solar spectrum. There is, therefore, a need to synthesise red absorbing dendrimers.

A further advantage to using dendrimer materials is the lowered risk of phase separation when using a blend. Blends of dendrimers could be used to cover the whole spectrum (materials permitting) in order to create a device that would harvest as much light as possible. Until now only blue or green absorbing dendrimer materials existed which is limiting, but as demonstrated in section 5.2.5, work has been performed to synthesise and test 'redder' materials in the form of cyanine dye derivatives. The combination of red, blue and green absorbing materials without phase separation would be a great advantage to light absorption, ultimately leading to more efficient devices.

The work presented in this chapter investigates several conjugated dendrimers (primarily dendrimers used in previously published work on LED devices) both as neat films and as blends with PCBM. Since dendrimers have been shown to be efficient materials for LEDs, they were investigated as potential materials for PV applications. Materials used range from porphyrin dendrimers to the much newer (and more efficient) iridium cored dendrimers, and further onto the newest dendrimer materials; those based upon cyanine dyes which have been specifically designed for solar cell purposes.

5.2 Dendrimer Materials

Due to the flexibility of the intrinsic molecular design, there are many possible dendrimer materials that could be synthesised. In simple terms, it is merely a case of 'swapping' cores in order to change the absorption (or emission) properties since this is the chromophore. By keeping the dendrons and surface groups constant, this (ideally) keeps the charge transport and molecular interactions consistent, whilst also maintaining solubility properties. This way, the effect of the core can be observed (almost) independently through each molecular variant, providing an opportunity to compare cores directly. The following results present work performed upon 1^{st} generation (G1) dendrimers in order to directly compare the properties of the cores. Materials range from porphyrins to metallic cored complexes and onto novel dye variants. Devices were fabricated and tested as described in chapter 3 using neat film and also blended with PCBM in a 1:2 ratio (dendrimer to PCBM) unless otherwise stated.

5.2.1 Porphyrins

Porphyrin materials have existed for millions of years in the Haem cycle of animals and in the form of chlorophyll in plants, the organic material responsible for photosynthesis. The molecular structure of chlorophyll is shown in figure 5.1. The fundamental part of the molecule is essentially a porphyrin ring, with a magnesium atom in the centre. This is very

similar to Haemoglobin; the main difference in this case being the iron core, rather than magnesium. Since this porphyrin ring is so effective

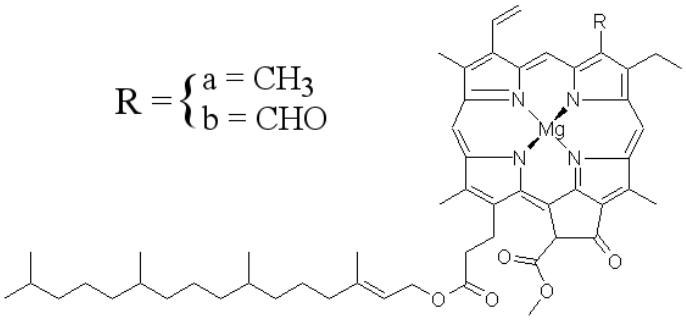

Figure 5.1: Molecular structure of chlorophyll. There are two types, *a* and *b*. The differences are in the side group, R.

at providing plants with energy in nature, it is certainly worthwhile to investigate it for power generation purposes. To this end, a porphyrin cored dendrimer was synthesised to test its effectiveness. The molecular structure of this material is shown in figure 5.2(a). This porphyrin had no metal core initially. Later it was modified into the structure shown in figure 5.2(b) by adding a zinc atom, the reason for which will be discussed below.

Initially, the porphyrin dendrimer was designed as a red emitter [6–9], so its absorption spectrum was mainly 'blue' (300-500 nm) [7]. This provided a good starting point for investigation because the absorption of the molecule would be in the optical region which is desirable for PV materials. The measured absorption spectrum for the free base porphyrin is shown in figure 5.3. Film thicknesses were approximately 60 nm. There is a significant, narrow absorption peak at $\sim$ 430 nm. This spectrum is similar to that found in the work by Frampton *et al.* and Pillow *et al.* [9, 10]. Results from testing the devices under A.M. 1.5 simula-

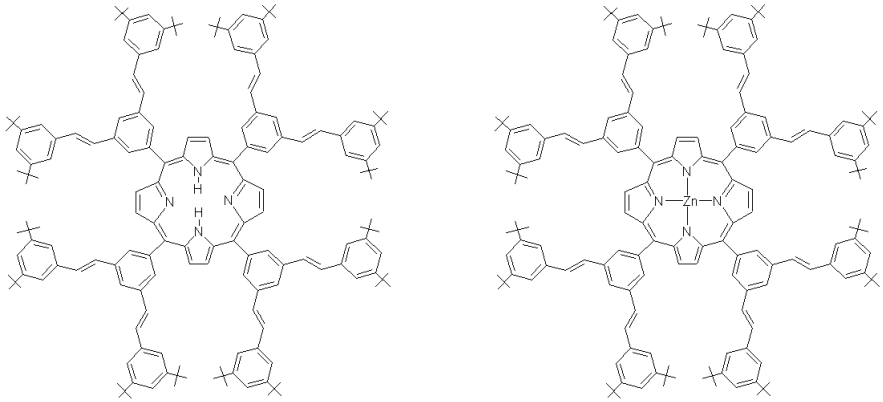

(a) Free base porphyrin dendrimer.

(b) Zinc porphyrin dendrimer.

Figure 5.2: Molecular structures of the porphyrin dendrimers used in this work.

tion show poor performance as solar cells, both as neat film and doped with PCBM. Typical IV curves are shown in figure 5.4. Efficiencies were approximately $\eta = 1 \times 10^{-4}$ %. This is certainly not useful for any applications. As one can see, there is only a modest improvement in the performance to $\eta = 1.5 \times 10^{-4}$ % by adding PCBM (in contrast to the effect of PCBM on polymer materials). This was possibly due to a slight mismatch in HOMO and LUMO levels within the device, causing electrons and/or holes to become trapped on one of the species within in the device. The approximate HOMO and LUMO levels of the device are HOMO $\sim$ 5.4 eV and LUMO $\sim$ 3.7 eV [11]. Poor performance is expected in neat films as discussed in chapter 2 but the lack of significant improvement by doping was surprising. The low efficiencies are most likely due to at least two contributing factors. Firstly, the material does not absorb a significant amount ($\sim$ 0.5% absorbed) of solar light which will reduce the efficiency. Secondly, if excitons are formed, it is unlikely that electrons will be transported to the electron acceptor (PCBM) due

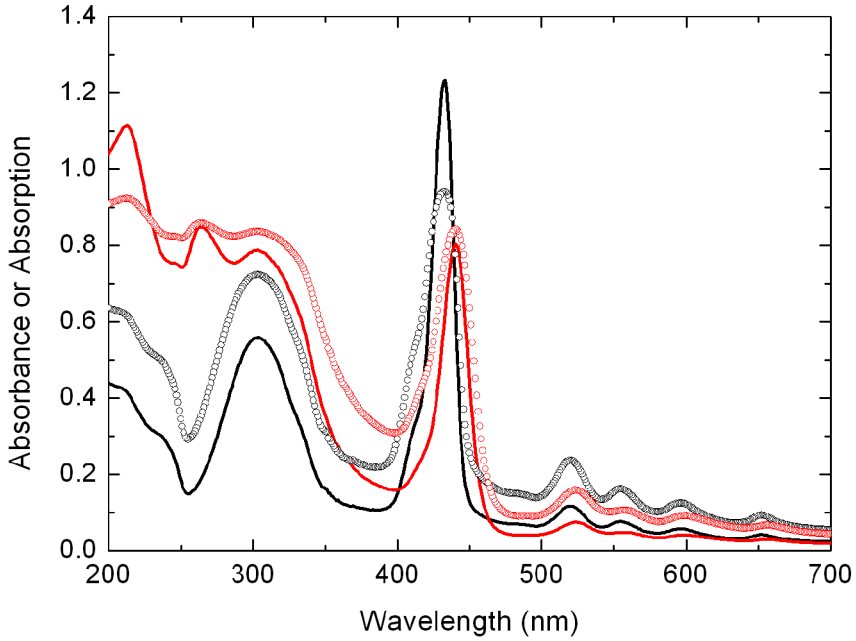

Figure 5.3: Absorbance (A, solid line) and absorption ($1 - 10^{-A}$, open circles) of the free base porphyrin dendrimer. Neat film is shown in black and blends with PCBM are shown in red.

to the LUMO levels being similar, see figure 5.5. Since no difference in LUMO levels exists between the two species, there is little inclination for electrons to move from porphyrin dendrimer to PCBM. This substantially inhibits the transport within a device, which is observed directly by an almost zero change in efficiency. For these reasons, the porphyrin was then doped with zinc in order to change the LUMO and possibly obtain higher efficiencies.

The absorption spectrum for the zinc porphyrin is shown in figure 5.6. One can see from the spectrum that there is little difference between the neat films of the two materials. The addition of zinc to the core has red-

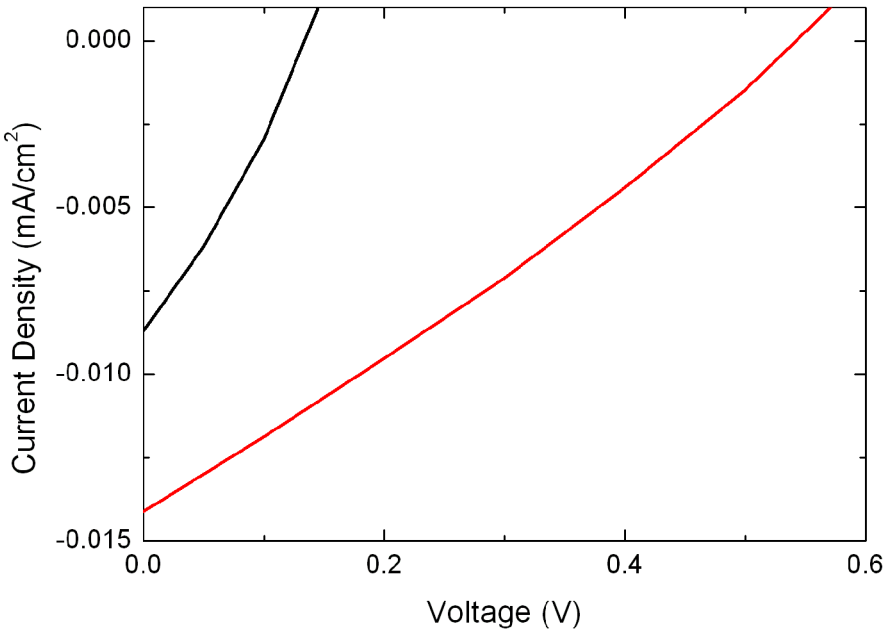

Figure 5.4: IV curve for free base porphyrin devices. Neat film (black line) and blend with PCBM (red line) were both tested.

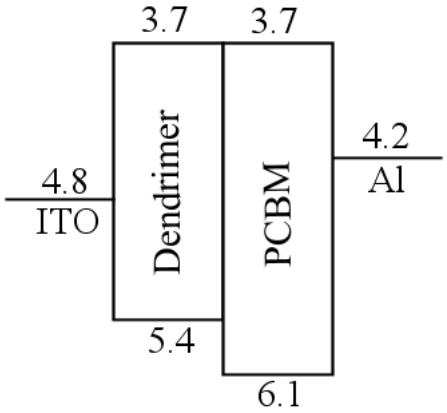

Figure 5.5: HOMO-LUMO schematic for free base porphyrin device. Energies are shown in eV relative to vacuum level [1, 11].

shifted the feature at 525 nm to 560 nm and has slightly enhanced the peak at 300 nm. This suggests that the LUMO has in fact been lowered to allow lower energy absorption. The addition of PCBM significantly increases the absorbing power of both films and red-shifts the 425 nm peak by approximately 20 nm. IV results show a reduced performance for

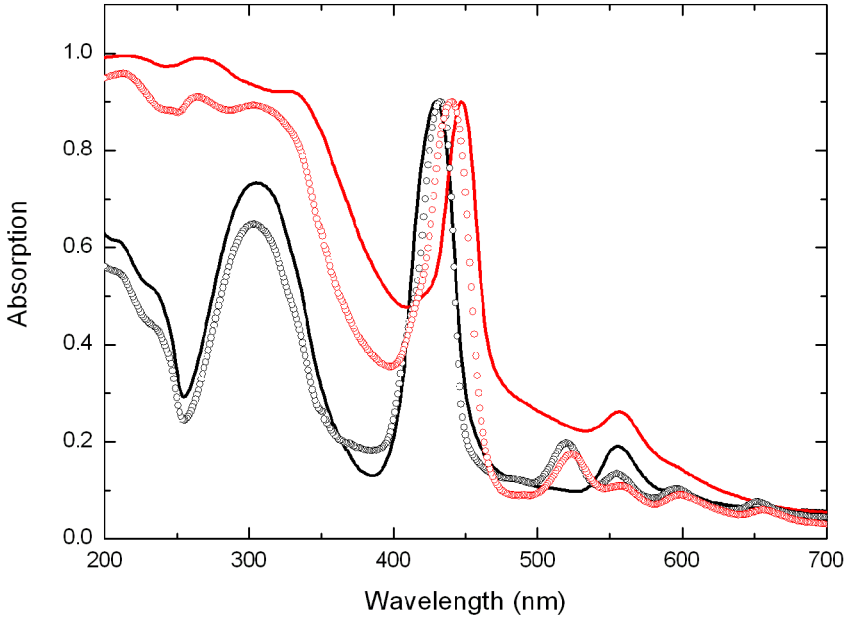

Figure 5.6: Absorption spectra for both porphyrin dendrimers. Zinc core is shown as solid lines and free base is shown as open circles. Neat films are shown in black and blends with PCBM are shown in red.

the zinc porphyrin, by almost a factor of approximately 10 times smaller than the free base porphyrin producing efficiencies of $\eta = 1 \times 10^{-5}$ %. A similar decrease in performance in the blend was observed. However, PCBM did improve the device performance compared to neat film, but only by a factor of 3, similar to the free base porphyrin case. This poor performance could be explained by the redshifted spectrum. The low-

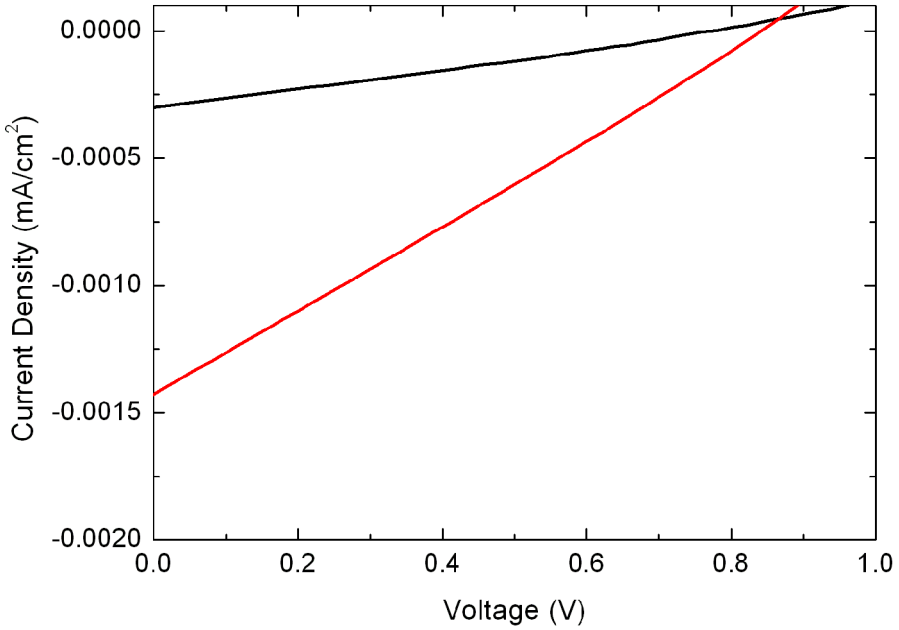

Figure 5.7: IV curve for zinc porphyrin devices. Neat film (black line) and blend with PCBM (red line) were both tested.

ering of the LUMO of the dendrimer would decrease the likelihood of charge transport from dendrimer to PCBM. The dendrimer would act as a charge trapping site, disallowing electrons or holes to move to the acceptor. This would reduce both charge separation and charge transport (The energy levels of the Zn porphyrin are currently unknown). These effects, coupled with poor light absorption, show that using porphyrins as PV materials is unfortunately an ineffective exercise in this case.

5.2.2 $Ir(ppy)_3$

The development of conjugated dendrimers over recent years has produced a great variety of materials for light emitting purposes. The most promising of which has been a dendrimer based upon the $Ir(ppy)_3$ molecule [2, 3]. This produced the IrG1 (Iridium cored, 1^{st} generation) dendrimer. The molecular structure of the IrG1 material is shown in figure 5.8. Light emission is produced through phosphorescence, rather

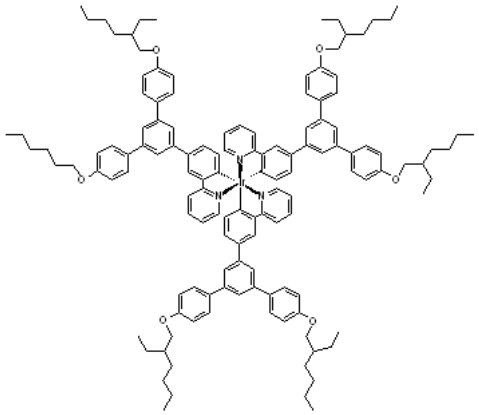

Figure 5.8: Molecular structure of IrG1.

than fluorescence. This increases the maximum possible internal efficiency from approximately 25% (singlets only) to almost 100% by emitting from triplet excitons as well. LED devices have been fabricated with external quantum efficiencies of up to 16% using this dendrimer material [12–14]. The dendrimer was chosen for solar cell devices due to the long PL lifetime of phosphorescent materials. This holds the potential for highly efficient charge extraction as the excitons exist for a comparatively longer time, providing more opportunity for charge separation. As with other dendrimers in this thesis, the blends were made 1:2 in favour

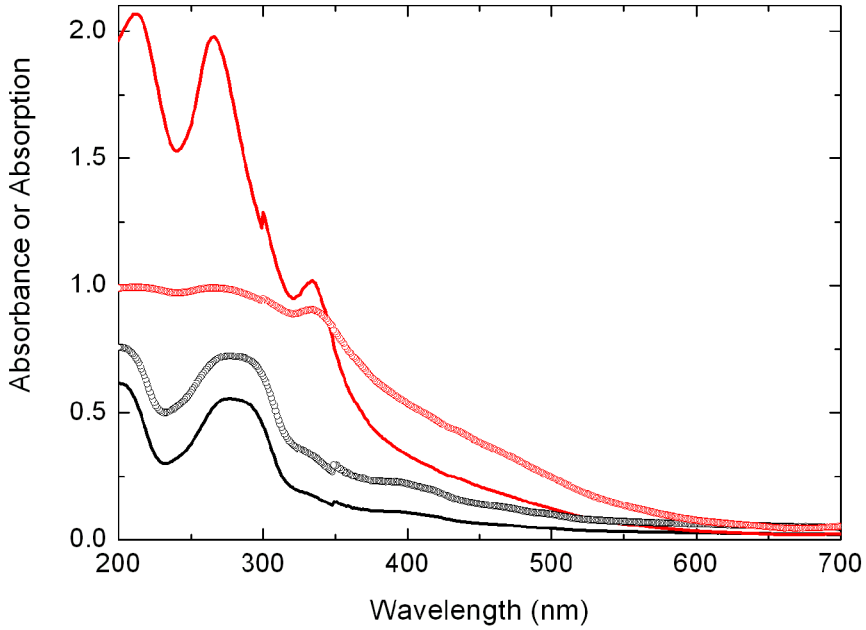

Figure 5.9: Absorbance (A, solid line) and absorption ($1 - 10^{-A}$, open circles) of the IrG1 dendrimer. Neat film is shown in black and blends with PCBM are shown in red.

of PCBM. Film thicknesses in this case were approximately 60 nm for neat film and 220 nm for the blend. The absorption spectrum of the IrG1 is shown in figure 5.9. The majority of the absorption of the (neat) molecule lies in the UV, but there is a small part that overlaps with the solar spectrum. The addition of PCBM increases the absorption significantly, although most of this still lies within the UV domain.

IV curves for typical devices are shown in figure 5.10. Neat film devices fabricated showed no performance as photocurrents and open circuit voltages were almost zero. The addition of PCBM significantly improved the performance. Fill factor was measured to be 0.3 with $V_{OC} = 0.85$ V

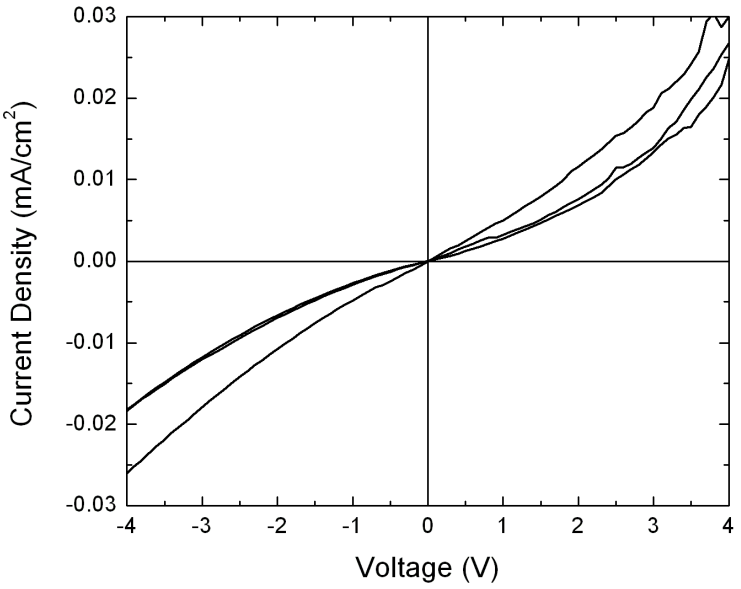

(a) Neat film IrG1 devices.

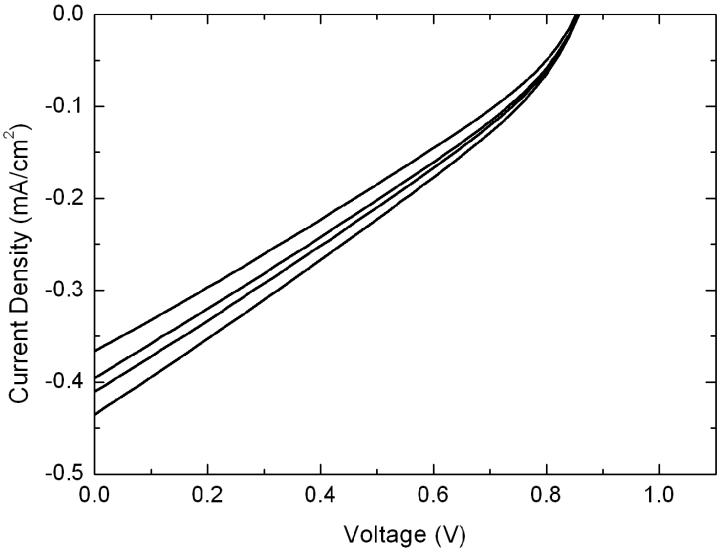

(b) IrG1 and PCBM blend devices.

Figure 5.10: IV curves for neat film (a) and blend (b) devices from IrG1. Curves show a number of devices from the same fabrication batch. Variations probably arise from differing pixel sizes.

and $J_{SC} = 0.43$ mA/cm^2. Device efficiency was calculated to be 0.11% for blend devices.

On comparison of the absorbance (or absorption) spectrum and the performance curves for the IrG1 blends, it is noticed that there is a (relatively) high performance gained from a small amount of absorbed solar light due to a blue absorption spectrum. This raises the possibility of high internal efficiency of the IrG1/PCBM blend system. Comparing this result to a typical literature OC_1C_{10}-PPV blend device (efficiencies typically greater than 2% [1]) and taking into account the absorption of a film of the polymer material, it is observed that there is a significantly higher proportion of solar light being absorbed in the polymer blend device due to the redder absorption spectrum. This leads to the possibility of high internal efficiency within the dendrimer devices used here.

Testing the internal efficiency of the devices required measuring the Incident Photon to Conducted Electron (IPCE) efficiencies. This procedure is described in chapter 3. This provides an analogue to the LED *external* quantum efficiency of the devices. The internal efficiency (Absorbed Photon to Conducted Electron, APCE) requires the optical constants of each layer of the device to be taken into account. The optical constants were measured using ellipsometry by Chris Yates. A model was then constructed to calculate the contribution of the active layer. The model is based upon a matrix method devised by J.S.C. Prentice and assumes incoherent interference [15]. Each layer requires its optical constants (extinction coefficient, k, and refractive index, n) to be known. This can then be used to calculate the reflection, transmission and absorption for

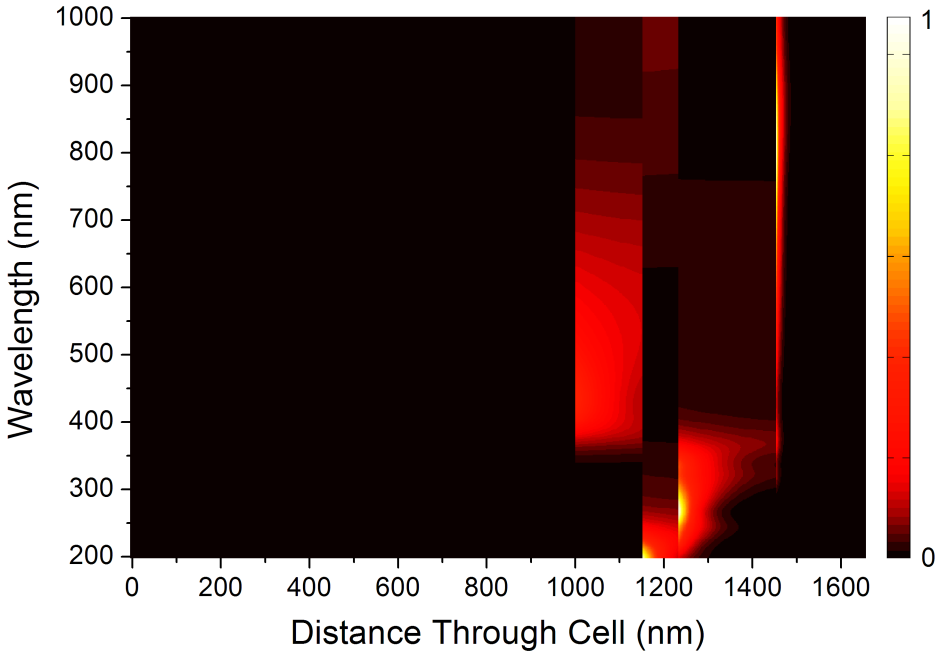

Figure 5.11: Contour plot showing the absorbing areas of an IrG1 blend device. There are obvious areas of high absorption, such as in the blend layer and in the ITO layer. The cell is split into layers (from left to right) Glass, ITO, PEDOT, Blend and the Al cathode.

each layer or interface. This is performed quite simply within the matrix model, with each matrix representing either an interface or an absorbing layer. All matrices are then multiplied together to give a profile for each wavelength. The resulting output produces a 3D surface. This is shown in figure 5.11 as a contour plot. One can see that the most significant amount of the absorption is performed by the blend layer within its first 100 nm. This indicates that the device can (or should) be made much thinner. There are also significant contributions from the other layers across the entire spectrum. ITO is highly absorbing in the optical which will detriment the cells performance. One can also see absorption in the

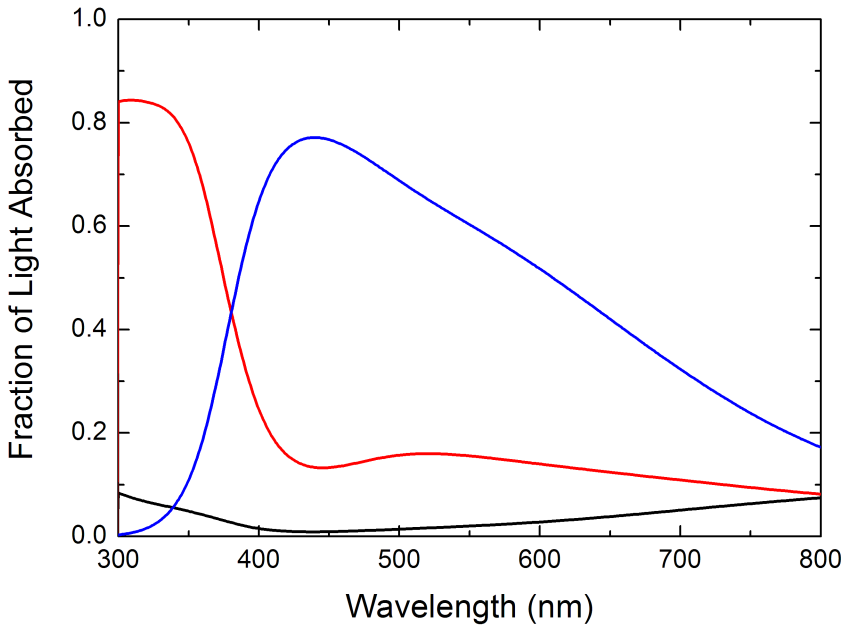

Figure 5.12: Absorption profiles for the IrG1 blend device layers. The layers correspond to ITO (blue), PEDOT (black) and the active blend (red). The curve shows absorption of light incident on each individual layer, rather than the incident light on the whole cell. Reflections are not shown.

aluminium and PEDOT layers, although to a lesser extent. Integrating each of these layers then provides the absorption profile $(1 - T - R)$ for each layer. These are shown in figure 5.12. By using equation 2.4, the blend absorption profile was then combined with the IPCE results to calculate the APCE. IPCE and APCE results are shown in figure 5.13. On inspection one can see that the IPCE is high (peaks at 40%) but this does not take into account reflection loss and light that is not absorbed. The APCE is much higher, as expected, calculated to be in excess of 90%. This result clearly shows that this blend of IrG1 and PCBM is highly efficient, both internally and externally, yielding a (moderately) high ef-

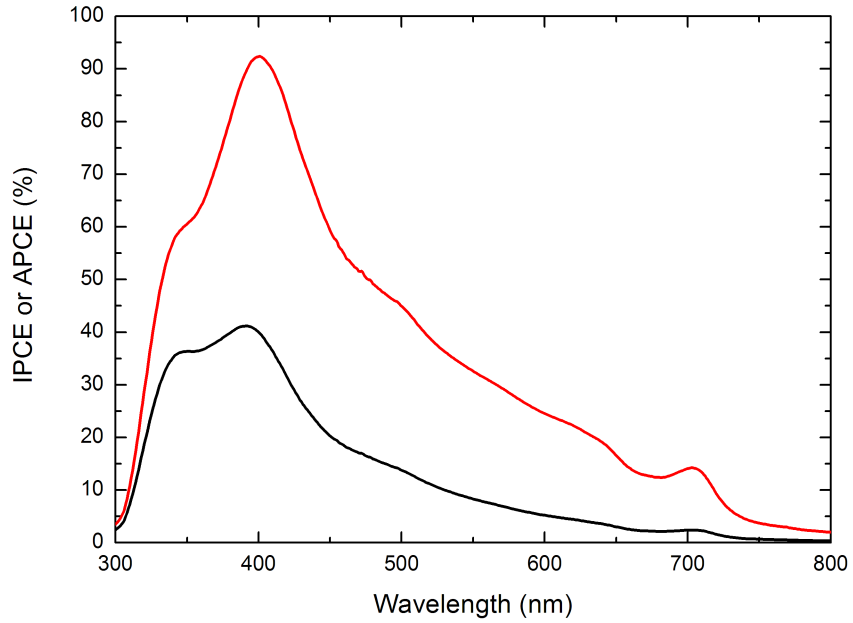

Figure 5.13: IPCE (black line) and APCE (red line) curves for a typical IrG1 blend device clearly show that the devices are highly efficient at converting solar light into conducted charge.

ficiency device that absorbs relatively little light.

The results show dendrimers may be interesting materials for solar cells as well as for LEDs. It has been demonstrated that the IrG1 dendrimer is highly efficient and further work on dendrimer solar cells would be certainly worth pursuing. The only disadvantage at this time is that the IrG1 molecule itself does not absorb a significant proportion of the solar spectrum. If such a molecule could be synthesised, combining high efficiency with broad absorption, it is conceivable that organic thin film PV devices could be fabricated to yield power conversion efficiencies competitive with other thin film devices with relative ease.

5.2.3 Ir(ppy)$_3$ Carbazole

Due to the success of the IrG1 molecule in LED devices, a further variation of the Ir(ppy)$_3$ molecule was tested to investigate whether the iridium core is responsible for the observed high internal quantum efficiency. Dendrimers in LED devices are usually put into a host material such as

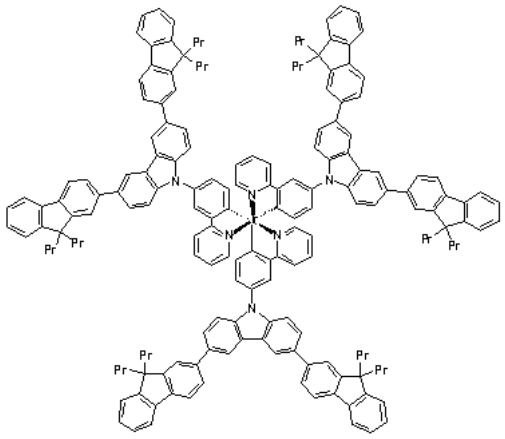

Figure 5.14: Molecular structure of the IrCz.

4,4‘-bis(*N*-carbazolyl) biphenyl (CBP) or polyvinyl carbazole (PVK). This is analogous to blending a polymer such as OC_1C_{10}-PPVwith PCBM in solar cells, where the PCBM effectively acts as a ‘host’ as it is more abundant in the mixture. The improvement applied to the successor molecule was the incorporation of the CBP or PVK host active group, the carbazole group, into the dendrimer structure. This would improve hole transport within the molecule, ultimately leading to much more effective charge extraction, especially when combined with PCBM. The molecular structure of the Iridium Carbazole dendrimer (IrCz) is shown in figure 5.14. As one can see in the structure, the carbazole group is incorporated into the dendrons instead of the standard biphenyl structure in IrG1.

The absorption spectrum of IrCz is shown in figure 5.15. The spectrum is similar to that of IrG1 due to the $Ir(ppy)_3$ core. Devices fabricated

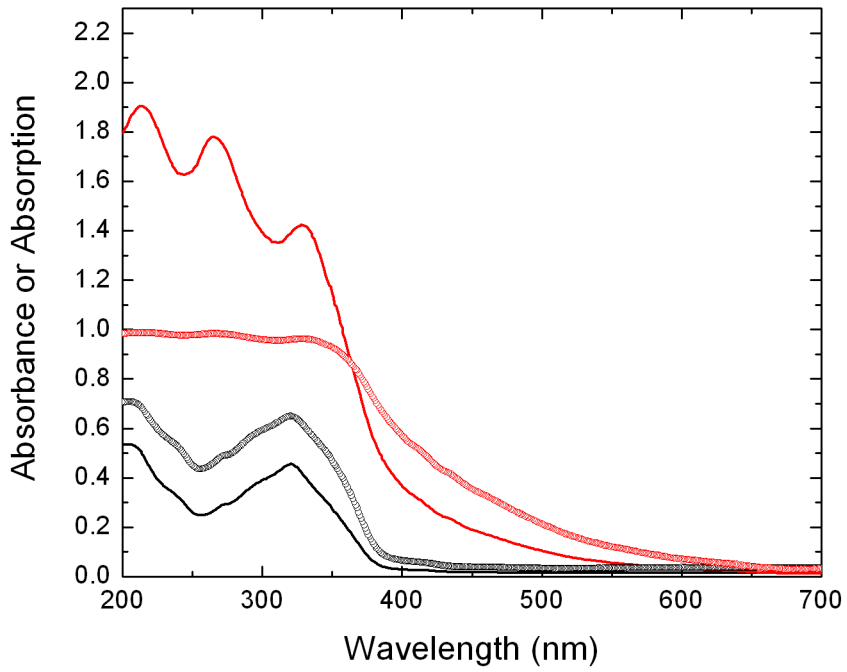

Figure 5.15: Absorbance (A, solid line) and absorption ($1 - 10^{-A}$, open circles) of the IrCz dendrimer. Neat film is shown in black and blends with PCBM are shown in red.

from IrCz had similar properties to IrG1 devices, although they were slightly less efficient overall. Neat film devices showed efficiencies of $\sim 3 \times 10^{-5}\%$ which is very low. Blending with PCBM increased efficiency significantly, by almost three orders of magnitude to 0.02%. However, these devices were still preliminary and little or no optimisation had been performed. IV curves are shown in figure 5.16. Due to the IrCz blend devices being (relatively) successful, they were tested for IPCE efficiency, similar to IrG1 devices. The IPCE results are displayed in

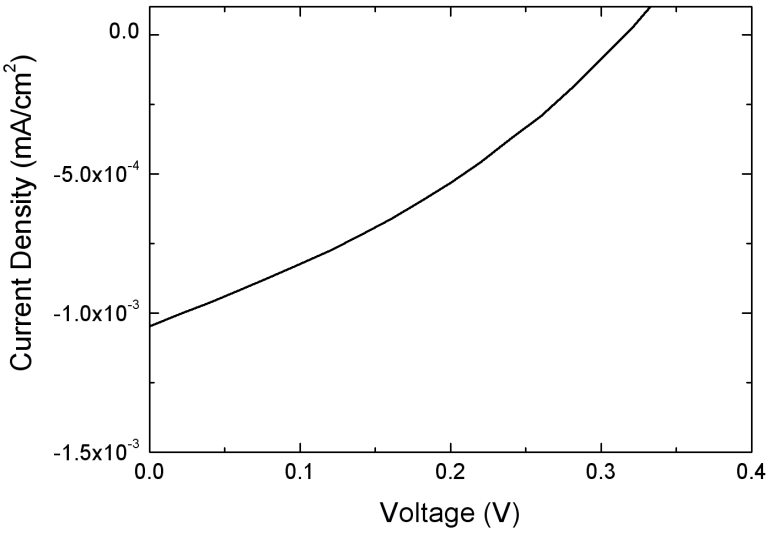

(a) Neat film IrCz device.

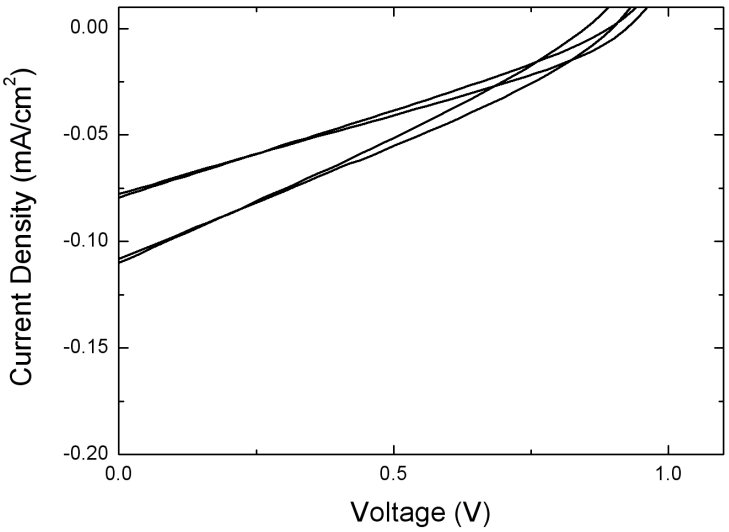

(b) IrCz and PCBM blend devices.

Figure 5.16: Typical IV curves for neat film (a) and blend (b) devices from IrCz. The graphs have been produced separately due to the difference in magnitudes. There is a significant improvement when PCBM is added.

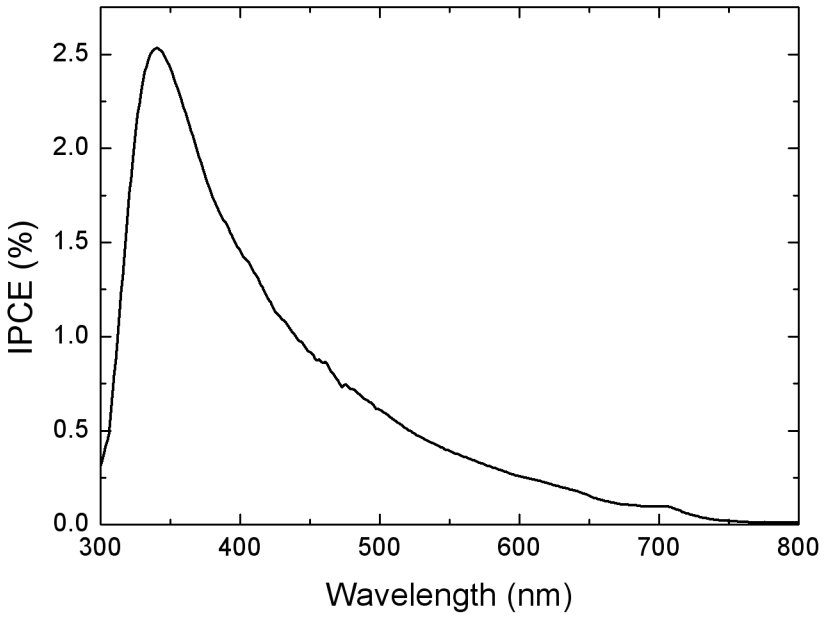

Figure 5.17: IPCE of IrCz blended with PCBM.

figure 5.17. In contrast to the IrG1 devices, the IrCz blends appear to be an order of magnitude less efficient. The IPCE results (maximum of 2.5%) seem to be comparatively lower than with IrG1 devices. However, these devices are preliminary at present. It is not unrealistic to expect an improvement for both measurements with device optimisation. The conversion efficiency is an order of magnitude lower (due to further optimisation needed) and the corresponding IPCE is an order of magnitude lower. Given a comparatively similar performance to the IrG1 blend, it is perhaps also conceivable that the IrCz blend is at least as internally efficient as the IrG1 blend, but this would need to be checked with APCE. Unfortunately, the optical constants for IrCz and blends thereof are currently unknown so a model could not be built to calculate the APCE. It

is highly likely that further work on the IrCz material would yield very promising results for devices.

5.2.4 Bisfluorene

A further example of a dendrimer applied to solar cell devices is the Bisfluorene dendrimer. Instead of a metal-ligand core structure, the Bis-

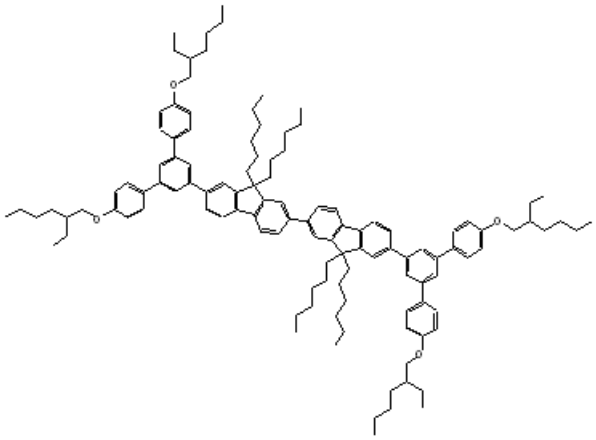

Figure 5.18: Molecular structure of the Bisfluorene dendrimer.

fluorene dendrimer has a pair of joined fluorene groups capped at each end by stilbene dendrons. This dendrimer is primarily used for emission of blue light in LED devices. The molecular structure of the Bisfluorene dendrimer is shown in figure 5.18. The absorption spectra for neat film and blend with PCBM are shown in figure 5.19. There is little absorption in the optical regime for the bisfluorene dendrimer so achieving a high efficiency was unlikely. Nevertheless, since the other dendrimers have proven to be highly efficient at charge separation (yielding high internal efficiencies) it was still worth investigating the material.

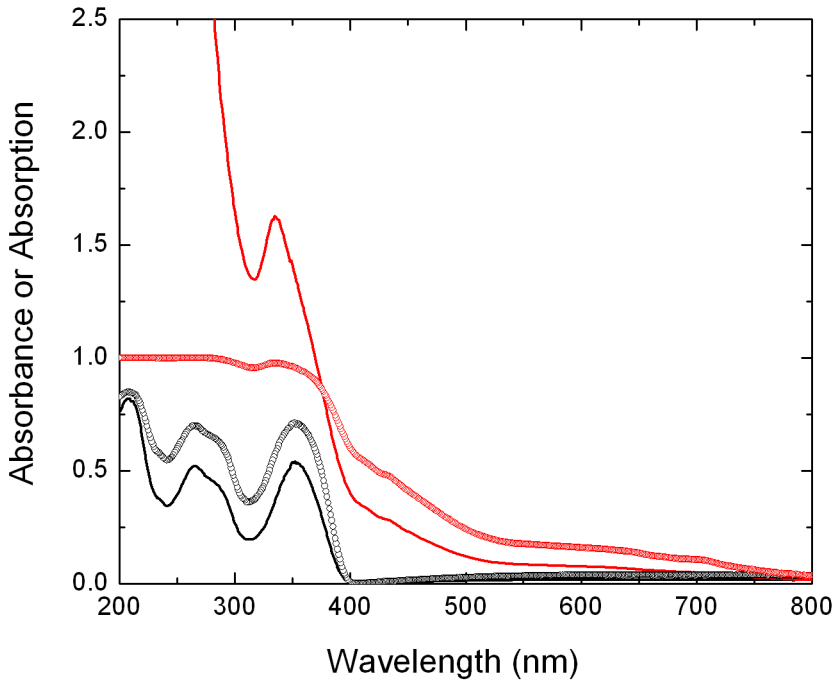

Figure 5.19: Absorbance (A, solid line) and absorption ($1 - 10^{-A}$, open circles) of the Bisfluorene dendrimer. Neat film is shown in black and blends with PCBM are shown in red.

IV curves for Bisfluorene devices are shown in figure 5.20. As one can see from the curves, there is no PV activity seen in either neat film or blend. This is most likely due to the poor light absorbing power of the dendrimer. This result supports the need for redder absorbing materials to take advantage of the solar spectrum. The absorbed photon energy is high for the Bisfluorene material and it is ideally desired to harvest the highest number of photons, rather than the highest energy photons. Since one absorbed photon produces one exciton, it is much preferred to absorb red and IR photons as they are comparatively more numerous in the solar spectrum.

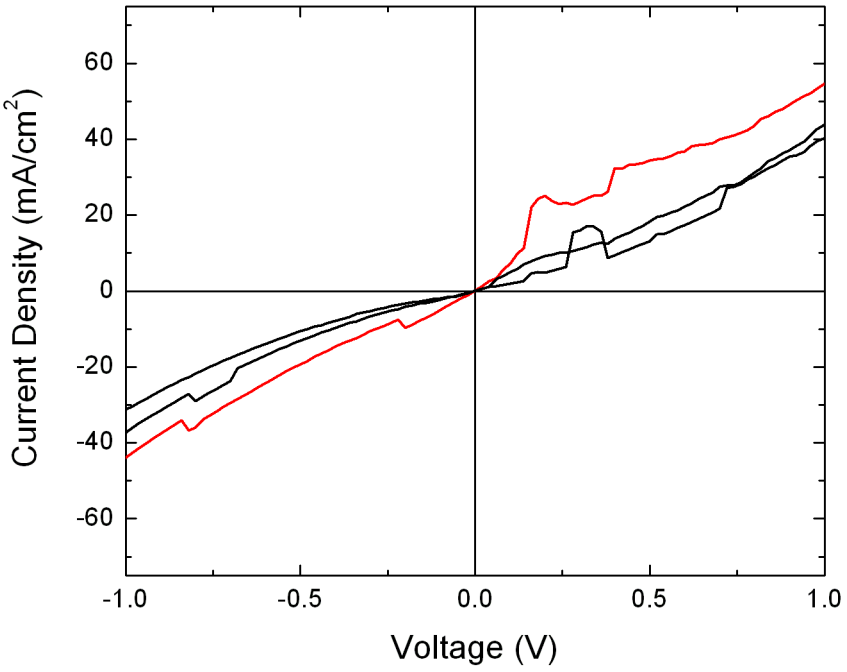

Figure 5.20: Typical IV curves for neat film (black) and blend (red) devices from Bisfluorene under solar simulation.

5.2.5 Cyanine Dyes

The results presented in the previous sections discuss materials that are primarily used for light emission and have a blue or green absorption spectrum. This is undesirable for a high conversion efficiency solar cell. The research towards synthesising redder absorbing materials has progressed relatively well for polymer materials, yielding such polymers as PTPTB [16–18], PDOST [19] and PFDTBT [20,21] (see chapter 4). All of these polymers are designed to absorb lower energy photons because they are more numerous in the solar spectrum. The same approach has

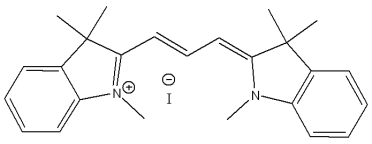

(a) PCD03-10

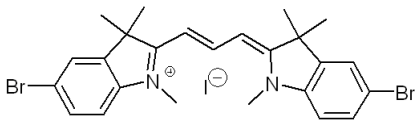

(b) PCD03-18

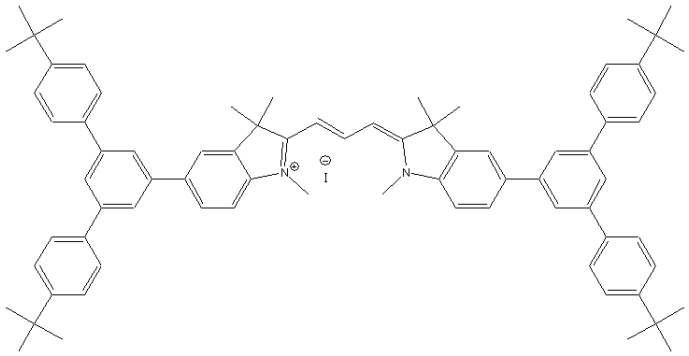

(c) PCD03-19

Figure 5.21: Molecular structures of the Cyanine dye dendrimer materials. The core is the same in all cases.

been taken with a brand new group of conjugated dendrimers. By changing the cores of the dendrimer structure, it has been possible to synthesise materials that absorb red light rather than green or blue. Three novel materials based upon cyanine dyes will be discussed in this section. The results presented here are preliminary and no device optimisation has been performed in any way. Currently, no IUPAC names have been created for these materials so they will be referred to by their batch numbers, PCD03-10, PCD03-18 and PCD03-19. The molecular structures for the new materials are shown in figure 5.21. They progress

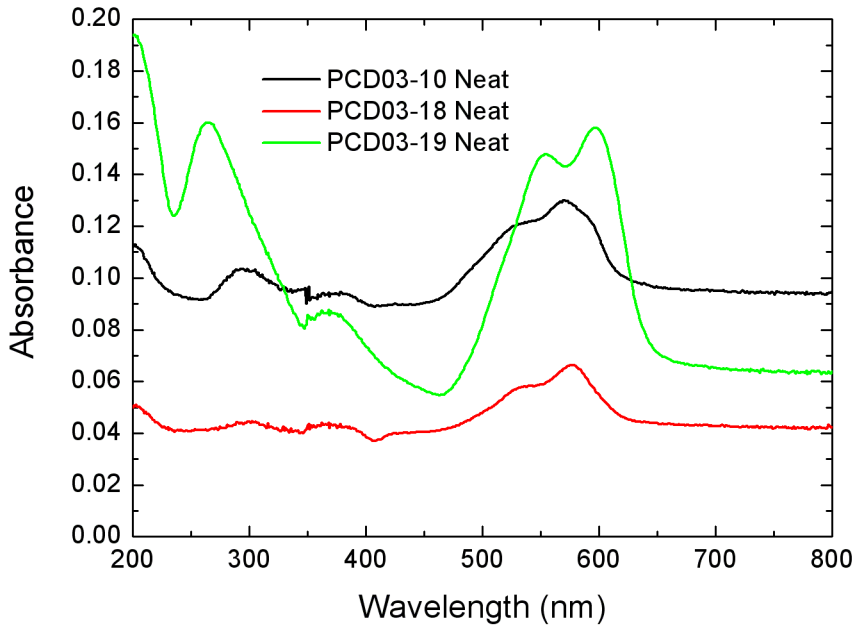

Figure 5.22: Cyanine dye neat film absorbance spectra.

from a simple core structure (PCD03-10) to a full dendrimer (PCD03-19). Preliminary photophysical measurements have been performed for each material. Absorbance spectra for neat films and blends are presented in figures 5.22 and 5.23. From each of these spectra one can see that there is the desired absorption peak in the red part of the spectrum as desired. However, there are a number of issues with the spectra at present.

Firstly, it is obvious that there is a high amount of reflection and/or scattering from the films during the measurement giving rise to the high zero level at around 700 nm. Spectra were measured four times each to verify that they were not bad readings. Unfortunately, Fresnel corrections cannot be applied as the refractive index of the materials is

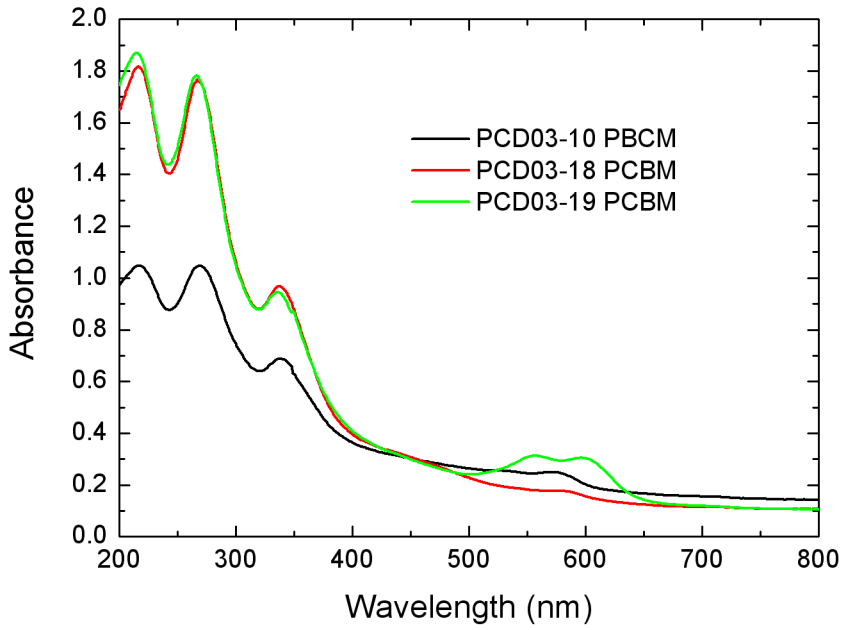

Figure 5.23: Cyanine dye-PCBM blend absorbance spectra.

unknown. Any possible scattering is attributed to the relatively poor quality of the films. The films looked slightly 'foggy' on inspection but this could most likely be solved by changing solvent. For the cyanine dye dendrimers the solvent was chlorobenzene to maintain consistency with device work. Chlorobenzene was chosen as PCBM is most soluble in it compared to other common solvents.

The second issue with the absorption spectra is the relatively low absorbing power of the films. This is attributed to low film thickness (< 30 nm) due to low molecular weight. Higher concentrations could not be readily made due to low amounts (few mg) of supplied material. Nevertheless, the spectra show absorption in the desired part of the spectrum which is

promising for solar cells. PL spectra are shown in figures 5.24 to 5.26

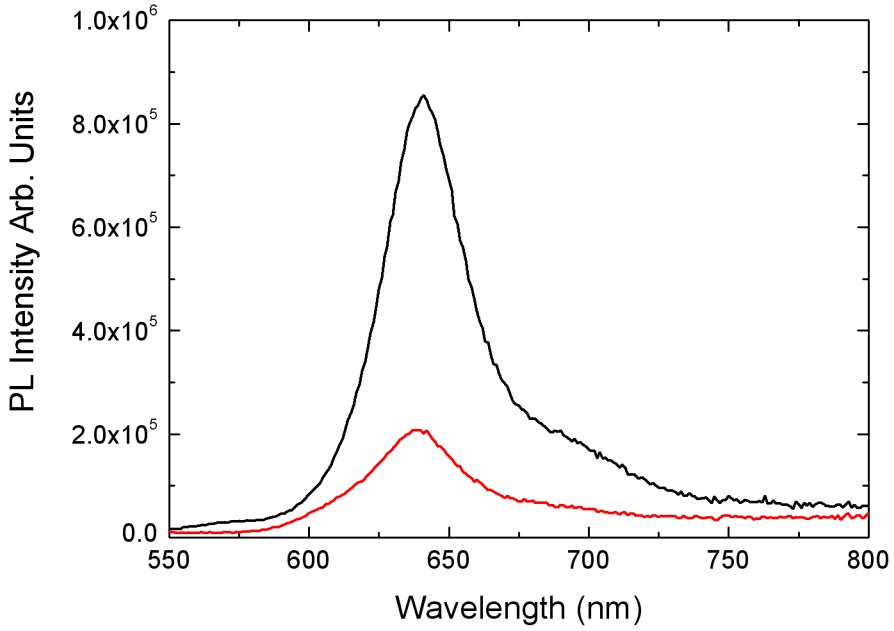

Figure 5.24: PL of PCD03-10 neat films (black) and blend with PCBM (red).

for neat films and blends. The PL spectra show desired attributes for applications in PV devices. Comparing each of the materials one can see that the emission is redder with increasing molecular weight (PCD03-10 increasing to PCD03-19) which is expected due to longer conjugation lengths. In addition, the inclusion of PCBM reduces the PL intensity as expected as the photogenerated excitons will be quenched by the presence of the electron acceptor. This is seen in all cases.

Given the promising results for initial photophysics, the materials were used to make devices. Device structure was as described previously.

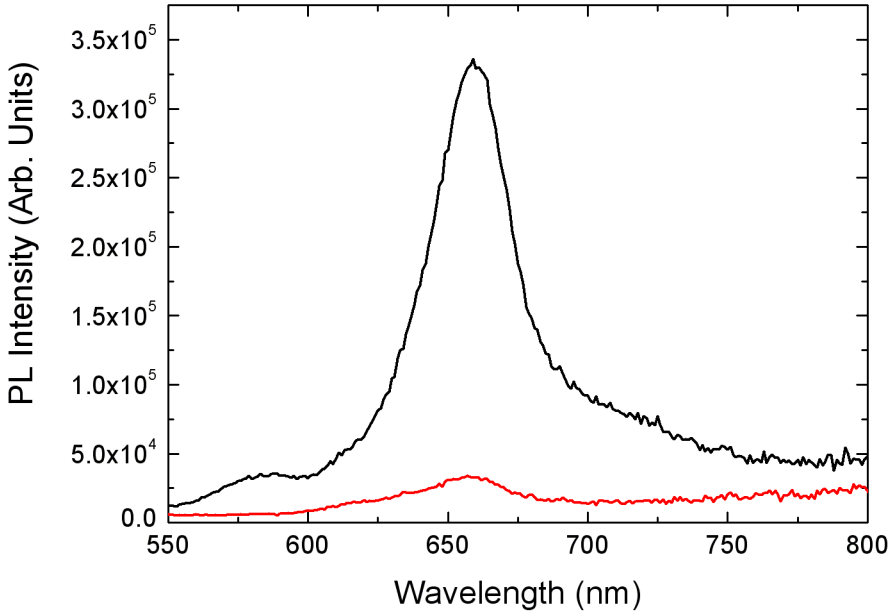

Figure 5.25: PL of PCD03-18 neat films (black) and blend with PCBM (red).

Three combinations of active layer were tried, neat film without a PEDOT layer, neat film with a PEDOT layer and blend with a PEDOT layer. The reason for using PEDOT is its stabilising properties. The presence of PEDOT appears to make the devices more robust, less prone to short circuits and also it appears to increase the open circuit voltage.

Neat film devices had limited performance (as expected and similar to previous dendrimer results) both with and without PEDOT present, although there was a noticeable improvement when PEDOT was used both in short circuit current and open circuit voltage. It was decided that PEDOT would be used with the blends due to this improved performance

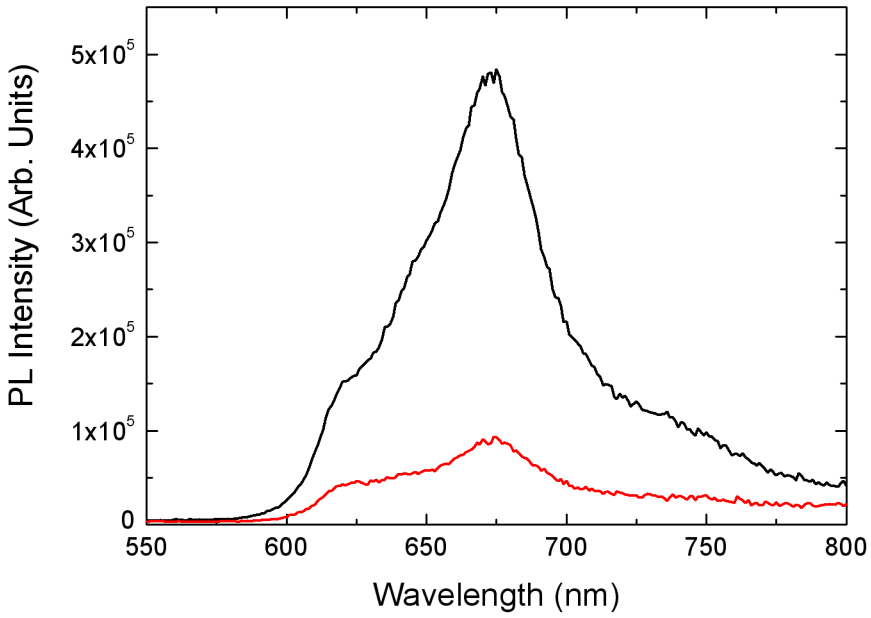

Figure 5.26: PL of PCD03-19 neat films (black) and blend with PCBM (red).

seen with PEDOT. The following figures show IV curves for devices under illumination by solar simulation.

The addition of PCBM to the active layer significantly improved the performance, although there was little change to V_{OC}. This may be dependent upon contact materials or simply a limiting factor of the materials themselves. However, performance was increased by two orders of magnitude, from a few$\times 10^{-4}$% to around 0.01% (comparable with other dendrimer devices). This provides a realistic opportunity for optimisation of device structure and active layer blend concentration. This optimisation however is beyond the scope of this thesis.

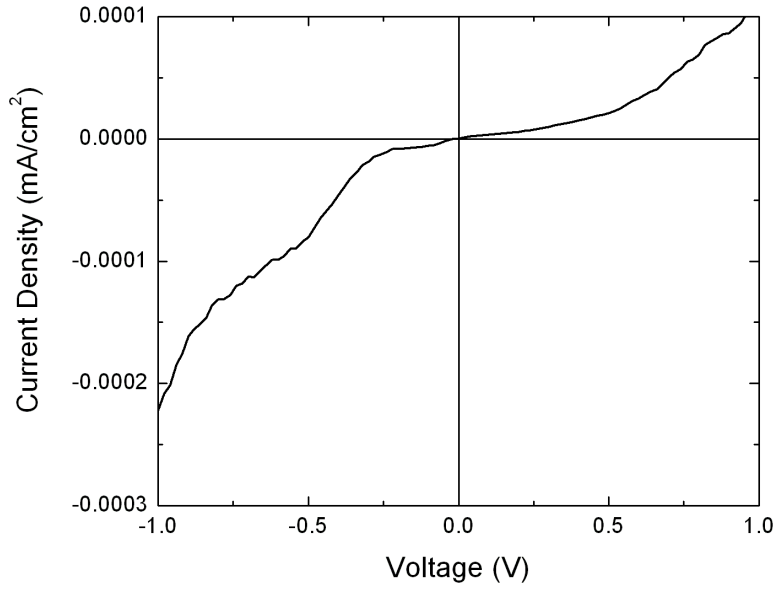

Figure 5.27: IV curves for PCD03-10 neat film devices.

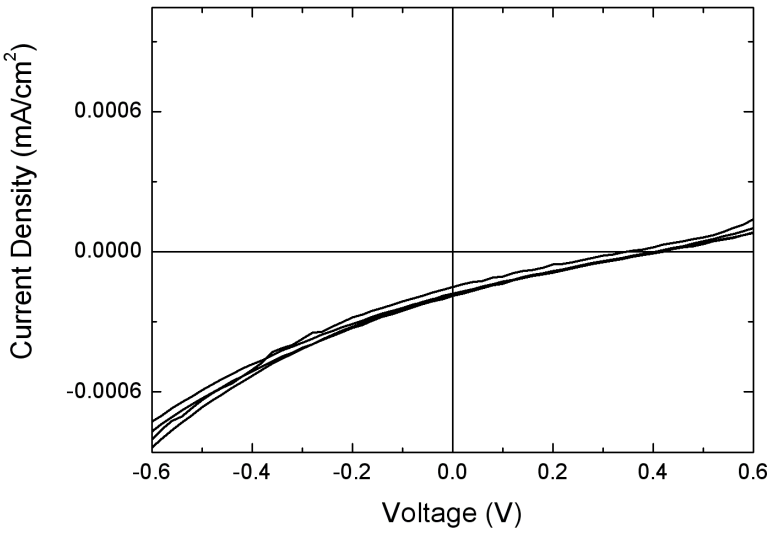

Figure 5.28: IV curves for PCD03-10 neat film devices (PEDOT).

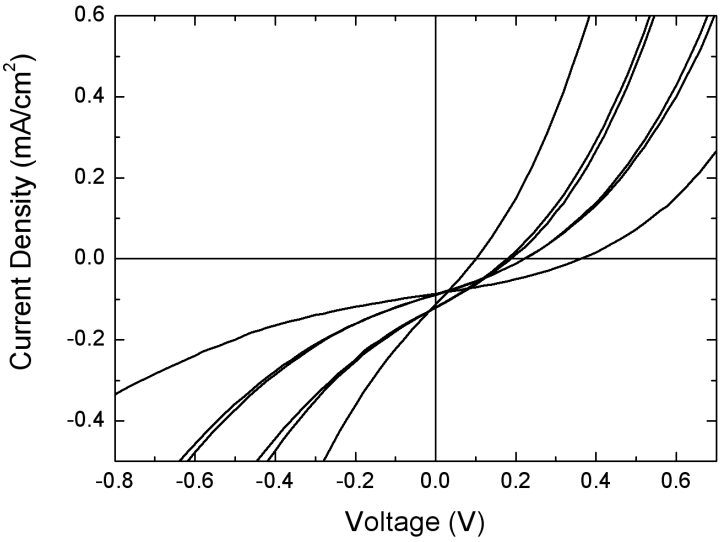

Figure 5.29: IV curves for PCD03-10 blend devices.

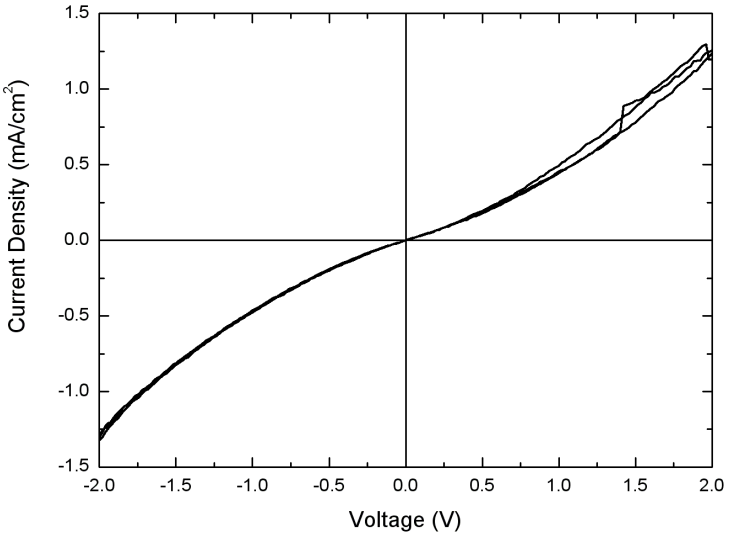

Figure 5.30: IV curves for PCD03-18 neat film devices.

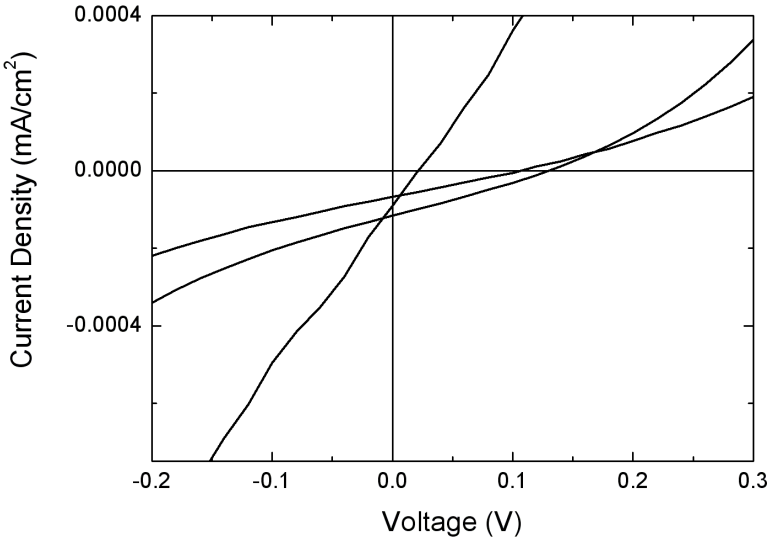

Figure 5.31: IV curves for PCD03-18 neat film devices (PEDOT).

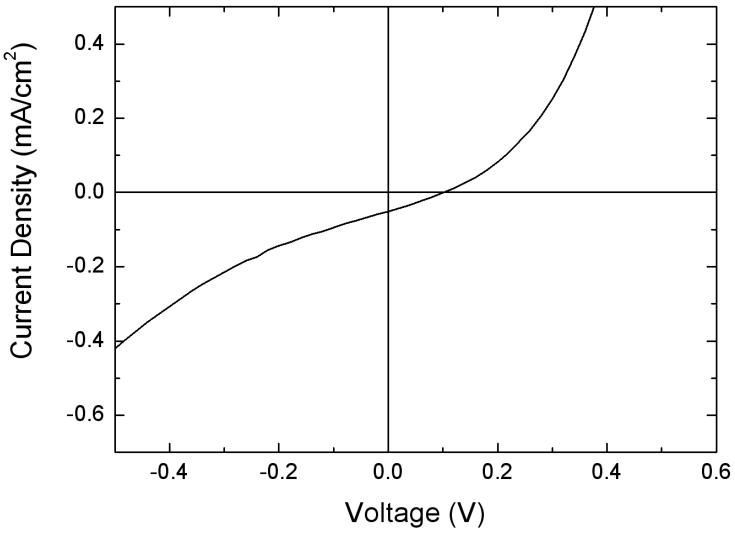

Figure 5.32: IV curves for PCD03-18 blend devices.

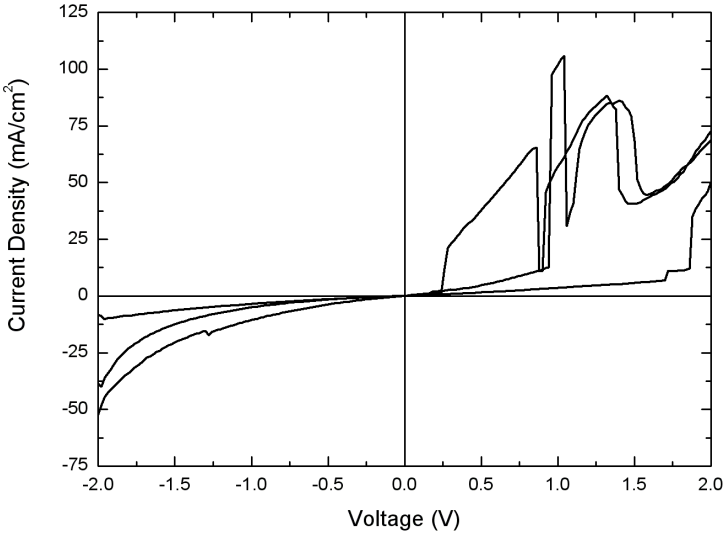

Figure 5.33: IV curves for PCD03-19 neat film devices.

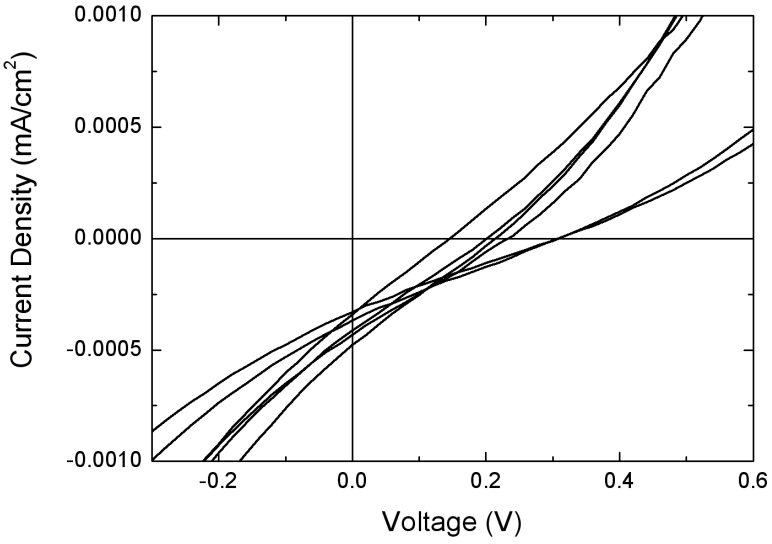

Figure 5.34: IV curves for PCD03-19 neat film devices (PEDOT).

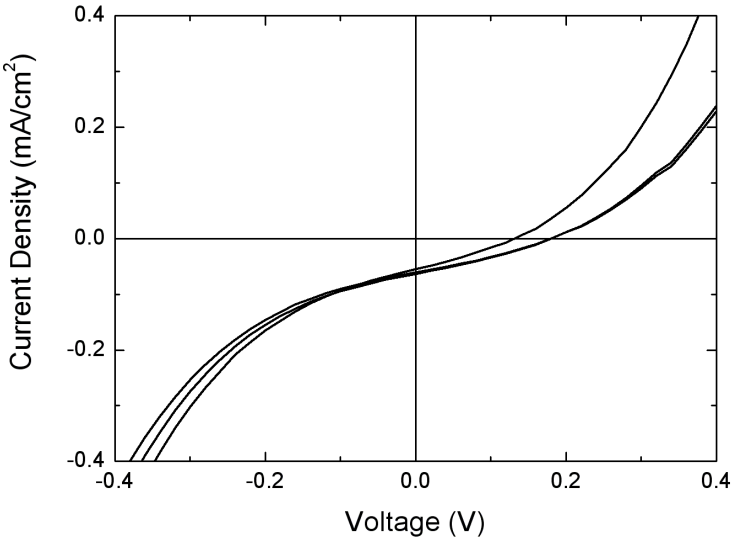

Figure 5.35: IV curves for PCD03-19 blend devices.

General observations for the device curves include the shape and reliability of the curves. Overall performance improved with the addition of PEDOT and the inclusion of PCBM in the active layers. In my experience of fabricating devices, I found a general trend of improvement and stability in devices with the addition of PEDOT. Neat films without PEDOT proved to be difficult to measure as they would quite often short out during, or shortly after, testing. Neat films alone also generally produced a large number of failed devices due to short circuits, although this is most likely linked to thin active layers. Spin coating thicker active layers should improve the device yield. There is also concern over the low value for V_{OC} ($\sim$ 0.2 V) for all devices, even those with PEDOT and PCBM. This will most likely be improved by optimising both blend ratio, film thickness and contact metal choices.

The cyanine dye materials investigated here show promise as potential materials for dendrimer solar cells. Even in these preliminary testing stages, the devices show comparatively good performance. Device efficiencies are still low, approximately 0.01% for blend devices, but this can certainly be improved as discussed above.

5.3 Discussion

For the majority of the dendrimers studied here, there has been an overall degree of success in applying the range of materials to PV devices. It has been especially successful since all of these materials (with the exception of the cyanine dyes) are primarily applied to light emitting roles, rather than light absorption.

For the case of the iridium materials (those based upon $Ir(ppy)_3$) it has been shown that they are both highly efficient at charge separation and transport, a property of the dendrimers that places them as an ideal candidate for solar cell device materials. Currently, the only drawback is that, despite their high internal efficiency, they are limited to the amount of the solar spectrum that is absorbed. Since they are designed to be green emitters, they absorb blue light, which is unsuitable in a PV device. The addition of an electron transporting host is still needed for the IrG1 molecule. This new carbazole molecule also produced high (external) efficiency and is a promising candidate for PV applications. It is conceivable that with the correct choice of core, a molecule could be

synthesised to absorb redder light, whilst keeping the high efficiency of the $Ir(ppy)_3$ dendrimer molecule.

The use of ellipsometry has provided a powerful tool in determining the internal efficiencies of these devices, and also information regarding the optimal device structure. Since the absorbing layers can now be modelled accurately, we can determine how thick a film should be to absorb as much light as possible whilst maintaining charge transport and exciton diffusion properties. In addition, combining the modelling with IPCE measurements provides an accurate estimate of the internal quantum efficiency (APCE) for devices. Currently it has been performed only on IrG1 but the technique could be used upon any material.

Since chlorophyll has been sucessfully providing plants with the means to convert solar energy for millions of years, it would seem that it would be worthwhile to incorporate the same or a similar structure of molecule into a solar cell. This was performed by using a porphyrin ring core (as opposed to $Ir(ppy)_3$). Unfortunately, the results were poor, providing little or no exciton charge separation which ultimately resulted in very low device efficiencies. This was caused by the similar LUMO levels of the active materials. The attempt to increase the LUMO by metallising the core resulted in even worse performance by providing an electon/hole trap resulting in recombination instead of charge separation. In addition, the absorption spectrum for the porphyrin dendrimer was not ideal, despite a significant peak in the green.

The modification and further understanding of materials over the last

few years has given rise to a methodology of synthesising materials for needs. This methodology has been applied here providing a whole new family of dendrimer materials which have been successful when used in PV devices. The cyanine dye materials described above have (although only in preliminary work) been successfully tested as solar cell materials, both in neat film and blended with PCBM. The successful shift in absorption spectrum, whilst keeping the dendrimer structure (core, dendrons and surface groups) provides proof that the dendrimer concept is indeed valid. The materials can be modified to suit a purpose simply by changing the core without changing the processability.

5.4 Summary

This chapter has introduced a number of dendrimer materials and shown that they are suitable for use as solar cell materials. Dendrimers have been shown to be highly efficient ($> 90\%$) at charge separation and subsequent transport, verified by APCE measurements. Porphyrin materials have been investigated but proved unsuccessful due to charge trapping on the dendrimer. A new group of dendrimers has been introduced, based upon cyanine dyes. They show potential to be excellent PV materials due to their suitable absorption spectra and (in dendrimer form) could be highly internally efficient similar to the IrG1 dendrimer.

References

[1] C.J. Brabec, N.S. Sariciftci, and J.C. Hummelen, *Advanced Functional Materials* **11**, 15 (2001).

[2] M.A. Baldo, S. Lamansky, P.E. Burrows, M.E. Thompson, and S.R. Forrest, *Applied Physics Letters* **75**, 4 (1999).

[3] K.A. King, P.J. Spellane, and R.J. Watts, *Journal of the American Chemical Society* **107**, 1431 (1985).

[4] M. Halim, J.N.G. Pillow, I.D.W. Samuel, and P.L. Burn, *Advanced Materials* **11**, 371 (1999).

[5] J.P.J. Markham, *Highly Efficient Dendrimers and Polymers for Solution Processed Organic Light Emitting Diodes*, PhD thesis, University of St. Andrews, 2003.

[6] M. Halim, J.N.G. Pillow, I.D.W. Samuel, and P.L. Burn, *Synthetic Metals* **102**, 1113 (1999).

[7] J.M. Lupton, *Nanoengineering of Organic Light-Emitting Diodes*, PhD thesis, University of Durham, 2000.

[8] J.M. Lupton, I.D.W. Samuel, M.J. Frampton, R. Beavington, and P.L. Burn, *Advanced Functional Materials* **11**, 287 (2001).

[9] M.J. Frampton, S.W. Magennis, J.N.G. Pillow, P.L. Burn, and I.D.W. Samuel, *Journal of Materials Chemistry* **13**, 235 (2003).

[10] J.N.G. Pillow, M. Halim, I.D.W. Samuel, and P.L. Burn, *Macromolecules* **32**, 5985 (1999).

[11] P.L. Burn, Private Communication.

[12] S.C. Lo, N.A.H. Male, J.P.J. Markham, S.W. Magennis, P.L. Burn, O.V. Salata, and I.D.W. Samuel, *Advanced Materials* **14**, 975 (2002).

[13] J.P.J. Markham, S.C. Lo, S.W. Magennis, P.L. Burn, and I.D.W. Samuel, *Applied Physics Letters* **80**, 2645 (2002).

[14] T.D. Anthopoulos, J.P.J. Markham, E.B. Namdas, I.D.W. Samuel, S.C. Lo, and P.L. Burn, *Applied Physics Letters* **82**, 4824 (2003).

[15] J.S.C. Prentice, *Journal of Physics D: Applied Physics* **32**, 2146 (1999).

[16] D. Muhlbacher, H. Neugebauer, A. Cravino, N.S. Sariciftci, J.K.J. van Duren, A. Dhanabalan, P.A. van Hal, R.A.J. Janssen, and J.C. Hummelen, *Molecular Crystals and Liquid Crystals* **385**, 205 (2002).

[17] C. Winder, G. Matt, J.C. Hummelen, R.A.J. Janssen, N.S. Sariciftci, and C.J. Brabec, *Thin Solid Films* **403-404**, 373 (2002).

[18] C.J. Brabec, C. Winder, N.S. Sariciftci, J.C. Hummelen, A. Dhanabalan, P.A. van Hal, and R.A.J. Janssen, *Advanced Functional Materials* **12**, 709 (2002).

[19] L. Goris, M.A. Loi, A Cravino, H. Neugebauer, N.S. Sariciftci, I. Polec, L. Lutsen, E. Andries, J. Manca, L. DeSchepper, and D. Vanderzande, *Synthetic Metals* **138**, 249 (2003).

[20] M. Svensson, F. Zhang, S.C. Veenstra, W.J.H. Verhees, J.C. Hummelen, J.M. Kroon, O. Inganäs, and M.R. Andersson, *Advanced Materials* **15**, 988 (2003).

[21] R.A.J. Janssen, J.C. Hummelen, and N.S. Sariciftci, *Materials Research Society Bulletin* **30**, 33 (2005).

Chapter 6

Exciton Transport in Organic Films

6.1 Introduction

The absorption of light in a photovoltaic device is essential to its operation. Absorbing light generates singlet excitons. Since thin film devices (as described in chapters 3, 4 and 5) are excitonic in operation [1–3] it is desirable to understand the behaviour of these excitons in order to further optimise devices and materials. The transport (or diffusion) of excitons within a solar cell device is important for efficient operation. Once an exciton has been created, it is then (relatively) free to move about the film provided it is energetically favourable for it to do so. This can be done in a number of ways; including intrachain transport and interchain hopping. This diffusion process will continue until the exciton decays or gets trapped. The decay process can either be radiative, releas-

ing a (lower energy) photon, or non-radiative producing phonons (heat). For the case of solar cells, neither of these events is desired so it is important to harvest excitons before they decay. This is performed by the separation of charges by overcoming the Coulombic binding energy of the exciton, which is generally accepted to lie between 0.3 and 1 eV [4–6] for conjugated polymer films, although lower values have been reported [7]. Because of this, charge separation generally occurs at an interface with an acceptor, which can either be a layer of organic or inorganic semiconductor [8] or dispersed molecules with a different ionisation and/or electron affinity [9].

For photovoltaic devices it is essential to convert excitons into charge carriers, so the transport (by diffusion) of excitons to the heterojunction is a very important step in the operation of an organic solar cell. Excitons are able to move about within a film as long as energetically possible. For the polymers studied in this work, this energy transfer is thought to be Förster transfer. The progression of an exciton through a film is known as diffusion, and the mean length of this motion is known as the *exciton diffusion length*, defined as L_d.

This characteristic length has been investigated here using two different approaches. By investigating diffusion to a quencher, it is possible to determine the diffusion length by measuring the photoluminescence lifetime of a conjugated polymer film. As film thicknesses decrease, there will be less distance for excitons to diffuse and a corresponding higher probability that they will encounter the quenching layer. This will then reduce the fluorescence lifetime of the material. Measuring the lifetime

in a material can yield information about many of its properties such as the diffusion coefficient, D, which in turn can be used to find the exciton diffusion length, L_d.

There is an alternative way to measure exciton diffusion by studying exciton-exciton annihilation (or exciton fusion). Exciton-exciton annihilation occurs when two excitons in close proximity (within an annihilation or reaction radius) combine, forming a higher excited state, which relaxes quickly to the lowest excited state. As a result, one exciton is lost into heat. This density is usually greater than $\sim 10^{17}$ cm^{-3} [10–13], although this does vary between materials. Annihilation leads to a quenching of excitons, resulting in non-radiative decay and a reduction of the density. This is obviously detrimental to the operation of a solar cell where as many excitons as possible are required to be harvested.

This chapter will focus upon the calculation and determination of exciton properties for two polymers using high resolution (5 ps) TRL spectroscopy. This approach has been successfully applied to diffusion length measurements for the first time here, yielding very promising results.

I would like to thank Olivier Gaudin for ellipsometry measurements to obtain the absorption coefficient for MEH-PPV.

6.2 Exciton-Exciton Annihilation

Exciton-exciton annihilation is an important process in determining interactions between excited states within materials [10–12, 14–17]. It can also yield information regarding temporary states within materials as a result of excitation [18]. It has previously been used to determine the exciton diffusion coefficient in light emitting conjugated dendrimers [19]. Understanding the charge transfer processes that occur in a device is key to optimisation, especially in PV devices containing more than one materal [20, 21]. It is generally interactions at interfaces, such as those in devices, that cause a significant build up of charges and excitons.

The interaction between excitons during annihilation is similar to that of Förster transfer. Dipoles oscillate, inducing an ocsillation in their neighbouring molecules. The timescale of this transfer is generally accepted

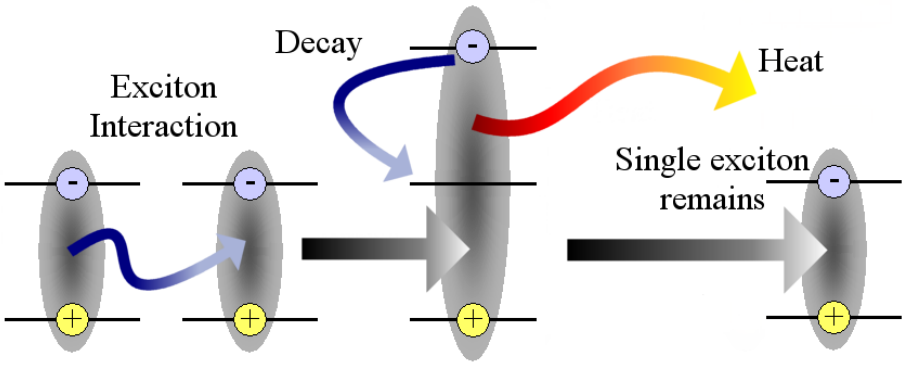

Figure 6.1: Schematic showing the process involved in exciton-exciton annihilation. Excitons interact forming a doubly excited state which relaxes resulting in a single exciton and phonons.

to be significantly faster (10-100 fs) than that of a standard Förster interaction [22] of 1-3 ps [13]. This interaction between excitons provides

a non-radiative decay route, removing the chance for exciton diffusion to a heterojunction. Annihilation involves two excitons in close proximity (within an annihilation or reaction radius), usually on neighbouring molecules. Figure 6.1 shows a schematic of the process. The oscillation further stimulates an already oscillating dipole (exciton) transferring its energy to produce a doubly excited state. This higher state then relaxes non-radiatively resulting in a single exciton. The energy is lost as phonons (heat).

The initial interaction can be described by the equation 6.1 where two excitons interact resulting in a doubly excited state and a ground state species. Excited species are denoted by a star. Degrees of excitation are denoted by subscripts.

$$S_1^* + S_1^* \rightarrow S_0 + S_n^* \tag{6.1}$$

The system then decays via the following route, resulting in a single exciton and phonon interaction.

$$S_n^* \rightarrow S_1^* + phonons \tag{6.2}$$

This process can be investigated through time-resolved spectroscopy in order to determine how the exciton decay varies with excitation density. As an exciton relaxes it emits a photon, which can be detected. If it is forced to recombine non-radiatively, there will be no emission and this will affect the fluorescence lifetime, reducing it. The greater the concentration of excitons, the more annihilation there will be and consequently there will be a more significant reduction in PL lifetime. This rate of

decay of excitons can be described by the following rate equation:

$$\frac{dn(t)}{dt} = -\kappa n(t) - \gamma n(t)^2 \tag{6.3}$$

which has solution for time independent γ

$$n(t) = \frac{n(0)\exp(-\kappa t)}{1 + \frac{\gamma}{\kappa} n(0)[1 - \exp(-\kappa t)]} \tag{6.4}$$

where $n(t)$ is the number of excitons at time t, κ is the decay rate with no annihilation and γ is the desired annihilation constant. This can be rearranged into a linear form for ease of plotting, shown in equation 6.5. These equations are also discussed in reference [11].

$$\frac{1}{n(t)} = \left[\frac{1}{n(0)} + \frac{\gamma}{\kappa}\right] \exp(-\kappa t) - \frac{\gamma}{\kappa} \tag{6.5}$$

Fluorescence lifetime measurements were performed as described in chapter 3. Samples were illuminated with varying laser powers to provide a number of different intensities, consequently producing a range of excitation densities. Laser spot sizes were measured using a variable slit at 10 μm intervals. Powers were recorded for each slit size for the upsweep and downsweep to ensure consistency. The normalised intensity peak after time zero was used to calculate $n(0)$ and all subsequent values of $n(t)$ since PL intensity is proportional to exciton density, $n(t)$ [19]. In order to achieve sufficient intensities, the output of a regenerative amplifier was used to excite the sample. The excitation beam used was at 400 nm with a repetition rate of 50 kHz. Excitation densities were calculated using

the following relation:

$$n(0) = \frac{4}{\pi r^2}\frac{\lambda}{hc}\frac{P(1-10^{-A})}{zr_{rep}} \tag{6.6}$$

where P is the average laser power used, λ is the wavelength of light, z is the film thickness, r is the diameter of the spot, A is the absorbance of the film at λ and r_{rep} is the repetition rate of the laser. Film thickness was measured using a dektak profilometer and checked using the measured absorbance spectrum and measured absorption coefficient. Due to the low film thickness and low absorption at 400 nm, it was assumed that there was uniform excitation of the samples.

6.2.1 Annihilation Constant of MEH-PPV

The use and study of MEH-PPV as a polymer is quite extensive, including LEDs [23], solar cells [24] and optically pumped polymer lasers [25]. Consequently, it is extremely beneficial to understand the processes involved in this polymer in order to enhance devices fabricated with it. Previously reported studies have shown a one-dimensional diffusion length of the exciton in MEH-PPV films in the range of 6-14 nm [26–28] using interface quenching methods. This variation can be explained to some extent by different morphology of bulk films and interfaces used in these studies as well as by different lifetime of the mobile intra-chain excitons. Excitation intensity dependent exciton lifetime has been reported in MEH-PPV films [17], but quantitative estimates of annihilation parameters were not given.

This section presents quantitative studies of exciton-exciton annihilation in MEH-PPV films using time resolved photoluminescence (PL). PL kinetics can be described with a time independent annihilation rate, which provides information on exciton diffusion in the bulk MEH-PPV films without the complexity of surface effects.

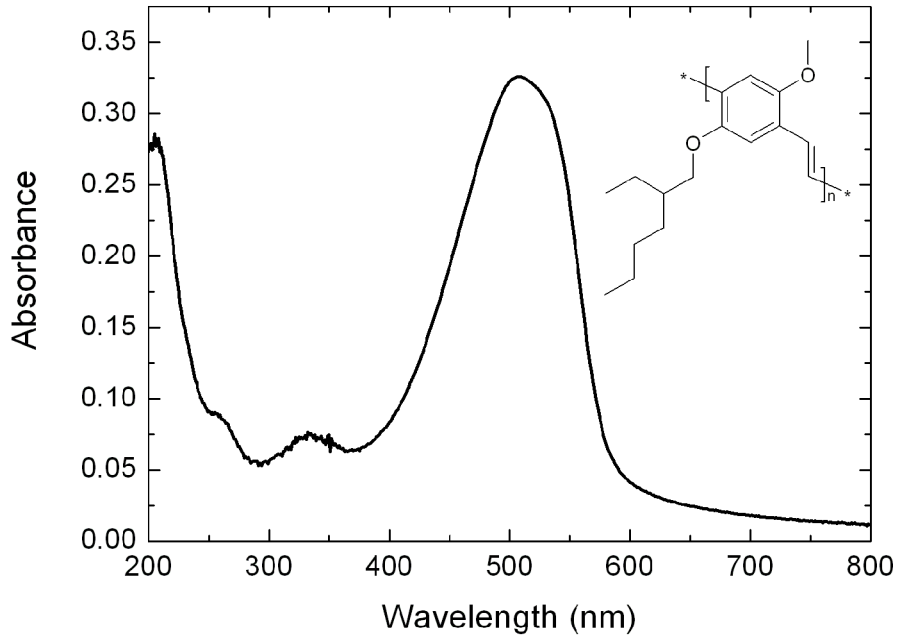

Figure 6.2: Absorbance spectrum of MEH-PPV. The absorbance was used to calculate the film thickness combined with ellipsometry data. The molecular structure of MEH-PPV is shown in the inset.

The measured PL lifetime in an MEH-PPV film at low excitation density ($< 10^{17}$ cm^{-3}) for these experiments was approximately 140 ps. This is consistent with previous literature work by Hayes *et al.* [29]. Film thickness was calculated from the measured absorbance (see figure 6.2) using an absorption coefficient determined by ellipsometry. A thin film of

35 nm was used to ensure no amplified spontaneous emission (ASE) was present, which could add a further decay channel for excitons [30]. Excitation was by 100 fs pulses at 400 nm with a repetition rate of 50 kHz. Emission detection was integrated over the spectral range of 550-680 nm using a synchroscan streak camera. The instrumental response function was $\sim$ 5 ps (FWHM). Excitation spot size was measured to have a diameter of 0.5 mm at $1/e^2$ of the maximum intensity and the excitation density ranged from 1.7×10^{16} cm^{-3} to 1.5×10^{18} cm^{-3} (assuming one absorbed photon produces one exciton). The absorbance of the 35 nm thick film at 400 nm is 0.086 (see figure 6.2), so the exciton density is essentially uniform through the film. A graph containing a number of repre-

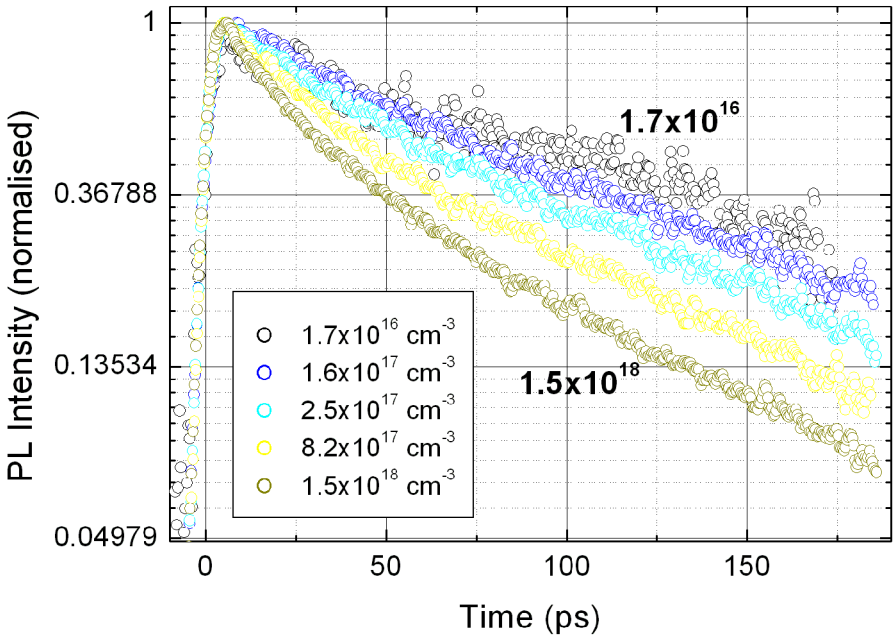

Figure 6.3: Time-resolved decay of MEH-PPV at a range of incident excitation densities. Lifetime decreases with increasing excitation density. Not all intensities used have been displayed for clearer viewing.

sentative PL decay curves is shown in figure 6.3. Curves are labelled

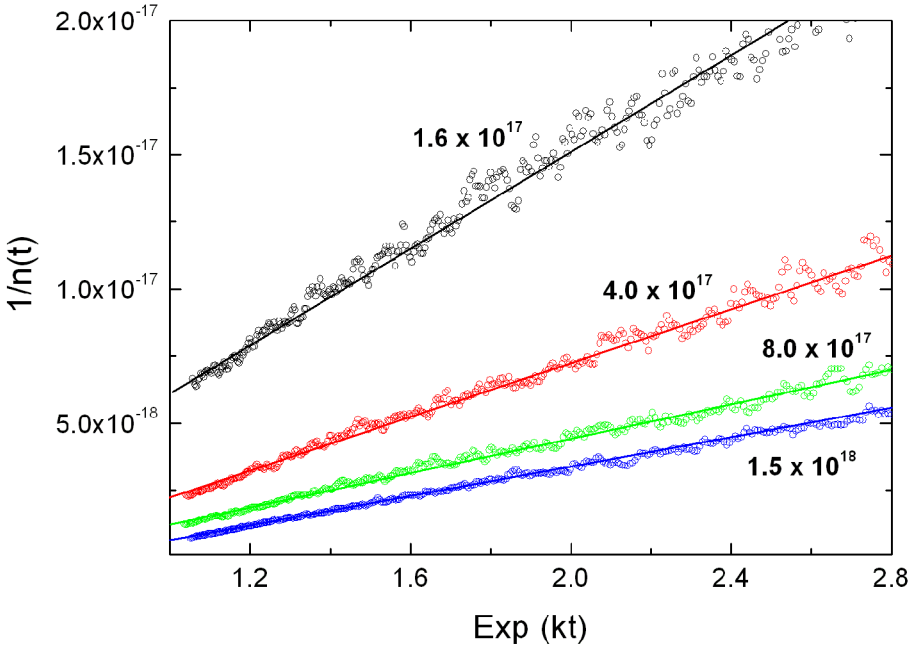

Figure 6.4: A representative range of linearised results of the measured PL decays for MEH-PPV. All lines had negative intercepts and the gradients were used to calculate γ as it was more reliable. Excitation densities are shown in cm^{-3}.

according to excitation density. As the excitation density is increased, the decays become progressively faster due to exciton-exciton annihilation. Once exciton density drops off below threshold levels, the decay proceeds monoexponentially, as expected. These decay curves were then linearised using equation 6.5. The results for this analysis are shown in figure 6.4. Annihilation constants were calculated from the gradient of each curve as this is more reliable than using the y-intercept. All intercepts were negative, as desired. Equation 6.3 predicts linear dependence of $1/n(t)$ vs $\exp(\kappa t)$, which is indeed verified in figure 6.4. The slope of these linearised curves gives the singlet-singlet annihilation rate for the

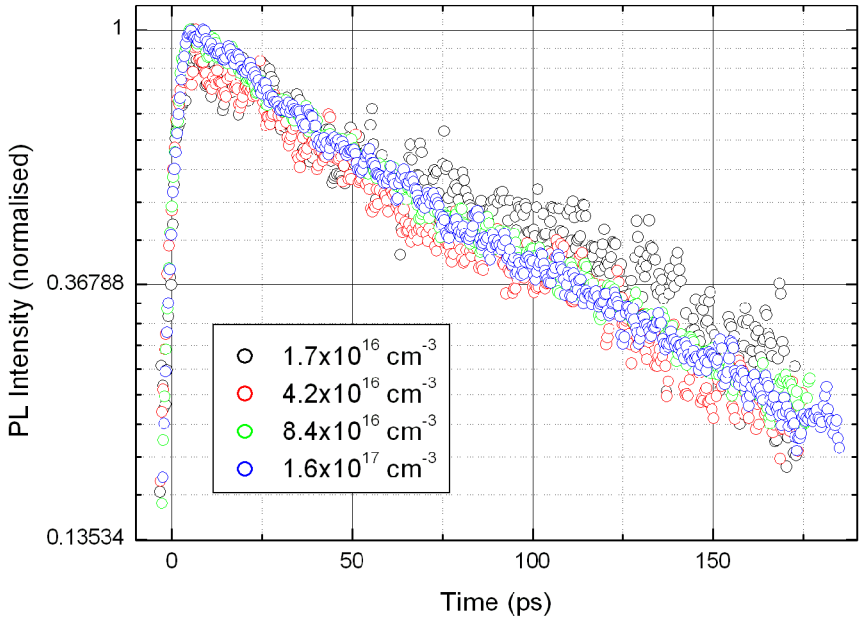

Figure 6.5: Curves show TRL decay for the lowest excitation densities used for MEH-PPV annihilation measurements. It is clear that there is little difference seen between the four, showing the onset of annihilation at approximately 1.6×10^{17} cm^{-3}.

MEH-PPV film.

It was noticed that there was little difference in lifetimes for excitation densities lower than 1.6×10^{17} cm^{-3}. This was then seen as the lowest limit for the excitation density required for annihilation to occur. Figure 6.5 shows the lowest excitation densities used to demonstrate this observation. Figure 6.6 shows the results for calculated annihilation constants for densities above 1.6×10^{17} cm^{-3}. One can see quite clearly that it is very consistent up to 5×10^{17} cm^{-3}. The annihilation constant was calculated to be $\gamma = (2.8 \pm 0.5) \times 10^{-8}$ cm^{3}s^{-1} due to the consistency of the results. This is comparable to previous work on PPV, which

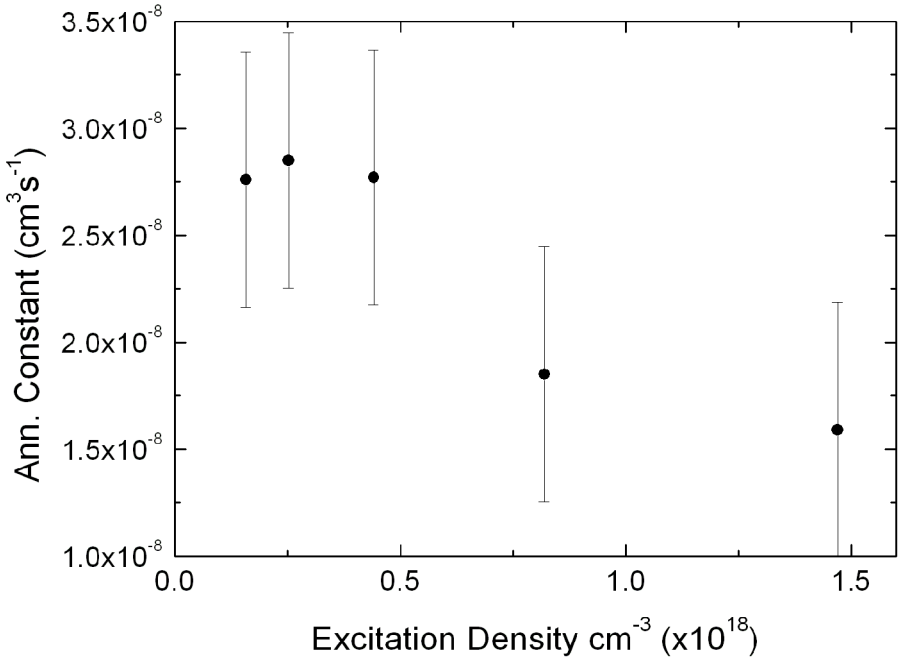

Figure 6.6: Final results for the values of γ obtained for each excitation density. Densities where annihilation was not observed ($n(0) < 10^{17}$ cm^{-3}) are not displayed.

quotes $\gamma = 4 \times 10^{-8}$ cm^{3}s^{-1} at 275 K [12]. There is an apparent reduction of the annihilation constant at higher excitation densities, which can be explained by the non-resolved PL decay due to rapid annihilation of excitons generated within the annihilation (reaction) radius. Neglecting this effect overestimates the initial exciton density used to calculate the annihilation rate, which then results in lower values of γ. The fact that annihilation kinetics fit well with time independent γ indicates that exciton diffusion is three-dimensional in MEH-PPV films [6]. The relationship between the diffusion length and the annihilation constant will be discussed further in section 6.4.

6.2.2 Annihilation Constant of P3HT

P3HT has recently become a potential material for photovoltaic devices due to its suitable absorption spectrum [31]. Device efficiency within a blend rose from $\sim$0.2% for untreated devices to over 3% for thermally annealed devices [32, 33].

Due to these results, it is therefore important to understand the interactions within this material. The need for thermal annealing presents the possibility that there exists different processes within P3HT compared to MEH-PPV due to a possible phase or structure change upon heating. The observation of exciton-exciton annihilation is one way of characterising these interactions. Results are now presented for P3HT showing data gathered from TRL spectroscopy measurements and subsequent analysis using the theory described in the previous sections.

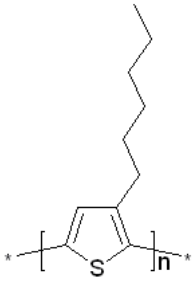

Figure 6.7: Molecular structure of P3HT.

The molecular structure of P3HT is shown in figure 6.7. Excitation densities ranged from approximately 2.3×10^{16} cm^{-3} to 1.0×10^{18} cm^{-3}. Excitation was by 100 fs pulses at 400 nm with a repetition rate of 50 kHz.

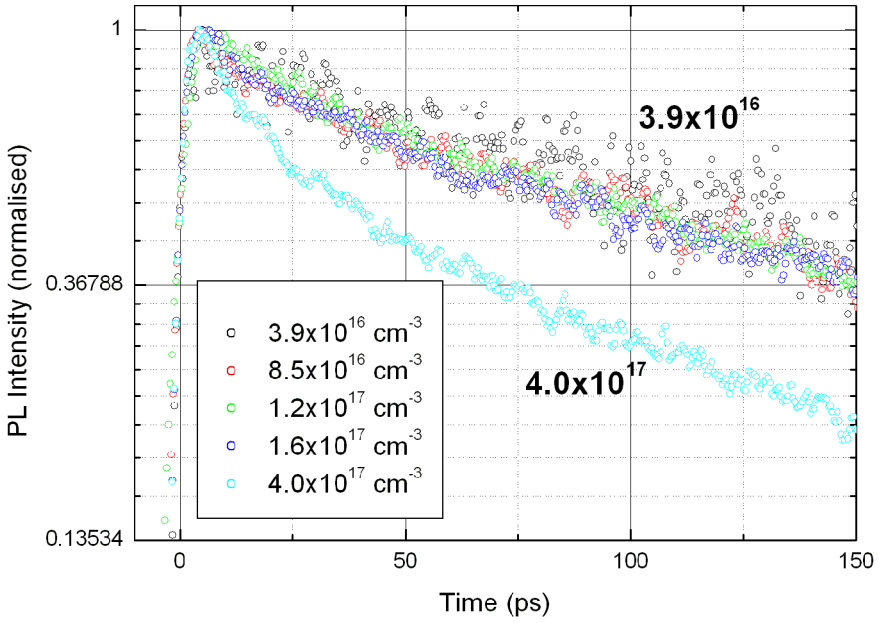

Figure 6.8: Time-resolved decay of P3HT at a range of incident excitation densities. Lifetime decreases with increasing power. Not all results have been displayed for ease of viewing.

Emission detection was integrated over the spectral range of 580-710 nm using a synchroscan streak camera. The instrumental response function was $\sim$ 5 ps (FWHM). Excitation spot size was measured to have a diameter of 0.5 mm at $1/e^2$ of the maximum intensity. Film thickness was measured to be 191 nm using a Dektak profilometer. This value can be confirmed by calculating the thickness from the absorbance spectrum and using the absorption coefficient. This has been measured by Al-Ibrahiam *et al.* [34] to be $\sim 3 \times 10^4$ cm^{-1} at 400 nm. This yields an estimated film thickness of $\sim$ 183 nm.

A graph containing a number of representative PL decay curves is shown

in figure 6.8. It is evident that lifetime decreases with increasing excita-

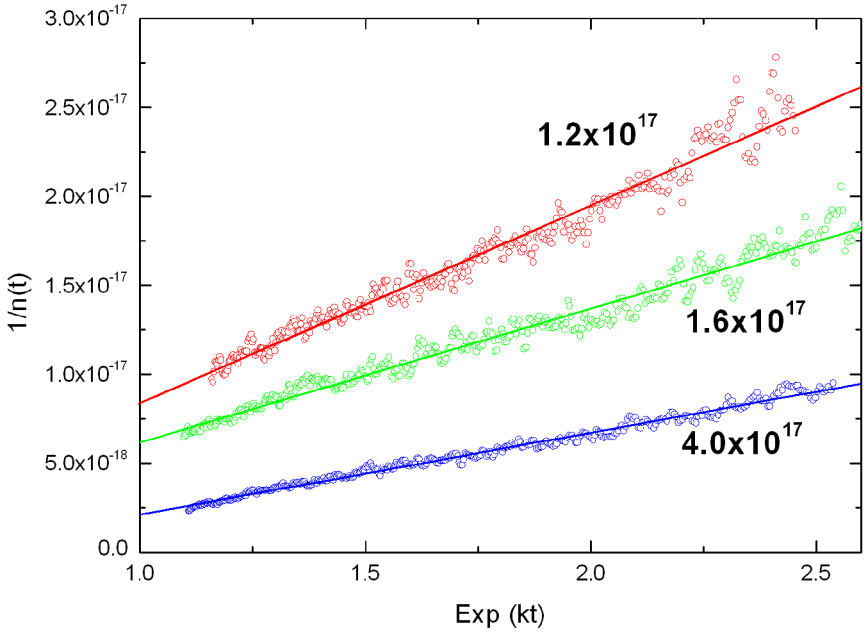

Figure 6.9: Representative curves showing results from P3HT annihilation linearisation. All y-intercepts were negative, as desired. Densities shown are in cm^{-3}

tion. This is due to exciton density increasing to the point where annihilation becomes dominant in the decay process. It is also noticed that annihilation does not begin until excitation densities reach approximately 1.2×10^{17} cm^{-3} because all lower intensities are of similar lifetime. This is a similar density to that in MEH-PPV for annihilation to occur. The decay curves above 1.2×10^{17} cm^{-3} were then linearised using equation 6.5. Figure 6.10 shows low intensity PL decays for P3HT. This demonstrates that there is no annihilation occurring at low intensity. These low power results have been ignored for the calculation of the annihilation coefficient. The results for linearisation are shown in figure 6.9. Annihilation

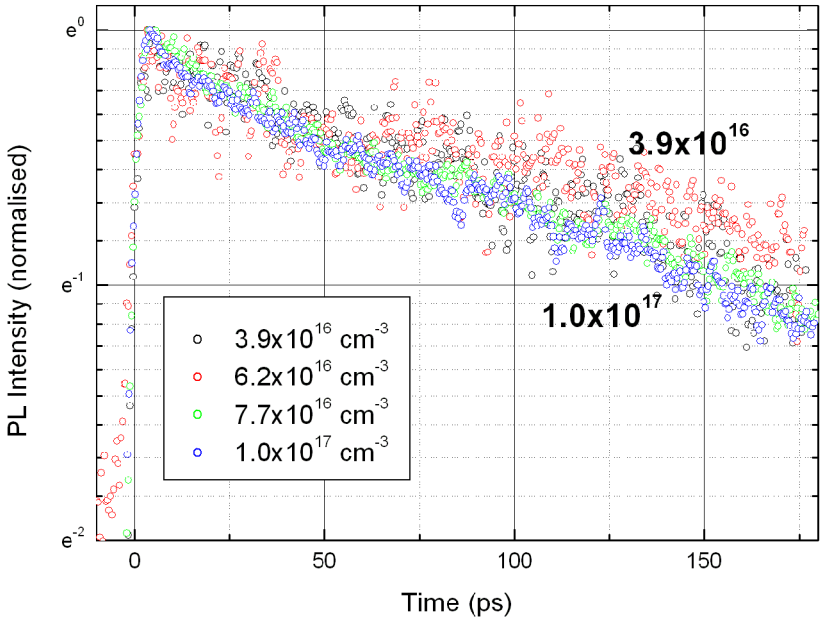

Figure 6.10: Low intensity PL decay curves for P3HT. Curves show TRL decay for the lowest powers used for annihilation measurements. It is clear that there is little difference seen between the curves.

constants were calculated from the gradient of each curve as this is more reliable than using the y-intercept. Figure 6.11 shows the results for calculated annihilation constants for excitation densities 1.2×10^{17} cm^{-3} and above. From the linearised results, the annihilation constant is found to be $\gamma = (1 \pm 0.5) \times 10^{-8}$ cm^{3}s^{-1} for P3HT. This is in very close agreement to previous work on P3HT which quotes $\gamma = 2.3 \times 10^{-8}$ cm^{3}s^{-1} from conductivity measurements [35]. The small difference arises from the fact that literature result was not time resolved. This would lead to the possibility of the annihilation constant being overestimated as charge recombination would not be taken into account.

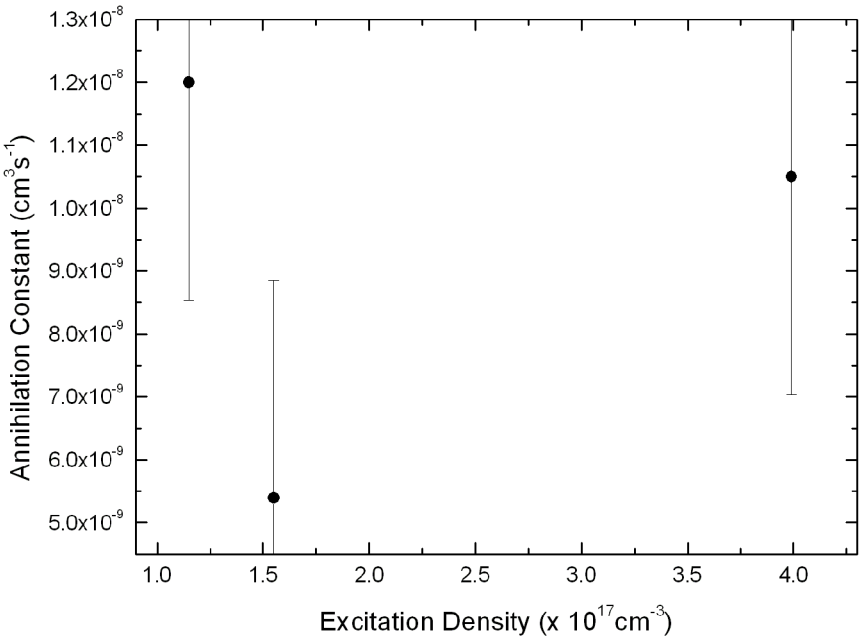

Figure 6.11: The variation of γ with incident power for P3HT. There is a fairly consistent result for most incident powers.

The results for exciton-exciton annihilation and how the annihilation constant can be related to the diffusion coefficient, D, and the diffusion length, L_d, will be discussed in section 6.4, after the interface quenching experiments have been presented.

6.3 Time-Resolved Determination of Exciton Diffusion Length

There have been many studies into the exciton diffusion length of organic materials, ranging from PPV and its various derivatives [26, 27, 36–38] through other materials such as phthalocyanines [39], phosphorescent dendrimers [19], perylenes [40, 41] and polythiophenes [35, 42, 43]. The results generally yield diffusion lengths lying in the range 2-20 nm. This length is obviously dependent upon material. Until very recently, all of these measurements have been performed under steady state. This approach has the advantage of being straightforward, but lacks any power to resolve short timescale events such as recombination or annihilation effects. Most recently, Markov *et al.* [44] have performed time-resolved measurements but these are low resolution (performed by Time Correlated Single Photon Counting, TCSPC) which lacks the ability to detect ultrafast events. The approach taken in this thesis uses ultrafast techniques to resolve these short timescale events and shows that there are factors that affect the lifetime of a material, for example the film thickness, that must be taken into account when analysing the data. The work described here uses ITO as a quenching layer and PL lifetime was measured with a streak camera, as described in chapter 3.

Samples were prepared as detailed in chapter 3. Film thicknesses were varied by varying solution concentration and spin speed. Concentrations used ranged from 6 mg/ml to 3 mg/ml for MEH-PPV and from 25 mg/ml to 3 mg/ml for P3HT. Films were spun onto silica substrates as refer-

ences and onto ITO coated glass under the same conditions. In these experiments, ITO was used as a quencher as it would not diffuse into the polymer layer. This has been found to occur in deposited layers of C_{60} which leads to an overestimation of the diffusion length [36]. Samples were excited with 0.5 mW of 400 nm laser light with a repetition rate of 80 MHz. This was chosen to ensure low excitation densities (with low peak power) so that no ASE or annihilation would occur to affect the decays. To test that there were no effects from the quartz substrates, a

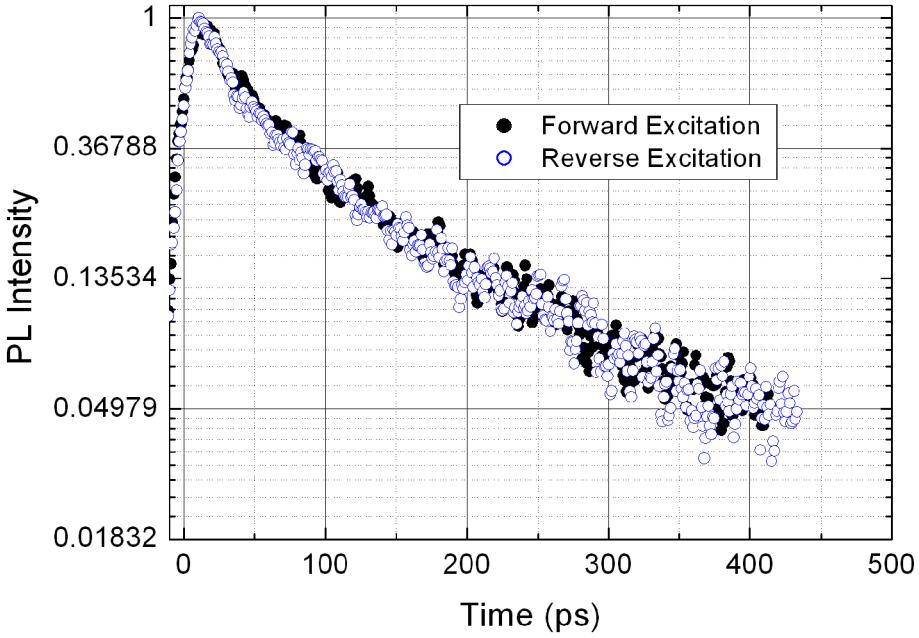

Figure 6.12: Decay curves showing the result of different orientations of a test sample of P3HT. One can see there is no difference between direct film excitation and excitation through the substrate.

test sample ($\sim$ 100 nm) of P3HT was excited from both sides. The decays are shown in figure 6.12. Excitation in this case was at 485 nm as this was close to the absorption maximum of P3HT. This would provide

a much greater excitation density difference (90%) between each edge of the film. There is no observed difference in decay lifetime, indicating that there is no (or identical, which is unlikely) quenching from the quartz and vacuum interfaces. This is an important result as it provides evidence for the assumption that the quartz and vacuum interfaces do not quench. This is useful for modelling the data by using only the ITO layer as a quencher. The model described here was written using *Mathematica*. Decays were modelled using a standard model for diffusion,

$$\frac{\partial n(z,t)}{\partial t} = D\frac{\partial^2 n(z,t)}{\partial z^2} - \kappa(t)n(z,t) - S(z)n(z,t) + \exp(-\gamma t^2) \qquad (6.7)$$

where D is the diffusion coefficient, n is the number of excitons, τ is the fluorescence lifetime, $S(z)$ defines the quenching interface and the final term on the right describes the instrument response function of the streak camera. The variables t and z represent time and distance through the film respectively. It was found during the course of these measurements (on both MEH-PPV and P3HT) that the fluorescence lifetime was dependent upon film thickness. This was unexpected, but nevertheless important. Since there was an extra component in the decay due to this thickness dependence, it needed to be accounted for in the model. This was performed by fitting a mathematical decay to the films on quartz and transferring the parameters gained from this fit to the corresponding film thickness on ITO, at which point the diffusion fit could be found. The thickness decay was incorporated into the lifetime of the film, $\kappa(t)$, and is defined in this model as

$$\kappa(t) = \left[\frac{1}{\tau_0} + \frac{\exp(-\xi t^p)}{\tau_{decay}}\right] \qquad (6.8)$$

where τ_0 is the fluorescence lifetime of a thick (>30 nm) film in the absence of any quenching and ξ, p and τ_{decay} are fitting parameters. It should be stressed that this provides a purely mathematical tool to take the observed thickness dependence into account.

A further addition to this model is the definition of a quenching interface. In all previous literature work, it has been assumed that there is an infinite quenching rate at a 'perfect' interface [36, 42, 44]. This means that excitons are assumed to be instantly quenched when they reach $z = 0$. This has been found to be insufficient when modelling the data and is also physically unrealistic. There will be a small distance over which excitons are quenched, so this has been factored into this model in the form of $S(z)$. Cited literature work defines $S(z)$ to be zero for non-quenching substrates (which is also used here) and (negatively) infinite at the polymer-quencher interface. $z = 0$ is defined here as the polymer-ITO interface (where $z = d$ is the polymer-vacuum interface). An exponential dependence of the quenching rate as distance z was used in this work, and is defined as

$$S(z) = \frac{\exp(-\zeta z)}{\tau_{ito}} \tag{6.9}$$

where ζ^{-1} is the depth of the quenching zone and τ_{ito} is the time over which the dissociation occurs at the interface.

Fits were made to fused silica substrate samples initially in order to take the film thickness dependence into account. This provided values for the parameters ξ, p and τ_{decay}. These values were then used in the corre-

sponding film thickness on ITO. Each film had different values for ξ, p and τ_{decay}, but as mentioned above, these were purely for mathematical fitting. The interface parameters were then varied for each film in turn until a fit was made. The parameters gained were then transferred to a different film to test for consistency. If no fit was achieved, then the parameters (D, ζ and τ_{ito}) were varied until all films used the same values for D, ζ and τ_{ito}. This provided realistic interface quenching for the model. Values for the interfaces will be discussed with the data for each polymer in turn.

Using the fit parameters, a mathematical surface was created (using variables t and z). This surface was then integrated across with respect to film thickness to obtain a decay curve which was then fitted to the experimental data. Once D was obtained it is then possible to obtain the maximum diffusion length of the material using the following relation:

$$L_d = \sqrt{mD\tau_0} \tag{6.10}$$

where m is the dimensionality, D is the diffusion coefficient as above and τ_0 is the (non-quenched) fluorescence lifetime.

As part of this work, two polymers were investigated for exciton diffusion length; MEH-PPV and P3HT. Since film thickness is an important factor in this investigation, it is essential to know this value quite accurately. Usually, a Dektak profilometer would be used to measure film thickness, but because films in this work were very thin, it is impossible to gain reliable results from such a method (nominal resolution of

the Dektak is quoted to be $\pm$ 5 nm). Alternatively, it is possible to measure the absorbance of a film and use this measurement to calculate the film thickness. Absorbance measurements were performed as described in chapter 3. The thickness of a 'thick' film of polymer was measured with a Dektak and then this value was scaled down linearly using the absorbance measurements. This was performed for P3HT because the absorption coefficient is not known precisely. Approximate values can be obtained from the publication by Al-Ibrahiam *et al.* [34] and are taken to be $\sim 3 \times 10^4$ cm^{-1} at 400 nm. These approximations agreed with the measured values to within 5%. A similar method was used for MEH-PPV, but the absorption coefficient was known precisely (measured by Olivier Gaudin using ellipsometry) so values can be calculated from the measured absorbance spectrum.

Results will be fully discussed in section 6.4 in addition to their relationship with the exciton-exciton annihilation results from section 6.2.

6.3.1 Interface Quenching using MEH-PPV

As described above, samples of MEH-PPV were prepared on quartz and ITO substrates with corresponding spin conditions to provide a range film thicknesses. Film thicknesses were measured to be 57, 9, 7 and 5 nm. The absorbance spectra measured for the films are shown in figure 6.13. Films on ITO were also measured and were found to be of similar thickness. PL decay was measured a number of times for each

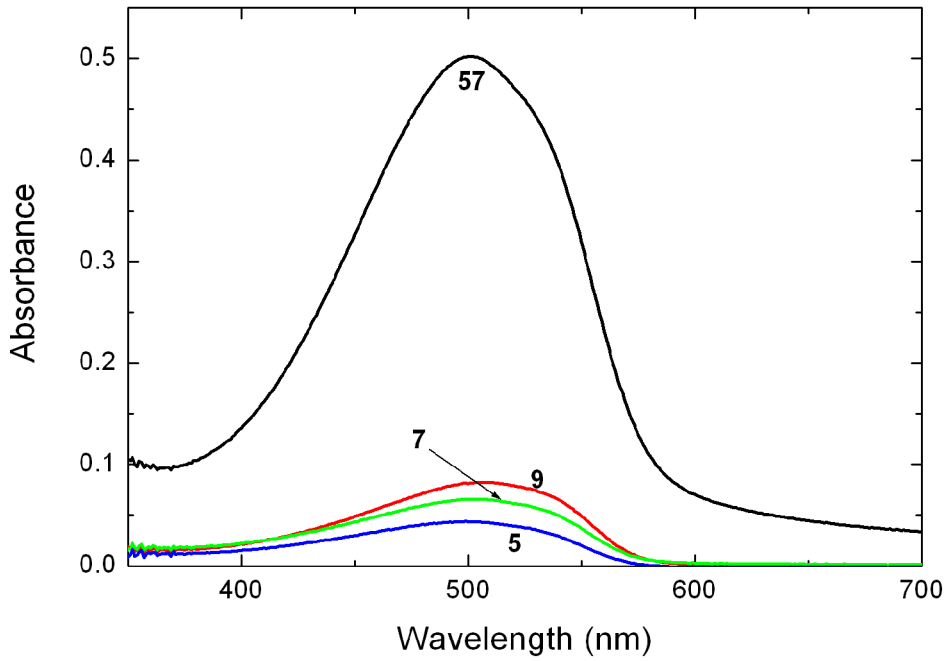

Figure 6.13: Absorbance spectra for various thicknesses of MEH-PPV films on quartz. The absorbance decreases linearly with reducing thickness.

thickness and averaged to obtain a more reliable reading. This also improved signal to noise ratios. Figure 6.14 shows the PL decay curves for MEH-PPV together with model fits. It was observed that there was no (or negligible) difference between the fused silica and ITO substrates at 57 nm. This is expected, since the majority of excitons will be formed more than a diffusion length away from the ITO interface, and therefore will not be quenched. This is reflected in the consistent lifetime in the two films. It is possible to see the film thickness dependence of the decay, even on the fused silica substrates. The decay is expected to become faster with decreasing film thickness on ITO because excitons will diffuse to this interface and become quenched. This is not the case for

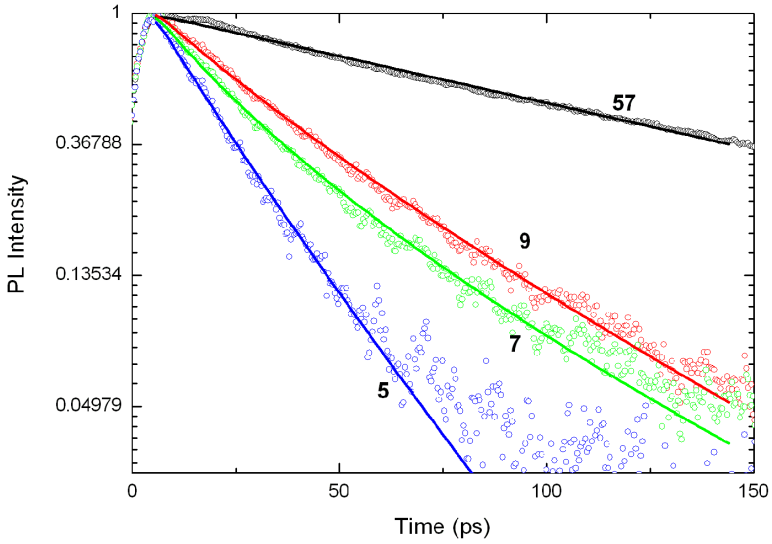

(a) MEH-PPV on quartz substrates.

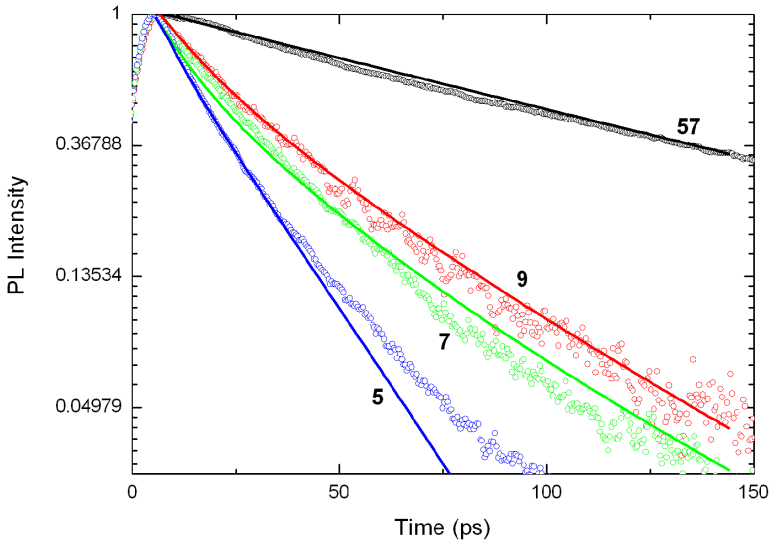

(b) MEH-PPV on ITO substrates

Figure 6.14: TRL decays for films of MEH-PPV. Decay is seen to be dependent upon film thickness, even in the absence of a quencher. Experimental data is shown as open circles, model fits are shown as solid lines.

fused silica substrates as there is no quenching. This thickness dependence therefore needs to be taken into account.

Once fits were found for the fused silica substrates, fit parameters for ITO substrates were found to be $\zeta = 5$ nm^{-1} and $\tau_{ito} = 1$ ps. These parameters defined the quenching interface over which excitons were dissociated and were fixed for all films of MEH-PPV. These are considered to be realistic values as it is reported that the dissociation time for an exciton in MEH-PPV at the interface with SnO_2 is of the order 1 ps [45] and 2 Å is approximately the transverse size of a PPV backbone [46]. This left the diffusion coefficient as the only fitting parameter. Best fits were found for $D = 3 \times 10^{-3}$ cm^{2}s^{-1}. Using this value for D, in addition to the obtained lifetime for MEH-PPV of 140 ps, the result obtained for the exciton diffusion length for MEH-PPV is $L_d = 6 \pm 2$ nm. This result is consistent with previous work on PPV derivatives [26, 27, 36, 38]. Error in this measurement arises from the possible fit tolerances for D. Tolerance on the fits gives $D = (3 \pm 2) \times 10^{-3}$ cm^{2}s^{-1}.

6.3.2 Interface Quenching using P3HT

In a similar way to MEH-PPV, samples of P3HT were prepared on fused silica and ITO substrates with corresponding spin conditions to provide a range film thicknesses. Film thicknesses were measured to be 25, 19, 7, and 3 nm. The absorbance spectra measured for the films are shown in figure 6.15. Films on ITO were also measured and were found to be

of similar thickness. PL decay was measured a number of times for

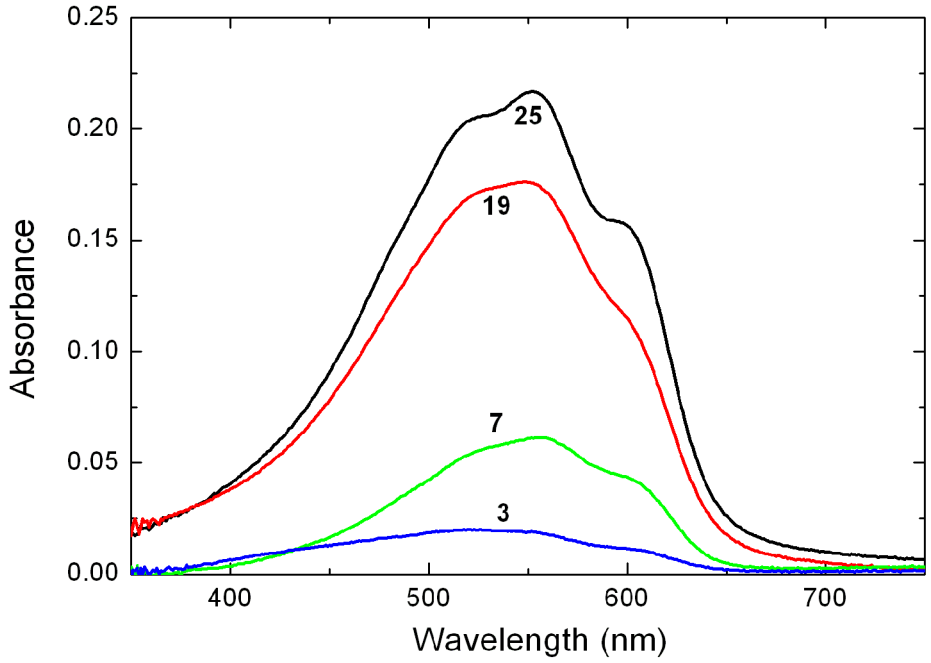

Figure 6.15: Absorbance spectra for various thicknesses (shown in nm) of P3HT films on fused silica. The absorbance decreases with decreasing thickness.

each thickness and averaged to obtain a more reliable reading. This also improved signal to noise ratios. Figure 6.16 shows the PL decay curves for P3HT together with model fits. It is possible to see the film thickness dependence of the decay on the fused silica substrates. The decay is expected to become faster with decreasing film thickness on ITO because excitons will diffuse to this interface and become quenched. This is not the case for fused silica substrates as there is no quenching. This decay, as with MEH-PPV, needs to be taken into account.

Fit parameters for ITO substrates were found to be $\zeta = 1.2$ nm^{-1} and

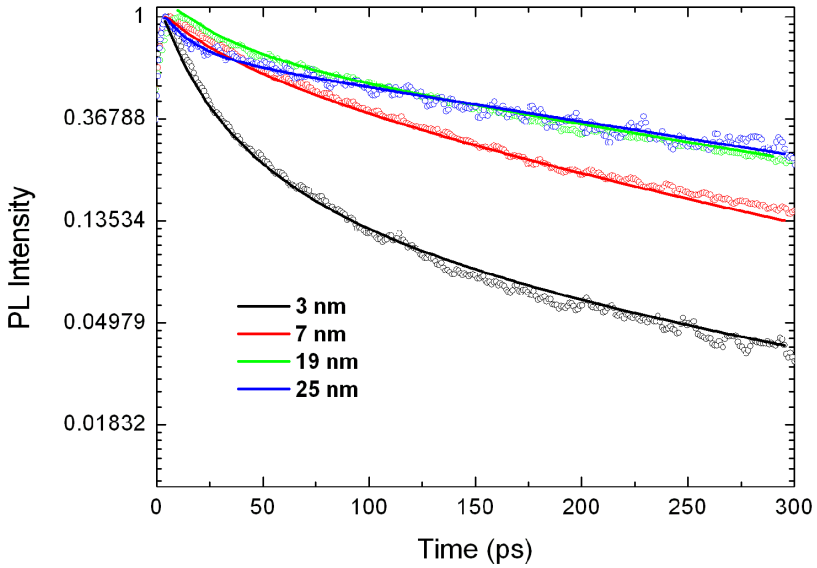

(a) P3HT on fused silica substrates.

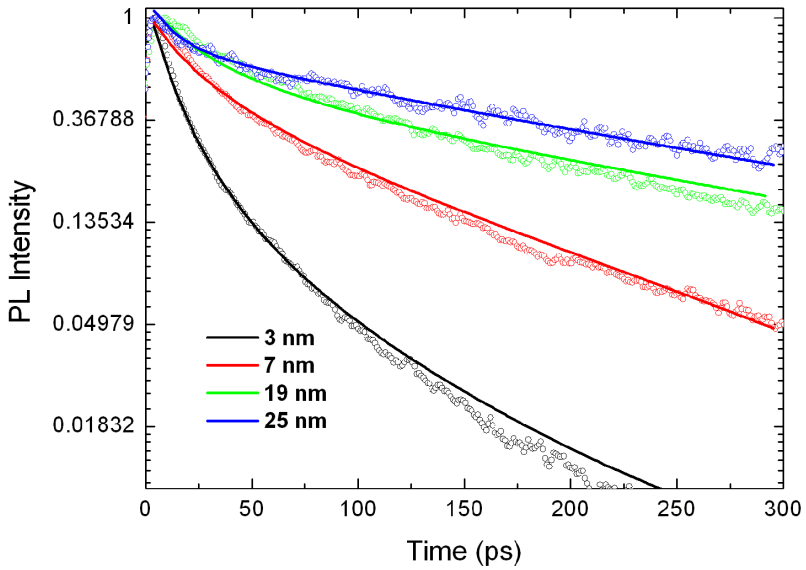

(b) P3HT on ITO substrates.

Figure 6.16: TRL decays for films of P3HT. Decay is seen to be dependent upon film thickness, even in the absence of a quencher. Experimental data is shown as open circles, model fits are shown as solid lines.

$\tau_{ito} = 6$ ps. These are considered to be realistic values as it has been stated that the dissociation time for an exciton in oligothiophene is in the range 1-8 ps [47]. The size of the quenching zone, ~ 8 Å, is larger than expected. However, this could be explained in terms of the exciton being delocalised between chains in P3HT as observed in other polythiophenes with a small interchain distance [48, 49]. The parameters (ζ, τ_{ito}) defining the quenching interface over which excitons were dissociated were fixed for all films of P3HT. This left the diffusion coefficient as the only fitting parameter. Best fits were found for $D = 1 \times 10^{-4}$ cm^{2}s^{-1}. Error in this measurement arises from the possible fit tolerances for D and also possible film thickness inaccuracies due to the measuring method. Tolerance on the fits gives $D = (1.0 \pm 0.5) \times 10^{-4}$ cm^{2}s^{-1}. The values used for fitting the silica substrates are shown in table 6.1.

Thickness (nm)	ξ	**p**	τ_{decay} **(ps)**
25	0.3	2/3	10
19	0.4	5/10	11
7	1.2	4/17	8
3	0.43	6/14	6.1

Table 6.1: A summary of the fitting parameters used for films of P3HT on silica substrates.

6.4 Comparison and Discussion

The presented results above show several key characteristics for MEH-PPV and P3HT. Each polymer will now be discussed in more detail, comparing the results from each experimental method in order to determine

any consistencies and further conclusions that can be drawn from the experimental outcome.

6.4.1 MEH-PPV

For the case of MEH-PPV there is strong consistency between the two methods used above. Using equation 6.11, it is possible to determine the exciton diffusion coefficient for MEH-PPV from the annihilation constant.

$$\gamma = 8\pi D R_a \tag{6.11}$$

where R_a is the annihilation radius of excitons, which corresponds to the distance at which annihilation is faster than diffusion [11]. This is only valid for diffusion-limited annihilation, where the exciton has to diffuse a significant distance before annihilation occurs. This condition is satisfied in this case. If this was not the case, then γ would show strong time dependence, and the plots in figure 6.4 would be nonlinear. Singlet-singlet annihilation is likely to be dominated by dipole-dipole interaction, and so the R_a value is smaller than the Förster radius for excitation transfer onto the excited segment. This depends on the spectral overlap of the PL and the excited state absorption, and is currently unknown. Generally the Förster radius in organic materials is $<$5 nm [50], and the largest reported value of 8 nm was obtained for the perfectly overlapping PL spectrum of the glassy phase of polyfluorene with the absorption spectrum of the crystalline phase [51]. Using $R_a = 5$ nm as the upper estimate, we obtain the lower limit of the diffusion coefficient

$D_{min} = 2.2 \times 10^{-3}$ cm^{2}s^{-1}. This is a factor of two larger than the reported value in MEH-PPV films from surface quenching, where an infinitely large exciton capture rate by polymerised C_{60} was assumed [27]. Given the errors in both measurements the agreement is acceptable. Using $R_a = 2$ nm as the lowest estimate, which is about five times smaller than the length of the singlet exciton in MEH-PPV [52], we obtain an upper limit of $D_{max} = 5 \times 10^{-3}$ cm^{2}s^{-1}.

The diffusion length of the singlet exciton can be calculated using equation 6.10. An approximate value for the diffusion length in three dimensions ($m = 3$), L_{3D} can be determined from the annihilation data using the density at which annihilation begins to occur, found here to be $n(0) \sim 10^{17}$ cm^{-3}. Assuming that exciton diffusion is isotropic the volume sampled by the exciton can be approximated as a sphere and the density of these spheres is $n(0)$, so that

$$\frac{4}{3}\pi n(0) L_{total}^3 = 1 \tag{6.12}$$

This results in $L_{total} \sim 13$ nm, which is in fact the sum of L_{3D} and R_a, so this value can be taken as an upper estimate for the three-dimensional diffusion length. It corresponds to $D_{max} = 4 \times 10^{-3}$ cm^{2}s^{-1}, which gives a stronger constraint on D_{max} than the surface quenching by TiO_2 [28]. Taking this value and the estimated value of D_{min} we obtain $D = (3 \pm 1) \times 10^{-3}$ cm^{2}s^{-1}. The diffusion length, L_d, depends upon the dimensionality, m, which needs to be appropriate to the situation being considered. in addition, the calculations for L_{3D} assume isotropic diffusion which may not apply for P3HT (see section 6.4.2). For exciton diffusion across a

film to a planar heterojunction or quenching interface, only diffusion in one direction matters, and so it is the one-dimensional diffusion length ($m = 1$ in equation 6.10) which is relevant. The range of values here for the diffusion coefficient indicates that L_{1D} lies in the range 5 to 8 nm.

The agreement between diffusion coefficients (using an approximate 5 nm annihilation radius, R_a) in both annihilation and diffusion measurements is remarkably close. Using $R_a = 5$ nm, this gives $D = (3 \pm 1) \times 10^{-3}$ cm^{2}s^{-1}. This is certainly in good agreement with $D = (3 \pm 2) \times 10^{-3}$ cm^{2}s^{-1} obtained from the diffusion to the interface with ITO. Using the value of D obtained from the interface quenching measurements, the one-dimensional diffusion length, L_{1D} using $m = 1$, is found to be 6 ± 2 nm. From this agreement it can be concluded that the diffusion in MEH-PPV is isotropic in all directions due to the uniformly consistent values of the diffusion coefficient and exciton diffusion length.

6.4.2 P3HT

The results for P3HT are slightly in contrast to those of MEH-PPV. The PL lifetime for P3HT was 300 ps. This is comparable with previous literature work by Magnani *et al.* [53]. There have been a number of other polythiophenes studied in addition to P3HT with fluorescence lifetimes ranging from $\sim$ 60 ps to over 500 ps [13, 42, 49]. Using equation 6.11 and the annihilation data, the value found for the diffusion coefficient is $D = 8.0 \times 10^{-4}$ cm^{2}s^{-1}. Comparing this to the interface quenching value

of $D = 1 \times 10^{-4}$ cm^{2}s^{-1}, there is a discrepancy. Using equation 6.12 and $n(0) = 1.2 \times 10^{17}$ cm^{-3}, an approximate value for the three-dimensional diffusion length is found to be 13 nm. This is the sum of R_a and L_d. It leads to a maximum diffusion length of $L_{3D} = 8$ nm assuming R_a is 5 nm as with MEH-PPV. This leads to a one-dimensional diffusion length to be $L_{1D} = 5$ nm. Using the value of D obtained from the annihilation data in equation 6.10, the diffusion length is found to be $L_{1D} = 5$ nm. These resulting values from both methods agree well. However, using the result for D from the interface quenching work and equation 6.10, the one-dimensional diffusion length is found to be $L_{1D} = 2 \pm 1$ nm. This result is in good agreement with work performed by Kroeze *et al.* [43]. However, there is at least a factor of two difference in the values for L_d and a factor of eight between the obtained diffusion coefficients. Since the results for both experiments each agree with previous literature, it is reasonable to say that the results are reliable with respect to their individual experiments.

The difference in values of D could be due to the ordering within films of P3HT. It has been shown that films of P3HT display a degree of ordering within the film structure, shown by X-ray diffraction studies [54, 55]. More recently, Sirringhaus *et al.* have used conduction studies in P3HT transistors to verify this structural variation [56]. The degree of ordering appears to be dependent upon regioregularity, molecular weight and head-to-tail (HT) conformity [54–58]. These cited works discuss the observation that polythiophenes order themselves into semi-regular structures when spin coated or drop cast into films. This ordering forms 'lamellae', which are long, two-dimensional structures that comprise of a

number of P3HT molecules lying planar to each other. Figure 6.17 shows a schematic of the lamellae and how P3HT molecules can stack. Since the P3HT used in my work is regioregular (50% HT), then only this case will be discussed here. The difference in orientation of the 'lamellae' will have a significant effect upon exciton diffusion. The ease of diffusion (or charge transport) in a given direction will depend on whether the orientation of the lamellae are parallel or normal to the substrate. Exciton diffusion is expected to be faster along the individual lamellae due to a shorter distance between conjugated segments. It will also be faster from chain to neighbouring chain when they are arranged in a planar fashion due to overlapping π clouds between neighbouring molecules.

The results presented above for exciton diffusion to an interface and for annihilation (sections 6.2.2 and 6.3.2) show a significant difference in the diffusion coefficients obtained from each experiment. As previously mentioned, both results are consistent with published literature so it is assumed that they are acceptable. The value of $D = 1 \times 10^{-4}$ cm^{2}s^{-1} for diffusion to an interface is essentially a one dimensional measurement. This will be sensitive to the preferential ordering of the P3HT molecules in a spun film. The result for the annihilation constant (and subsequently the derived diffusion coefficient, $D = 8 \times 10^{-4}$ cm^{2}s^{-1}) will be less affected by this orientation dependence as it is sensitive to 3D diffusion. This implies that the P3HT stacks are oriented preferentially parallel to the substrate resulting in higher diffusion along the film and much slower towards an interface with ITO (or other quencher). It has also been reported that this is the way that molecules are arranged for spun films of P3HT [55].

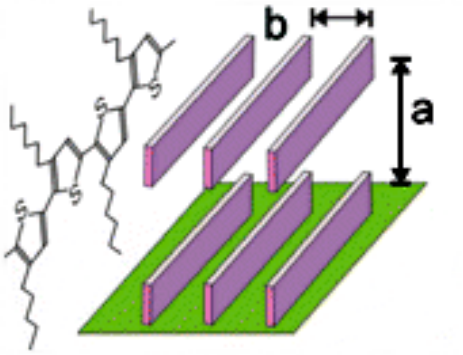

(a)

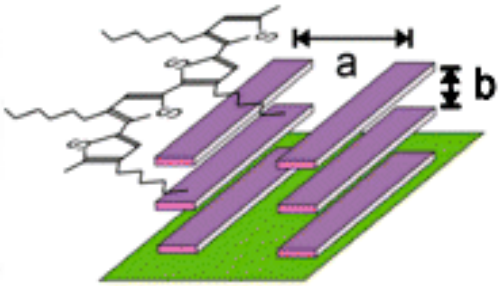

(b)

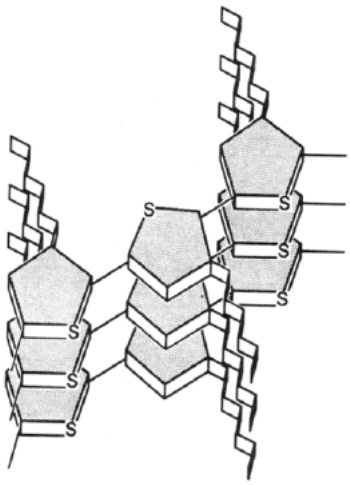

(c) Coplanar stacking within P3HT.

Figure 6.17: (a) and (b) Schematics of the structure of lamellae on a substrate. The configuration in (a) allows preferential transport parallel to the substrate and is more difficult towards it due to overlapping π orbitals between molecules. (b) shows the alternative arrangement where transport to the substrate is easier. (a) and (b) taken from [56]. (c) The arrangement of coplanar regioregular P3HT molecules within a domain. Taken from [58].

This agreement in the discussed literature and in my results here suggests that there is ordering present in films of P3HT in favour of transport parallel to the substrate. This case is illustrated in figure 6.17(a). The lamellae have ordered themselves to produce exciton diffusion along the stacks, which in turn produces a higher value of D measured by the 3D annihilation experiment and a lower value of D for the 1D interface quenching experiment. If the orientation of stacks could be controlled (it is uncertain of the cause but might be an effect of molecular weight and/or regioregularity [56]) it would enable an increase in the diffusion coefficient in a preferred direction (for example towards electron acceptor layers in PV devices) and hinder it in other directions.

Structural studies on P3HT [54–58] also suggest an explanation for the thickness dependence of PL lifetime. The effect is only seen on films thinner than $\sim$ 20 nm. It is possible that the morphology of the film itself (possibly due to the lamallae) is responsible for the effect. Since P3HT is polycrystalline [54], it will possess an arrangement of domains (crystals) with a common order within them. Regioregular molecules such as P3HT are known to exhibit this behaviour [58]. These domains have been measured to be approximately 170 Å in size for P3HT [54,55]. In the interface quenching work presented in section 6.3.2, it was found that the PL lifetime was similar for films 19 nm and higher. This is comparable to the limit of domain size within a P3HT film. The thickness dependence observed in my work suggests that order within each of these domains is high, promoting easier exciton migration. The coplanar arrangement, see figure 6.17(c), facilitates non-radiative decay of excited states [58]. If there is better transport then charges (or excitons) will

migrate more easily, reducing the time between excitation and emission, producing a shorter lifetime. Since the substrate is (assumed to be) flat with little or no disorder, is is plausible to surmise that the molecules in contact with and near to the substrate are most ordered. Above 20 nm it is perhaps the case that a second layer of domains form, with their own order that is arranged differently to those directly on the substrate. It has also been suggested that there are two ordering systems within polythiophene films [54]. The primary is caused by the 'stacking' of the coplanar chains to form lamellae, whilst the second is a much more 3D effect, possibly caused by the chain end groups. This is a bulk effect and will only be seen with more than one layer of domains upon the substrate. This is again supported by the data shown in my work. With two or more layers of domains, the lifetime becomes more dependent upon bulk 3D effects and the thickness dependence is not seen. The stacking of many layers of chains causes significant disorder [54] which will result in poorer exciton mobility, resulting in a longer, invariant PL lifetime in thicker films.

6.5 Summary

This chapter has presented TRL studies of MEH-PPV and P3HT. Exciton-exciton annihilation and interface quenching studies have been performed for both polymers, resulting in slight differences between the two materials. Exciton diffusion coefficients, diffusion lengths and annihilation constants have been calculated for each polymer. It has also

been shown that polymer PL lifetimes depend strongly on film thickness. Work performed on MEH-PPV shows very strong consistency between the two methods, resulting in isotropic exciton diffusion within the films due to close agreement in values of D. P3HT analysis shows preferential diffusion parallel to the substrate resulting in a higher diffusion coefficient in the plane of the film, and a much lower value for diffusion towards the quenching interface. This is caused by assembly of the film into lamellae. The thickness dependent PL lifetime can be explained by the physical size of the small crystals (domains) that form within films of P3HT. The crystal size is comparable to the maximum thickness at which this dependence begins. These crystals are highly ordered within their boundaries which cause faster recombination resulting in a shorter lifetime. For films thicker than $\sim$ 20 nm, the effect is not seen due to bulk ordering of the films from end group interactions.

References

[1] B.A. Gregg and M.C. Hanna, *Journal of Applied Physics* **93**, 3605 (2003).

[2] B.A. Gregg, *Journal of Physical Chemistry B* **107**, 4688 (2003).

[3] M.A. Green, *Physica E* **14**, 11 (2002).

[4] M. Scheidler, U. Lemmer, R. Kersting, S. Karg, W. Riess, B. Cleve, R. F. Mahrt, H. Kurz, H. Bassler, E. O. Gobel, and P. Thomas, *Physical Review B* **54**, 5536 (1996).

[5] S. F. Alvarado, P. F. Seidler, D. G. Lidzey, and D. D. C. Bradley, *Physics Review Letters* **81**, 1082 (1998).

[6] V. Gulbinas, Y. Zaushitsyn, V. Sundström, D. Hertel, H. Bassler,

and A. Yartsev, *Physical Review Letters* **89**, 107401 (2002).

[7] D. Moses, J. Wang, A.J. Heeger, N. Kirova, and S. Brazovski, *Proceedings of the National Association of Sciences of the USA* **98**, 13496 (2001).

[8] K.M. Coakley and M.D. McGehee, *Applied Physics Letters* **83**, 3380 (2003).

[9] D. Chirvase, Z. Chiguvare, M. Knipper, J. Parisi, V. Dyakonov, and J.C. Hummelen, *Journal of Applied Physics* **93**, 3376 (2003).

[10] T. Nguyen, I.B. Martini, J. Liu, and B.J. Schwartz, *Journal of Physical Chemistry* **104**, 237 (2000).

[11] N. Ikeda, A. Yoshimura, M. Tsushima, and T. Ohno, *Journal of Physical Chemistry* **104**, 6158 (2000).

[12] R.G. Kepler, V.S. Valencia, S.J. Jacobs, and J.J. McNamara, *Synthetic Metals* **78**, 227 (1996).

[13] A. Ruseckas, M. Theander, L. Valkunas, M.R. Andersson, O. Inganäs, and V. Sundstrom, *Journal of Luminescence* **76 & 77**, 474 (1998).

[14] E.J.W. List, U. Scherf, K. Mullen, W. Graupner, C.H. Kim, and

J. Shinar, *Physical Review B* **66**, 235203 (2002).

[15] W. Holzer, A. Penzkofer, R. Stockmann, H. Meysel, H. Liebegott, and H.H. Horhold, *Synthetic Metals* **125**, 343 (2002).

[16] V.A. Malyshev, H. Glaeske, and K.H. Feller, *Journal of Luminescence* **76 & 77**, 455 (1998).

[17] I.B. Martini, A.D. Smith, and B.J. Schwartz, *Physical Review B* **69**, 035204 (2004).

[18] Q. Xu, D. Moses, and A.J. Heeger, *Physical Review B* **68**, 174303 (2003).

[19] E.B. Namdas, A. Ruseckas, I.D.W. Samuel, S.C. Lo, and P.L. Burn, *Applied Physics Letters* **86**, 091104 (2005).

[20] J. Parisi, V. Dyakonov, M. Pientka, I. Riedel, C. Deibel, C.J. Brabec, N.S. Sariciftci, and J.C. Hummelen, *Zeitschrift fur Naturforschung Section A: Journal of Physical Sciences* **57**, 995 (2002).

[21] H. Lin, Y. Weng, H. Huang, Q. He, M. Zheng, and F. Bai, *Apllied Physics Letters* **84**, 2980 (2004).

[22] A. Ruseckas, Private Communication.

[23] G. Gustafsson, G.M. Treacy, Y. Cao, F. Klavetter, N. Colaneri, and A.J. Heeger, *Synthetic Metals* **57**, 4123 (1993).

[24] S.E. Shaheen, C.J. Brabec, N.S. Sariciftci, F. Padinger, T. Fromherz, and J.C. Hummelen, *Applied Physics Letters* **78**, 841 (2001).

[25] I.D.W. Samuel and G.A. Turnbull, *Materials Today* **7**, 28 (2004).

[26] A. Haugeneder, Neges C. Kallinger, W. Spirkl, U. Lemmer, J. Feldmann, U. Scherf, E. Harth, A. Gugel, and K. Mullen, *Physical Review B* **59**, 15346 (1999).

[27] D.E. Markov, C. Tanase, P.W.M. Blom, and J. Wildeman, *Physical Review B* **72**, 045217 (2005).

[28] V.M. Burkalov, K. Kawata, H.E. Assender, G.A.D. Briggs, A. Ruseckas, and I.D.W. Samuel, *Physical Review B* **72**, 075206 (2005).

[29] G.R. Hayes, I.D.W. Samuel, and R.T. Phillips, *Physical Review B: Rapid Communications* **52**, 569 (1995).

[30] A.K. Sheridan, G.A. Turnbull, A.N. Safonov, and I.D.W. Samuel, *Physical Review B: Rapid Communications* **62**, 11929 (2000).

[31] D. Chirvase, Z. Chiguvare, M. Knipper, J. Parisi, V. Dyakonov, and

J.C. Hummelen, *Synthetic Metals* **138**, 299 (2003).

[32] G. Li, V. Shrotriya, Y. Yao, and Y. Yang, *Journal of Applied Physics* **98**, 043704 (2005).

[33] V. Dyakonov, *Applied Physics A* **79**, 21 (2004).

[34] M. Al-Ibrahim, H. Klaus Roth, M. Schroedner, A. Konkin, U. Zhokhavets, G. Gobsch, P. Scharff, and S. Sensfuss, *Organic Electronics* **6**, 65 (2005).

[35] G. Dicker, M.P. de Haas, L.D.A. Siebbeles, and J.M. Warman, *Physical Review B* **70**, 045203 (2004).

[36] D.E. Markov, E. Amsterdam, P.W.M. Blom, A.B. Sieval, and J.C. Hummelen, *Journal of Physical Chemistry A* **109**, 5266 (2005).

[37] J.J.M. Halls, K. Pichler, R.H. Friend, S.C. Moratti, and A.B. Holmes, *Applied Physics Letters* **68**, 3120 (1996).

[38] T. Stubinger and W. Brutting, *Journal of Applied Physics* **90**, 3632 (2001).

[39] H.R. Kerp, H. Donker, R.B.M. Koehorst, T.J. Schaafsma, and E.E. von Faassen, *Chemical Physics Letters* **298**, 302 (1998).

[40] B.A Gregg, J. Sprague, and M.W. Peterson, *Journal of Physical Chemistry B* **101**, 5362 (1997).

[41] V. Bulovic and S.R. Forrest, *Chemical Physics* **210**, 13 (1996).

[42] M. Theander, A. Yartsev, D. Zigmantas, V. Sundstrom, W. Mammo, M.R. Andersson, and O. Inganäs, *Physical Review B* **61**, 12957 (2000).

[43] J.E. Kroeze, T.J. Savenije, M.J.W. Vermeulen, and J.W. Warman, *Journal of Physical Chemistry B* **107**, 7696 (2003).

[44] D.E. Markov, J.C. Hummelen, P.W.M. Blom, and A.B. Sieval, *Physical Review B* **72**, 045216 (2005).

[45] N.A. Anderson, E. Hao, X. Ai, G. Hastings, and T. Lian, *Chemical Physics Letters* **347**, 304 (2001).

[46] M. Kemerink, J.K.J van Duren, P. Jonkheijm, W.F. Pasveer, P.M. Koenraad, R.A.J. Janssen, H.W.M. Salemink, and J.H. Wolter, *Nanoletters* **3**, 1191 (2003).

[47] M. Helbig, A. Ruseckas, M.M.-L. Grage, E. Bickner, S. Rentsch, and V. Sundström, *Chemical Physics Letters* **302**, 587 (1999).

[48] A. Ruseckas, E.B. Namdas, T. Ganguly, M. Theander, M. Svensson,

M.R. Andersson, O. Inganäs, and V. Sundström, *Journal of Physical Chemistry* **105**, 7624 (2001).

[49] A. Ruseckas, E.B. Namdas, M. Theander, M. Svensson, A. Yartsev, D. Zigmantas, M.R. Andersson, O. Inganäs, and V. Sundström, *Journal of Photochemistry and Photobiology* **144**, 3 (2001).

[50] J.R. Lakowicz, *Principles of Fluorescence Spectroscopy*, Kluwer Academic/ Plenum Publishers, 1999.

[51] A.L.T. Khan, P. Sreearunothai, L.M. Herz, M.J. Banach, and A. Köhler, *Physical Review B* **69**, 085201 (2004).

[52] A. Ruseckas, P. Wood, I.D.W. Samuel, G.R. Webster, W.J. Mitchell, P.L. Burn, and V. Sundström, *Physical Review B* **72**, 115214 (2005).

[53] L. Magnani, G. Rumbles, I. D. W. Samuel, K. Murray, S. C. Moratti, A. B. Holmes, and R. H. Friend, *Synthetic Metals* **84**, 899 (1997).

[54] T.J. Prosa, M.J. Winokur, J. Moulton, P. Smith, and A.J. Heeger, *Macromolecules* **25**, 4364 (1992).

[55] H.J. Fell, E.J. Samuelson, J. Als-Nielsen, G. Grübel, and J. Mårdalen, *Solid State Communications* **94**, 843 (1995).

[56] H. Sirringhaus, P.J. Brown, R.H. Friend, M.M. Nielson, K. Bech-

gaard, B.M.W. Langeveld-Voss, A.J.H Spiering, R.A.J. Janssen, E.W. Meijer, P. Herwig, and D.M. de Leeuw, *Nature* **401**, 685 (1999).

[57] M. Huanyu, B. Xu, and S. Holdcroft, *Macromolecules* **26**, 1163 (1993).

[58] B. Xu and S. Holdcroft, *Macromolecules* **26**, 4457 (1993).

Chapter 7

General Conclusions

There are a number of conclusions that can be drawn from the work in this thesis. Since the work falls primarily into two sections, devices and spectroscopy, they can be dealt with individually.

Device work presented here encompasses a large number of materials in two distinct categories, polymers and dendrimers. Despite the differences in the material types, there are certain aspects that remain constant. For a successful solar cell device, there are a number of key factors required. These are high light absorption over a suitable wavelength range, charge separation, charge transport (covered in more detail by spectroscopy) and even device structure. It has been shown that, independent of material type, the need for charge separation and transport is crucial for an effective device. This has been demonstrated using polymer materials designed for charge separation. This approach was

successful in separating charges on a molecule without the need for a dopant, shown by comparing the polymers DPFEH-PPV and NDPFEH-PPV. The latter of these polymers includes a dipole across the molecule to assist in charge separation, which is highly effective, reducing the PL lifetime by a factor of five with respect to the non-polar molecule.

The synthesis of suitable materials is also essential in device fabrication. Light must be absorbed in order to generate excitons. The polymer DM-PPV has been synthesised to potentially increase the molecular packing in a polymer film, creating a higher density of light absorbing centres. This was successful and increased light absorption by 17% compared to MEH-PPV.

Suitable wavelengths for light absorption have been a common problem in recent years for organic materials [1] as the majority of conjugated materials absorb light that is too high in energy. Since there is an abundance of red photons in solar light, it is therefore beneficial to synthesise materials to absorb these photons in favour of higher energy photons. This has been successfully achieved using conjugated dendrimers based upon cyanine dyes.

Conjugated dendrimers have also been demonstrated to be highly efficient at charge separation and transport when blended with a host. A novel technique using IPCE measurements and ellipsometrical data has been described which shows that the internal quantum efficiency of iridium based dendrimer solar cells is in excess of 90% when blended with PCBM.

The transport of excitons within organic films is a key factor in the operation of thin film solar cell devices. In the presented work it has been shown using two techniques that exciton transport in polymers is highly dependent upon the material used. For the case of MEH-PPV, using a combination of exciton-exciton annihilation and interface quenching methods, the diffusion within a film is isotropic in all directions. For the case of P3HT, the results were in contrast. Due to self ordering of the polymer as it is spin coated onto a substrate, the PL lifetime of the material depends strongly upon film thickness and the diffusion process is anisotropic. The material orders itself into 'lamellae' [2–6] which are made up of a number of P3HT molecules stacking planar to each other. This then enables exctions to diffuse preferentially in the plane of these lamellae due to overlapping π electron clouds. These lamellae also form domains which have been shown to be of order 20 nm in size. These dimensions are similar to those where the PL lifetime begins to depend upon film thickness. The ordering of domains is controlled by the polymer end groups [3] which ultimately gives an upper limit of the PL lifetime. By reducing the film thickness, the disorder in the film is decreased and consequently, so is the PL lifetime.

Future work should be focussed upon the optimisation of device structure for cyanine dye materials, as well as the further synthesis of similar red absorbing materials. By providing a range of materials it may be possible to not only absorb light where needed, but also provide attractive alternatives for solar panel placement to suit surroundings and commercial demand.

Further investigation of materials should also be carried out with respect to the charge transport properties. The techniques introduced in chapter 6 can be used on any potential material in order to determine its exciton transport properties and, to some extent, any microscopic ordering that may occur during the film formation process. The ordering may be key to how a material operates in a device, and as such, the device design could be tailored to accommodate these properties.

References

[1] C.J. Brabec, N.S. Sariciftci, and J.C. Hummelen, *Advanced Functional Materials* **11**, 15 (2001).

[2] H. Sirringhaus, P.J. Brown, R.H. Friend, M.M. Nielson, K. Bechgaard, B.M.W. Langeveld-Voss, A.J.H Spiering, R.A.J. Janssen, E.W. Meijer, P. Herwig, and D.M. de Leeuw, *Nature* **401**, 685 (1999).

[3] T.J. Prosa, M.J. Winokur, J. Moulton, P. Smith, and A.J. Heeger, *Macromolecules* **25**, 4364 (1992).

[4] H.J. Fell, E.J. Samuelson, J. Als-Nielsen, G. Grübel, and J. Mårdalen, *Solid State Communications* **94**, 843 (1995).

[5] M. Huanyu, B. Xu, and S. Holdcroft, *Macromolecules* **26**, 1163 (1993).

[6] B. Xu and S. Holdcroft, *Macromolecules* **26**, 4457 (1993).

Appendix A

Publications Arising from this Thesis

A.J. Lewis, A. Ruseckas, O.P.M. Gaudin, G.R. Webster, P.L. Burn and I.D.W. Samuel, *"Singlet Exciton Diffusion in MEH-PPV Films Studied by Exciton-Exciton Annihilation"*, **Accepted by Organic Electronics**.

P.E. Shaw, A.J. Lewis, A. Ruseckas and I.D.W. Samuel, *"Exciton Diffusion and Annihilation in semiconducting polymers"*, **In preparation for submission to SPIE**.

A.J. Lewis, C.J. Yates, I.D.W. Samuel, S. Staton and P.L. Burn, *"High Quantum Efficiency Ir(ppy)$_3$ dendrimer solar cells"*, **In preparation for submission**.